(2)



UNCLASSIFIED
SECURITY CLASSIFICATION OF THIS PAGE (When Data Entered)

## REPORT DOCUMENTATION PAGE

READ INSTRUCTIONS BEFORE COMPLETING FORM

| REPORT NUMBER | 2. GOVT ACCESSION NO. | 3. RECIPIENT'S CATALOG NUMBER |
|---|---|---|
| ARO 22801.8-MS | N/A | N/A |

**TITLE (and Subtitle)**

A Self Consistent RF Discharge, Plasma Chemistry and Surface Model for Plasma Enhanced Chemical Vapor Deposition

**5. TYPE OF REPORT & PERIOD COVERED**
Final Report
14-Oct-1985 to 15-June-1988

**6. PERFORMING ORG. REPORT NUMBER**
11.321.

**AUTHOR(s)**

Mark J. Kushner and Michael J. McCaughey

**8. CONTRACT OR GRANT NUMBER(s)**
DAAG29-85-C-0031

**PERFORMING ORGANIZATION NAME AND ADDRESS**
Spectra Technology Inc., 2755 Northup Way, Bellevue, WA 98004; and University of Illinois, Dept. of Electrical & Comp. Engr., Urbana, IL

**10. PROGRAM ELEMENT, PROJECT, TASK AREA & WORK UNIT NUMBERS**
N/A

**11. CONTROLLING OFFICE NAME AND ADDRESS**
U. S. Army Research Office
Post Office Box 12211
Research Triangle Park, NC 27709

**12. REPORT DATE**
30 June 1988

**13. NUMBER OF PAGES**

**14. MONITORING AGENCY NAME & ADDRESS (if different from Controlling Office)**

**15. SECURITY CLASS. (of this report)**
Unclassified

**15a. DECLASSIFICATION/DOWNGRADING SCHEDULE**

**16. DISTRIBUTION STATEMENT (of this Report)**

Approved for public release; distribution unlimited.



**17. DISTRIBUTION STATEMENT (of the abstract entered in Block 20, if different from Report)**

NA

**18. SUPPLEMENTARY NOTES**

The view, opinions, and/or findings contained in this report are those of the author(s) and should not be construed as an official Department of the Army position, policy, or decision, unless so designated by other documentation.

**19. KEY WORDS (Continue on reverse side if necessary and identify by block number)**

Plasma Enhanced Chemical Vapor Deposition, amorphous silicon, modeling, electron kinetics, plasma chemistry, deposition kinetics, rf discharge, silane, film properties, silicon, [illegible]

**20. ABSTRACT (Continue on reverse side if necessary and identify by block number)**

A self consistent model for the plasma enhanced chemical vapor deposition of thin films of amorphous hydrogenated silicon (a-Si:H) is presented. The model consists of three submodels for the electron kinetics, plasma chemistry, and surface deposition kinetics for a-Si:H deposited from radio frequency plasmas containing silane. Results from the model are discussed for a variety of discharge conditions, and recommendations are made for optimizing film properties.

DD FORM 1 JAN 73 1473 EDITION OF 1 NOV 65 IS OBSOLETE

UNCLASSIFIED
SECURITY CLASSIFICATION OF THIS PAGE (When Data Entered)

ARO 22801.8-MS

# A SELF CONSISTENT RF DISCHARGE, PLASMA CHEMISTRY, AND SURFACE MODEL FOR PLASMA ENHANCED CHEMICAL VAPOR DEPOSITION

Mark J. Kushner and Michael J. McCaughey

FINAL REPORT

June 1988

U. S. ARMY RESEARCH OFFICE
Contract No. DAAG29-85-C-0031

University of Illinois
Department of Electrical and Computer Engineering
1406 W. Green Street
Urbana, Illinois 61801

and

Spectra Technology, Inc.
2755 Northup Way
Bellevue, Washington 98004

The view, opinions, and/or findings contained in this report are those of the authors and should not be construed as an official Department of the Army position, policy, or decision, unless so designated by other documentation.

Table of Contents

# I. Introduction

Plasma Enhanced Chemical Vapor Deposition (PECVD) is a process whereby thin films of amorphous, microcrystalline and crystalline films my be deposited. As the activation energy for the production of radicals in PECVD is provided by electron impact collisions in the plasma, the substrate temperature may be significantly lower in PECVD than that used in thermally activated chemical vapor deposition (CVD). Hence, PECVD is attractive for applications which are thermally sensitive.

A typical PECVD reactor and operating conditions are shown in Fig. 1. PECVD is usually performed at low pressures (< 0.5 Torr) in a parallel plate capacitively coupled radio frequency (rf) discharge. The power deposition is a few to 100's of $mW\text{-}cm^{-3}$ at frequencies of 100's of kHz to 10's of MHz. Feed stock gases are flowed through the discharge with residence times of 10's of ms to 1 s, resulting in an energy investment of 1 - 10's of eV per molecule. Electron impact dissociation and ionization collisions create neutral and charged radicals which diffuse or drift out of the plasma to the substrate. While approaching the substrate, the radicals may undergo further chemical reactions. At the substrate, the radicals adsorb, bond, sputter, and otherwise react with the surface to form the film. Saturated molecules may be desorbed from the surface and enter the plasma.

The PECVD of amorphous hydrogenated silicon (a-Si:H) has received a great deal of attention during the past few years as this material is used in the fabrication of thin film transistors, photo-voltaic devices (eg., solar cells) and photo-receptors, as used in copiers. In this process, feedstock gases consisting of mixtures of silane ($SiH_4$), disilane ($Si_2H_6$), and buffers (eg., $H_2$, Ar) are used to generate radicals such as $SiH_3$ and $SiH_2$ which are the major contributors to film growth. The a-Si:H film consists of a network of Si-Si and Si-H bonds having an atomic hydrogen fraction of 5-20%. Device quality material may be deposited at growth rates of 10's - 100's of Å/min.

The processes leading to the deposition of a-Si:H, described below, are complex. As a result, there has in the past been no a priori method to predict film properties (ie., growth rate, hydrogen fraction, hydride/dihydride bond ratios, surface roughness) given physical parameters such as gas mix, power deposition and reactor geometry. The technology associated with thin film growth has therefore been an empirical discipline, and the optimization of film properties has been slow to occur.

The PECVD process is conceptually divisible into three interlinked subprocesses:

- Gas phase electron kinetics
- Heavy particle plasma chemistry and transport
- Surface deposition kinetics.

Gas phase electron kinetics includes the processes in which power is coupled through the free electrons and deposited in the gas by electron impact

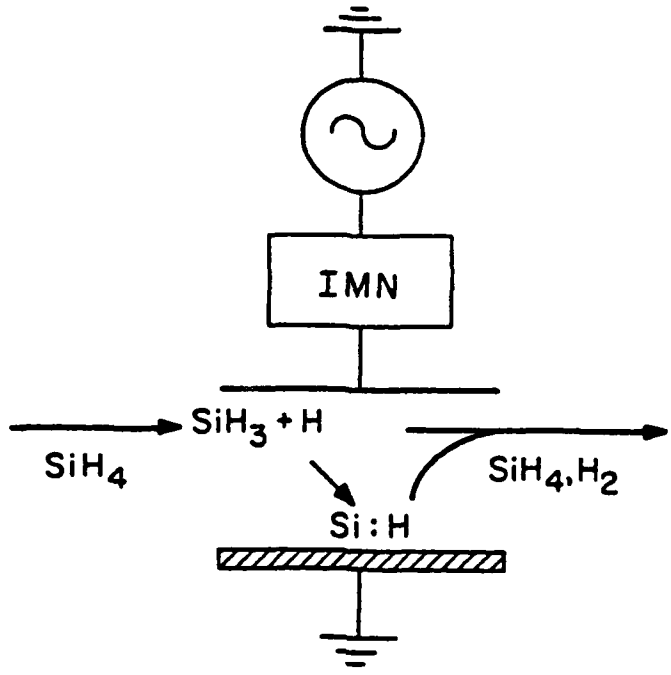


- Pressure: 10's - 100's mTorr
- Power: 10's - 100 $mW/cm^3$
- Electrode Separation: 1-10 cm
- Electron Density: $10^9 - 10^{10}/cm^3$
- Bulk Electron Temperature: 1-2 eV
- Gas Residence Time: 10's ms - 1 s
- Fractional Dissociation: 1-10's %

Figure 1 - Typical plasma reactor conditions for low pressure PAMP (eg., etching, deposition)

collisions. To describe these processes, one must be able to specify the electron distribution function for energy, position in the reactor and time during the rf cycle; $f(\epsilon,x,t)$. The heavy particle plasma chemistry and transport includes the processes during which radicals and ions are generated by electron impact and further reactions occur between the radicals and with the feed stock gases. These processes also include the transport of radicals and charged species in the plasma by either diffusion, convection, or drift of charged species in the electric field. The surface deposition kinetics include those processes occuring on and near the substrate which result in the formation of the film.

Although conceptually divisible, these three subprocesses are strongly coupled. The electron impact dissociation of, say, silane creates radicals which by further reactions change the electron transport coefficients and hence the electron distribution function. This change in the electron distribution function causes a change in the rate of radical generation. Radicals and ions impacting on the substrate form the amorphous silicon film. While doing so, these processes generate species which are released back into the plasma which affect the plasma and electron kinetics.

To obtain a predictive capability for the PECVD of a-Si:H, one must address the three sub-processes described above in a self consistent fashion. In this research project, a computer model for the PECVD of a-Si:H has been developed consisting of interlinked sub-models for the electron kinetics, plasma chemistry, and surface deposition kinetics. A Monte Carlo simulation is used to generate the electron distribution function and electron impact rate coefficients as a function of position and time in a parallel plate capacitively coupled rf discharge. These rate coefficients are used as input to a 1-1/2 dimensional, time dependent plasma chemistry model. The plasma chemistry model produces the densities and fluxes of radicals and ions. These fluxes are then used as input to a model for the surface deposition kinetics which simulates bulk and surface properties of the film. This work represents the first iteration of a totally self consistent model for the PECVD of a-Si:H.

## II. Research Results

The results of this research project are summarized in publications included in the Appendix. The abstracts from those publications are reproduced below.

On the Balance Between Silylene and Silyl Radicals in RF Glow Discharges in Silane: The Effect on Deposition Rates of a-Si:H (M. J. Kushner, J. Appl. Phys. 62, 2803 (1987))


### Abstract

Plasma Enhanced Chemical Vapor Deposition (PECVD) of amorphous hydrogenated silicon (a-Si:H) is typically performed in low pressure ($\lesssim$ 0.5 Torr) radio frequency (RF) discharges in gas mixtures containing silane ($SiH_4$). The initiating step is electron impact dissociation of silane whose products are primarily the silylene ($SiH_2$) and silyl ($SiH_3$) radicals. The ratio of $SiH_2$ to $SiH_3$ in the plasma is important because these radicals incorporate differently into the $\alpha$-Si:H film; and therfore the characteristics of the film are a function of the ratio $[SiH_3]/[SiH_2]$. The initial step is followed by a series of hydrogen abstraction, silylene insertion, and silyl association reactions which subsequenty alter this ratio. The branching ratios for electron impact dissociation of silane as well as the rate constants for the subsequent reactions have not been measured or are uncertain. Using a model for an RF discharge in silane gas mixtures, the effects of branching ratios for silane dissocation and rate constants for key reactions are investigated. We find that in order for $SiH_3$ to be the dominant radical, as currently thought, its branching ratio from electron impact dissociation of $SiH_4$ must exceed 0.75, and the yield for H atoms in the branch for $SiH_2$ must also exceed 0.75. The deposition rate of a-Si:H is then controlled by the yield of H atoms and the subsequent generation of radicals by hydrogen abstraction from $SiH_4$. These results require that the silyl association reaction must have a rate constant $\lesssim 10^{-11} cm^3 s^{-1}$, and that the rate constant for insertion of $SiH_2$ into silane must exeed $10^{-11} cm^3 s^{-1}$.


. . . . . .

A Phenomenological Model for Surface Deposition Kinetics During Plasma and Sputter Deposition of Amorphous Hydrogenated Silicon (M. J. Kushner, J. Appl. Phys. 62, 4763 (1987))


### Abstract

The surface processes during the plasma enhanced chemical vapor deposition and reactive sputter deposition of amorphous hydrogenated silicon (a-Si:H) are investigated by use of a phenomenological model. The model consists of an accounting, in rate equation form, of adsorption of radicals from the plasma onto the surface, surface

diffusion, incorporation into the lattice, interconnection of bonds in the lattice, and burial of species on the surface, thereby constituting film growth. By accounting for the coordination partners of Si atoms in the film, the atomic fraction of hydrogen in the film is computed for both the lattice and for hydrogen in polymeric or isolated configurations. Results from the model are discussed while parameterizing the probability for hydrogen elimination during incorporation, and the probability for saturation of dangling bonds by gas phase species. We find that the mode of hydrogen elimination during incorporation distinguishes films grown dominantly from $SiH_2$ or $SiH_3$ radicals. Characteristics of films grown by sputter deposition are investigated as a function of the composition of the radical flux. We find that films grown from hydrogen rich fluxes are composed dominantly of dihydride ($=Si\begin{smallmatrix}H\\H\end{smallmatrix}$) configurations, whereas hydrogen lean mixtures are composed of dominantly hydride ($\equiv Si-H$) configurations.

. . . . . .

A Model for the Discharge Kinetics and Plasma Chemistry During Plasma Enhanced Chemical Vapor Deposition of Amorphous Silicon (M. J. Kushner, J. Appl. Phys. 63, 2532 (1988))

Abstract

A model for the plasma enhanced chemical vapor deposition (PECVD) of amorphous hydrogenated silicon (a-Si:H) in rf and dc discharges is presented. The model deals primarily with the plasma chemistry of discharges sustained in gas mixtures containing silane ($SiH_4$). The plasma chemistry model uses as input the electron impact rate coefficients generated in a separate simulation for the electron kinetics and therefore makes no apriori assumptions as to the manner of power deposition. Radical densities and contributions to film growth are discussed as a function of gas mixture, electrode separation, and locale of power deposition; and comparisons are made to experiment. A compendium of reactions and rate constants for silane neutral and ion chemistry is also presented.

. . . . . .

Phase and Energy Distribution of Ions on Electrodes in Radio-Frequency Discharges (G. Hebner and M. J. Kushner, J. Appl. Phys. 62, 2256 (1987))

Abstract

A Monte Carlo particle simulation and parametric models for the sheath voltage and thickness were used to calculate the arrival phase and energy of ions striking the electrodes in low-pressure capacitively coupled rf discharges. Ion phase and energy

distributions are presented as a function of rf frequency, ion mass, rf voltage, dc bias, sheath thickness, and gas pressure. When the rf frequency is below the ion response frequency, the ions arrive at the electrode in phase with the applied rf voltage. As the rf frequency increases, the highest ion arrival probability shifts towards higher phase until, at sufficiently high frequencies, it is nearly uniform. The transition from a highly peaked ion phase distribution at low frequencies to a uniform distribution at high frequencies requires at least an order of magnitude change in rf frequency. The implication of these calculations on the electron energy distribution is discussed.

. . . . . .

Important Considerations for Optimizing Production Rates in RF Discharge Chemistry (M. J. Kushner and A. Garscadden in L. G. Christophorou and D. Bouldin, Gaseous Dielectrics V (Pergammon, New York, 1987) pp. 334-341)

Abstract

Important issues which should be considered when optimizing RF discharges for use in plasma processing are discussed using results from electron kinetics and plasma chemistry models. Mixtures of $Ar/SiH_4$ and $H_2/SiH_4$ are discussed as exemplary systems for the plasma deposition of amorphous silicon. The effect of dissociation of the feed stock gas on subsequent rates of dissociation is discussed, as is the effect of diluting silane discharges with argon.

. . . . . .

Simulation of the Bulk and Surface Properties of Amorphous Hydrogenated Silicon Deposited from Silane Plasmas (M. J. McCaughey and M. J. Kushner, submitted to J. Appl. Phys.)

Abstract

A Monte Carlo simulation for the growth of amorphous hydrogenated silicon (a-Si:H) thin films by plasma enhanced chemical vapor deposition (PECVD) is presented. The focus of the model is to predict the bulk properties of films having thicknesses of $\leq$ 2000Å (eg., hydrogen content, buried hydride/dihydride ratios, porosity, and surface roughness). the effects on the film properties of the composition of the radical flux incident on the surface are examined. Film properties were found to be critically dependent on the ratio of $SiH_3/SiH_2$ in the radical flux, with high values for this ratio causing depositon resembling chemical vapor deposition and low values resembing physical vapor deposition. Rough films (rms roughness of 10's of Å) result from radical fluxes having high $SiH_2$ fractions. We find that surface roughness and hydrogen fraction increase with increasing growth rate and increasing film thickness,

though thin films have large hydrogen fractions due to there being a hydrogen rich surface layer with a thickness approximately equal to the surface roughness. We also find correlation between porosity (subsurface voids) and hydrogen fraction, implying that hydrogen is trapped in voids as a result of their being lined with $\equiv$Si-H configurations.

III. Publications and Technical Presentations

The following publications and techninal presentations were prepared under this contract.

## Book Chapters

L. E. Kline and M. J. Kushner, "Computer Simulations of Materials Processing Plasma Discharges", to be published in CRC Critical Reviews in Solid State and Materials Science.

## Journal Articles

M. J. Kushner, "Mechanisms for Power Deposition in $Ar/SiH_4$ Capacitively Coupled RF Discharges," IEEE Trans. Plasma Sci. PS-14, 188 (1985).

G. Hebner and M. J. Kushner, "The Phase and Energy Distribution of Ions Incident on Electrodes in Radio Frequency Discharges," J. Appl. Phys. 62, 2256 (1987)

M. J. Kushner, "On the Balance Between Silyle and Silylene Radicals in RF Glow Discharges in Silane: The Effect on Deposition Rates of $\alpha$-Si:H," J. Appl. Phys. 62, 2803 (1987)

M. J. Kushner, "A Phenomenological Model for the Surface Deposition Kinetics During Plasma and Sputter *Deposition of Amorphous* Silicon," J. Appl. Phys. 62, 4763, (1987)

M. J. Kushner, "A Model for the Discharge Kinetics and Plasma Chemistry During Plasma Enhanced Chemical Vapor Deposition of Amorphous Silicon", J. Appl. Phys. 63, 2532 (1988)

M. J. McCaughey and M. J. Kushner, "A Simulation of the Bulk and Surface Properties of Amorhous Hydrogenated Silicon Deposited From Silane Plasmas", submitted to J. Appl. Phys.

## Invited Conference Presentations with Proceedings

M. J. Kushner, "A Plasma Chemistry and Surface Model for the Deposition of $\alpha$-Si:H from RF Glow Discharges: A Study of Hydrogen Content," Plasma Proceedings, Symposia Proceedings, vol. 68, J. W. Coburn, R. A. Gottscho and D. W. Hess, Editors, Material Research Society, Pittsburgh, pp. 293-307, 1986.

M. J. Kushner and A. Garscadden "Important Considerations for Optimizing Production Rates in RF Discharge Chemistry", Gaseous Dielectrics V, Proceedings of the Fifth International Symposium on Gaseous Dielectrics, Knoxville, Tennessee 1987, L. G. Christophorou and D. W. Bouldin, eds. (Pergamon, New York, 1987), pp. 334-342.

## Contributed Conference Presentations with Abstracts Only

M. J. Kushner, "Radical Fluxes in $SiH_4/Si_2H_6$ RF Discharges of Various Compositions," 13th IEEE Conference on Plasma Science, Saskatoon, Saskatchewan, Canada, 1986.

M. J. Kushner, "Modeling Plasma and Surface Chemistry in Deposition Plasmas," Gordon Research Conference on the Chemistry of Electronic Materials, Concord, New Hampshire, 1986.

M. J. Kushner, "Reactions Leading to the Formation of Large Clusters in $SiH_4$/Ar RF Plasmas," 39th Gaseous Electronics Conference, Madison, WI, 1986.

M. J. Kushner, "Modeling of Plasma Enhanced Chemical Vapor Deposition", (INVITED SPEAKER), Westinghouse R&D Center, Pittsburgh, PA, 1987.

M. J. Kushner, "Modeling of Plasma Enhanced Chemical Vapor Deposition", (INVITED SPEAKER), Department of Nuclear Engineering and Applied Science, University of Wisconsin, 1987.

M. J. McCaughey and M. J. Kushner, "A Model for the Surface Morphology of a-Si:H Films", Fall Meeting of the Materials Research Society, Boston, MA, 1987.

M. J. Kushner, "A Computational Perspective of Plasma Enhanced Chemical Vapor Deposition", (INVITED SPEAKER), Department of Chemical Engineering Seminar Series, University of Illinois, 1988.

M. J. McCaughey and M. J. Kushner, "Modeling Growth of Thin Films of Amorphous Silicon", Winter Meeting of the Illinois Chapter of the American Vacuum Society, Urbana, Illinois, 1988.

M. J. Kushner and L. E. Kline, "A Review of the Modeling of Low Pressure Discharges for Plasma Chemistry and Plasma Processing", IEEE Conference on Plasma Science, Seattle, WA, 1988.

M. J. Kushner and L. E. Kline, "Models of Plasma Deposition and Etching", Gordon Conference on Plasma Chemistry, 1988.

M. J. McCaughey and M. J. Kushner, "The Plasma Surface Interface in PECVD of Amorphous Silicon", Gaseous Electronics Conference, Minneapolis, MN, 1988.

## Invited Colloquium Presentations

M. J. Kushner, "Modeling of Plasma Enhanced Chemical Vapor Deposition", Westinghouse R&D Center, Pittsburgh, PA, 1987.

M. J. Kushner, "Modeling of PECVD", ARCO Solar, Chatsworth, CA, 1987.

M. J. Kushner, "Modeling of Plasma Enhanced Chemical Vapor Deposition", Department of Nuclear Engineering and Applied Science, University of Wisconsin, 1987.

M. J. Kushner, "A Computational Perspective of Plasma Enhanced Chemical Vapor Deposition", Department of Chemical Engineering Seminar Series, University of Illinois, 1988.

## IV. Scientific Personnel and Degrees Earned

Principal Investigator: Mark J. Kushner

10/85 - 8/86
Spectra Technology, Inc
2755 Northup Way
Bellevue, WA 98004

8/86 - 6/88
University of Illinois
Department of Electrical and Computer Engineering
1406 W. Green Street
Urbana, Illinois 61801

Graduate Research Assist.: Michael J. McCaughey
Department of Electrical and Computer Engineering
1406 W. Green Street
Urbana, Illinois 61801

Advanced Degrees Earned: Michael J. McCaughey
MS in Electrical and Computer Engineering
Thesis Title: "A Three-Dimensional Monte Carlo Simulation for Growth of Amorphous Hydrogenated Silicon Thin Films"

V. Appendix: Reprints of Pertinent Publications

On the Balance Between Silylene and Silyl Radicals in RF Glow Discharges in Silane: The Effect on Deposition Rates of a-Si:H (M. J. Kushner, J. Appl. Phys. 62, 2803 (1987))

A Phenomenological Model for Surface Deposition Kinetics During Plasma and Sputter Deposition of Amorphous Hydrogenated Silicon (M. J. Kushner, J. Appl. Phys. 62, 4763 (1987))

A Model for the Discharge Kinetics and Plasma Chemistry During Plasma Enhanced Chemical Vapor Deposition of Amorphous Silicon (M. J. Kushner, J. Appl. Phys. 63, 2532 (1988))

Phase and Energy Distribution of Ions on Electrodes in Radio-Frequency Discharges (G. Hebner and M. J. Kushner, J. Appl. Phys. 62, 2256 (1987))

Important Considerations for Optimizing Production Rates in RF Discharge Chemistry (M. J. Kushner and A. Garscadden in L. G. Christophorou and D. Bouldin, Gaseous Dielectrics V (Pergammon, New York, 1987) pp. 334-341)

Simulation of the Bulk and Surface Properties of Amorphous Hydrogenated Silicon Deposited from Silane Plasmas (M. J. McCaughey and M. J. Kushner, submitted to J. Appl. Phys.)

# Phase and energy distribution of ions incident on electrodes in radio-frequency discharges

Gregory A. Hebner and Mark J. Kushner
*Gaseous Electronics Laboratory, Department of Electrical and Computer Engineering, University of Illinois at Urbana-Champaign, 607 East Healey, Champaign, Illinois 61820*

(Received 13 April 1987; accepted for publication 11 June 1987)

A Monte Carlo particle simulation and parametric models for the sheath voltage and thickness were used to calculate the arrival phase and energy of ions striking the electrodes in low-pressure capacitively coupled rf discharges. Ion phase and energy distributions are presented as a function of rf frequency, ion mass, rf voltage, dc bias, sheath thickness, and gas pressure. When the rf frequency is below the ion response frequency, the ions arrive at the electrode in phase with the applied rf voltage. As the rf frequency increases, the highest ion arrival probability shifts towards higher phase until, at sufficiently high frequencies, it is nearly uniform. The transition from a highly peaked ion phase distribution at low frequencies to a uniform distribution at high frequencies requires at least an order of magnitude change in rf frequency. The implication of these calculations on the electron energy distribution is discussed.

## I. INTRODUCTION

Low-pressure radio-frequency (rf) discharges are now commonly used for plasma processing of semiconductor materials.[1,2] In order to predict the characteristics of the plasma reactor and the materials produced, studies have been performed of the electron kinetics in such systems.[3-13] The results of theoretical[3-5] and experimental[6-12] investigations have indicated that the electron energy distribution is a function of space and time. In general, the majority or "bulk" of the electron energy distribution is composed of low-energy electrons with a small "tail" of high-energy electrons. The high-energy tail of the distribution results from secondary electrons produced by ion bombardment which are accelerated by the sheath potential, and from the acceleration of bulk electrons by the oscillating sheath boundary. Since a portion of the high-energy tail of the electron energy distribution is the result of ion bombardment, knowing the time and energy distributions of the ions striking the electrode is important to accurately describe the temporal and spatial behavior of the tail of the electron energy distribution. In this paper we report on a theoretical investigation of the time and energy dependence of ions bombarding the electrodes in a low-pressure rf discharge. Previous studies of ion bombardment of the electrodes in rf discharges have only examined the distribution of energies or angles of the ions that strike the electrode.[9-13] As a result, the main emphasis of this study is the investigation of the arrival time, or phase of the ions with respect to the applied rf voltage, and the energy distribution of the ions that strike the electrode after traversing the sheath.

The model is described in Sec. II, followed by a discussion of the results for frequency, ion mass, voltage, and sheath thickness in Sec. III. Concluding remarks are in Sec. IV.

## II. DESCRIPTION OF THE MODEL

The study was performed using a Monte Carlo simulation similar to that previously described.[13] Therefore, the model will only be discussed briefly. The voltage drop across the sheath and the sheath thickness are assumed to have the form

$$V(t) = \max(V_{dc} + V_{rf} \sin \omega_{rf} t, V_{min}) \quad (1)$$

and

$$l(t) = \max(X_{dc} + X_{rf} \sin \omega_{rf} t, X_{min}) , \quad (2)$$

where $V(t)$ is the time dependent voltage across the sheath, $l(t)$ is the sheath thickness, and $\omega_{rf}$ is the rf frequency. The subscripts on $V$ and $X$ denote to the time-independent (dc) and the time-dependent (rf) components of the applied voltage and sheath thickness, respectively. max $(a,b)$ indicates the maximum value of $a$ or $b$. As our concern is with electropositive plasmas where the plasma potential is always positive, the function max is used to guarantee a positive sheath potential. $V_{min}$ and $X_{min}$ as equal to 0.001. The spatial distribution of the electric field within the sheath is chosen to be linear and has the form

$$E(x,t) = E_0[l(t) - x] , \quad (3)$$

where

$$E_0 = 2[V(t)/l(t)] . \quad (4)$$

Using the above parametric models, the trajectories of the ions in the sheath are computed using standard Monte Carlo techniques.[14,15] The ions are injected into the simulation with a random velocity chosen from a Maxwellian distribution. Their initial spatial positions are greater than the maximum sheath thickness $(X_{dc} + X_{rf})$. As previously described,[13] elastic and charge exchange collisions are included in the simulation by specifying a mean free path $\lambda$, and randomly choosing a collision distance $l_c$, such that

$$l_c = -\lambda \ln(r) , \quad (5)$$

where $r$ is a random number on (0,1). When the ions strike the electrode, their energy and arrival time with respect to the applied rf voltage are recorded.

Simulations were performed in helium and argon for frequencies in the range of 0.1–40.0 MHz, rf voltages of 400–

 0021-8979/87/182256-05$02.40  

800 V, dc biases of 0–300 V, gas densities of $1.0\times10^{16}$–$5.0\times10^{16}$ cm$^{-3}$ and sheath thicknesses of 0.5–1.5 cm.

## III. RESULTS AND DISCUSSION

Unless noted otherwise, the discharge conditions for the simulation of helium and argon ions striking the electrodes were a peak rf voltage ($V_{rf}$) of 400 V, maximum sheath thickness ($X_{rf}$) of 0.5 cm, and gas density of $1.0\times10^{16}$ cm$^{-3}$. The dc bias ($V_{dc}$) and the time-independent sheath thickness ($X_{dc}$) were set to zero for the first cases discussed below. For the calculations in helium, an energy-independent charge exchange collision cross section of $1.5\times10^{-15}$ cm$^2$ and an elastic collision cross section of $1.0\times10^{-16}$ cm$^2$ were used. We found that the results were insensitive to the choice of the elastic collision cross section as long as $\sigma_{elastic} \ll \sigma_{charge\ exchange}$. The calculations with argon ions were performed with energy-independent charge exchange and elastic collision cross sections of $2.5\times10^{-15}$ cm$^2$. For both gases, the initial ion velocity was chosen to be close to the Bohm criterion for an electron temperature of 10 000 K. Trials showed that variation of the initial ion velocity had a very small effect on the final distributions. Good statistics were obtained with runs of 10 000 particles.

### A. rf frequency and ion mass

The dependence of the ion energy distribution and the arrival phase at the electrode of light and heavy ions is shown in Figs. 1–4. Figures 1 and 2 show the distribution of arrival times for He ions and Ar ions as a function of frequency and phase with respect to the rf cycle. A phase of 0–$\pi$ represents the cathodic part of the cycle, while a phase of $\pi$–$2\pi$ denotes the anodic part of the cycle. We define a parameter, the ion response frequency, $\omega_I = 1/\tau$, where $\tau$ is the time required for the ion to cross the sheath while being accelerated by the average sheath potential. The parameter $\omega_I$ for He and Ar ions are approximately 3.6 and 0.76 MHz, respectivly. For low rf frequencies, that is frequencies that are significantly below $\omega_I$, the ions "follow" the applied rf voltage with the majority of the ions arriving in phase with the voltage. The probability of ions arriving at the electrode during the anodic part of the cycle is small since the sheath region is swept free of ions during the cathodic part of the cycle. Ions must then diffuse into the sheath region from the plasma.

As the frequency increases, the phase of the highest ion arrival probability shifts towards higher phase since the ions no longer have sufficient time, during a single rf cycle, to be accelerated and traverse the sheath in phase with the voltage. At sufficiently high rf frequency, ions, due to their finite mass, can no longer respond to the time varying field but instead respond to a time-averaged field. As a result, the ions tend towards a uniform distribution. However, even at frequencies much higher than $\omega_I$, the ion distribution is not uniform but is skewed towards the cathodic portion of the

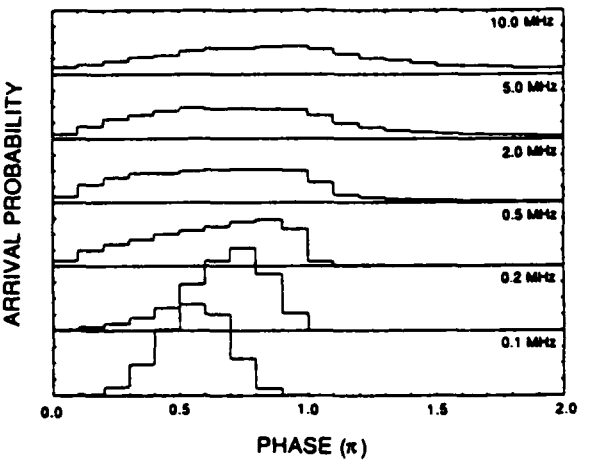


FIG. 2. Relative total arrival probability of Ar ions striking the electrodes as a function of phase and rf frequency for the conditions listed in Fig. 1.

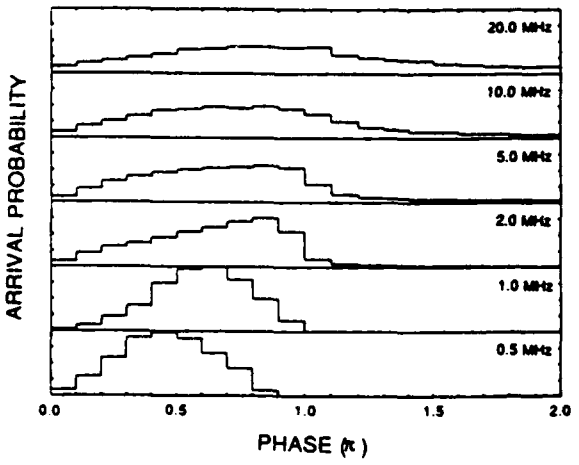


FIG. 1. Relative total arrival probability of He ions striking the electrodes as a function of phase and rf frequency for a peak rf voltage of 400 V, maximum sheath thickness of 0.5 cm, and a pressure of 0.3 Torr. A phase of 0 to $\pi$ represents the cathodic part of the cycle.

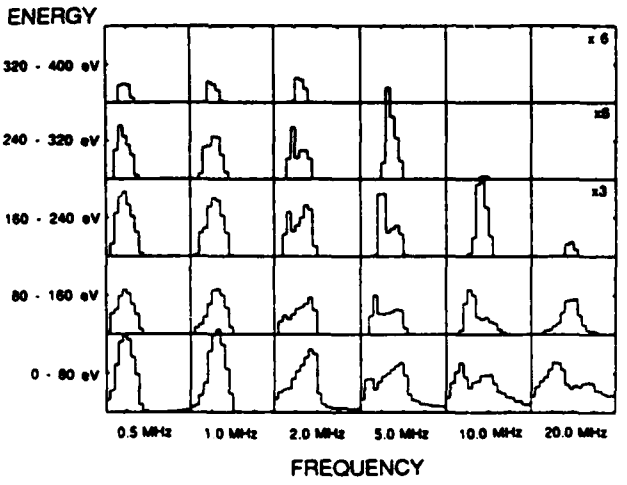


FIG. 3. Relative arrival probability of He ions striking the electrodes as a function of phase, energy range, and rf frequency for the conditions listed in Fig. 1. Within each small block the horizontal axis is phase from 0 to $2\pi$, while the vertical axis is relative arrival probability. The higher energy ranges have been multiplied by a display factor of 3 or 6.

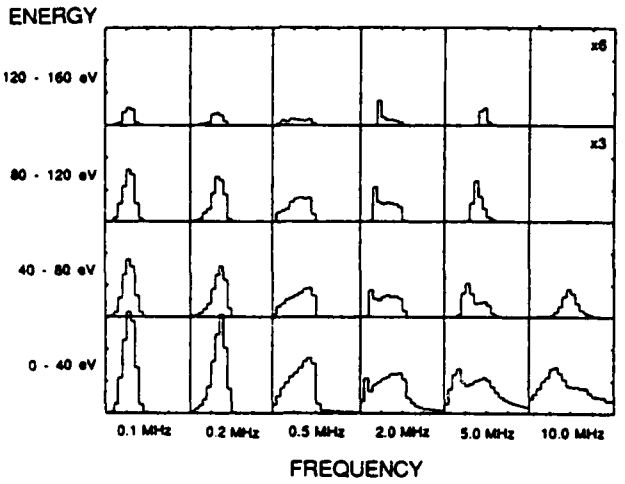


FIG. 4. Relative arrival probability of Ar ions striking the electrodes as a function of phase, energy range, and rf frequency for the conditions listed in Fig. 1. Within each small block the horizontal axis is phase from 0 to $2\pi$, while the vertical axis is relative arrival probability. The higher energy ranges have been multiplied by a display factor of 3 or 6.

cycle. The transition from a peaked behavior at low frequencies to a quasiuniform distribution at high frequencies does not happen rapidly, as illustrated in Fig. 5. The transition requires at least an order of magnitude in rf frequency.

As noted, the high-energy tail of the electron energy distribution is influenced by the ion bombardment of the electrode because of the production of secondary electrons which are then accelerated across the sheath potential. As the peak of the ion phase distribution moves towards higher phase, the production of high-energy secondary electrons will also move towards higher phase. Since the tail of the distribution is responsible for the optical excitation in the He rf discharge,[6] the optical emission from the discharge should show some shift with increasing frequency. This predicted phase shift of a portion of the high-energy tail of the electron energy distribution is suggested by recent experimental results using a high speed framing camera.[6] The time-dependent optical emission from a rf discharge has also been observed using an apertured photomultiplier tube (PMT) and an interference filter (Fig. 6). These results show that at low (0.4 MHz) frequencies, the optical emission peaks during the cathodic half cycle and is approximately in phase with the applied rf voltage. During the anodic half cycle the optical emission is small. At higher frequencies (2.5 MHz), the peak optical emission has moved towards higher phase. These results indicate that the arrival time of the ions on the electrode and the subsequent production of high-energy electrons is phase- and frequency-dependent and that this can have an influence on the discharge kinetics.

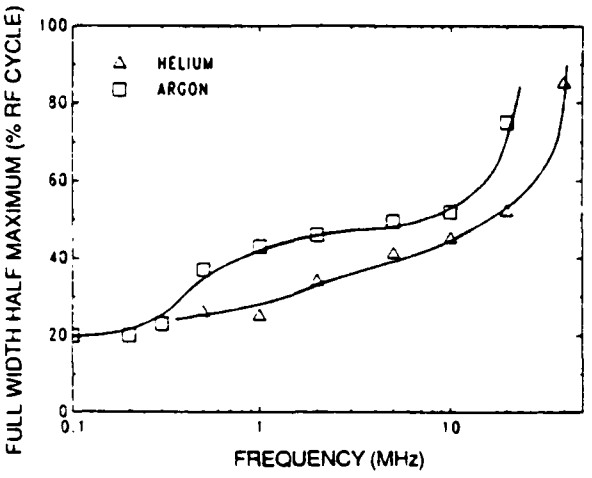


FIG. 5. Measured full width at half maximum of the relative total arrival probabilities shown in Figs. 1 and 2.

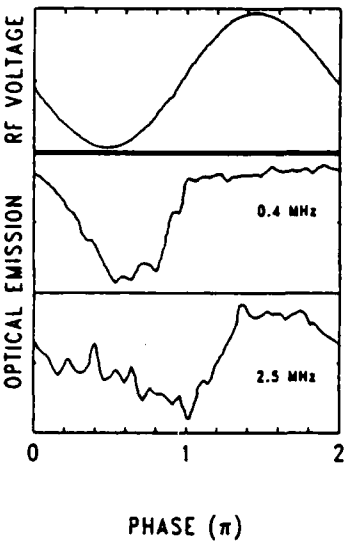


FIG. 6. Optical emission (5875 A, $\tau = 14$ ns) 1 cm below the rf driven electrode in a 0.5-Torr He rf discharge at two frequencies. The rf voltage on the driven electrode is as shown. The negative dc self bias was $\simeq 0$ V for 0.4 MHz and $\simeq 1/3$ the zero to peak voltage for 2.5 MHz. Increasing optical emission is plotted downward. The electrode seperation is 15 cm. The rf circuit is described in Ref. 6. At 0.4 MHz the optical emission peaks approximately in phase with the cathodic portion of the applied rf voltage. At 2.5 MHz, the peak emission is shifted to higher phase. The optical emission at 2.5 MHz is longer due to the negative dc self-bias.

As previously discussed, for low frequencies, the ions track the rf voltage. Those ions that arrive during the cathodic part of the cycle have a peak in the ion distribution at a phase of approximately $\pi/2$, independent of their energy bin. In addition, those ions which diffuse in from the plasma or are left outside the sheath region when the sheath retreats to the electrode are collected during the anodic part of the cycle with low energy, since the electric field is small. As the rf frequency increases, both the high- and low-energy ion distributions tend to shift toward higher phase. However, the higher energy ions shift towards $\pi$ and subsequently degrade to lower energy since the ions can no longer follow the field and acquire the maximum sheath potential. Those ions with high velocities during the anodic half cycle rapidly lose their energy through charge exchange collisions and populate the lower energy bins. A decrease in the peak ion energy above $\omega_i$ has been observed in chlorine rf discharges.[12] The ion distribution in the lowest energy bin tends to spread out and become more uniform over the entire rf cycle as a consequence of the ions now responding to a quasitime averaged sheath voltage. The end result is that the average ion energy

The energy distributions of the helium and argon ions striking the electrodes for the conditions of Fig. 1 are shown in Figs. 3 and 4. Each small plot in Figs. 3 and 4 represents a different energy range (stacked vertically) and rf frequency (horizontal). Within each small plot the horizontal axis is phase from 0–$2\pi$ and the vertical axis is the probability of an ion arriving at that phase within that energy range.

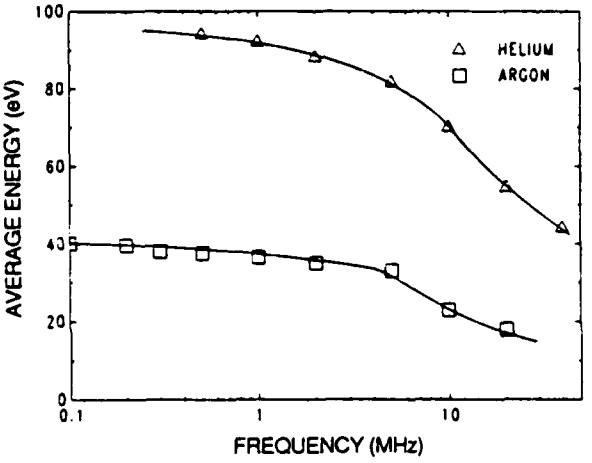


FIG. 7. Average ion energy as a function of rf frequency for He and Ar ions striking the electrodes. Conditions are as described in Fig. 1.

slowly decreases with increasing frequency until a frequency approximately equal to a few $\omega_i$ when the ions can no longer track the sheath field. At that point the average energy falls more rapidly (Fig. 7).

The effect of the ion mass (or $\omega_I$) can be observed by comparing Figs. 1 and 3 with Figs. 2 and 4. The frequency when the ions no longer follow the rf frequency is much lower in argon when compared to helium. In both gases the ion phase distributions follow the rf cycle at low frequency, with the most probable arrival time moving towards higher phase and spreading out with increasing rf frequency. However, while the frequencies where the average energy drops off and the ion phase distribution becomes more uniform in time are very different (Fig. 7), they nevertheless scale as $\omega_I$.

### B. rf voltage and dc bias

Increasing the rf voltage across the sheath from 400 to 800 V resulted in a linear increase of the average ion energy striking the electrode (Fig. 8). The probability distribution of ion arrival phase changed only slightly with increasing rf voltage. In general, there is a small increase in the height of the ion distribution peak (20%) at the expense of the ions that would normally arrive before the peak. In addition, the absolute position of the peak shifted slightly (less than $\pi/10$) towards the beginning of the cycle. Over this range of rf voltage, only the average energy appears to significantly differ. Thus, the linear relation between average energy and sheath voltage appears to be a valid and useful scaling law.

The effect of imposing a dc voltage and a dc sheath on the ion phase distribution and the average energy was also investigated. For these calculations, the dc voltage and sheath thickness were assumed to scale linearly with the rf voltage and sheath thickness. For example: with $V_{rf} = 400$ V and $X_{rf} = 0.5$ cm, if $V_{dc} = 200$ V, then $X_{dc} = 0.25$ cm. Using this assumption, the ion phase distributions were calculated for He ions, as shown in Fig. 9.

When the dc bias and dc sheath are increased, the ion distribution begins to take on the characteristics of both a rf system with its distinctly peaked behavior and a dc system, where the ion flux is constant in time. With larger bias, the peak becomes smaller and more ions are collected during what was the anodic part of the cycle. However, even though the distribution becomes more uniform with increasing dc bias, the average energy only increases by approximately 10%. This is likely a result of the competing processes of an increased sheath voltage raising the average energy while an increased sheath thickness decreases the average energy due to an increased probability for charge exchange collisions (to be discussed in Sec. III C). The same behavior was also observed for Ar ions.

### C. Sheath thickness and pressure

Increasing the rf sheath thickness and the pressure did not have a large effect on the ion phase distribution. With increasing sheath thickness (0.5–1.5 cm) and pressure ($1.0\times10^{16}$–$5.0\times10^{16}$ cm$^{-3}$), the peak height decreased by

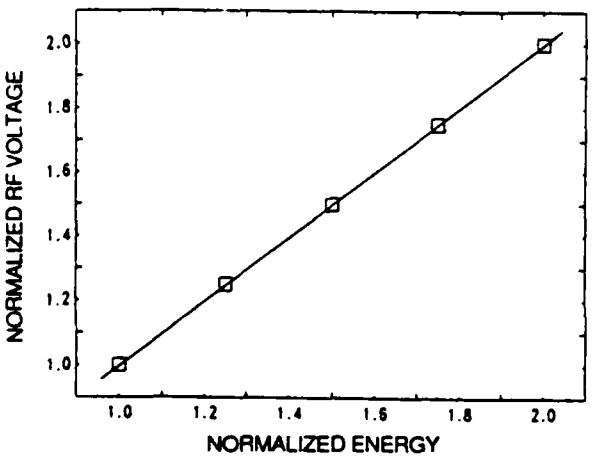


FIG. 8. Normalized He ion energy as a function of rf voltage normalized to 400 V. The ion energy is normalized to the 88.4 eV average energy obtained with a sheath potential of 400 V. The rf frequency is 2.0 MHz.

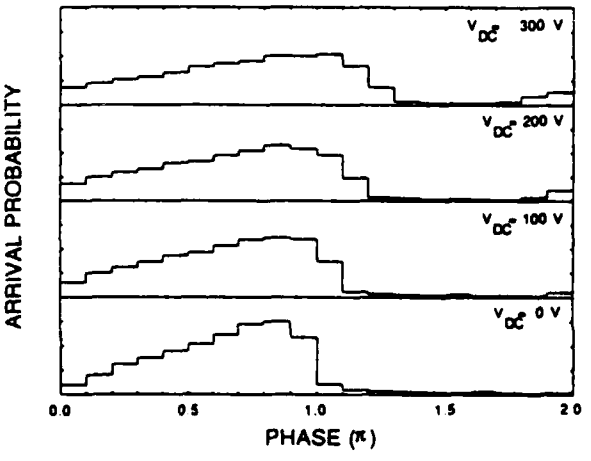


FIG. 9. Relative total arrival probability of He ions striking the electrode with an increasing dc bias and dc sheath thickness. The dc sheath thickness is assumed to increase linearly with increasing dc bias. The rf frequency is 2.0 MHz.

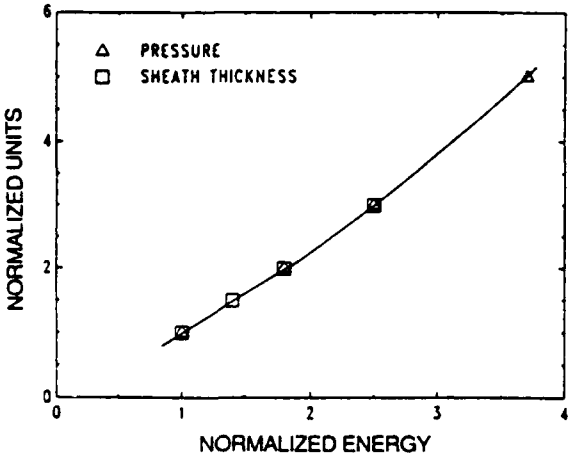


FIG. 10. Normalized He ion energy as a function of the reciprocal of the normalized pressure and sheath thickness. The ion energy is normalized to the 88.4 eV average ion energy in a 2.0 MHz discharge.

15% and 10%, respectively, with a resulting increase in the number of ions arriving before the peak of the distribution. In both cases the absolute position of the phase peak remained in approximately the same position. However, as stated previously, the average ion energy increased approximately linearly with respect to the reciprocal of the sheath thickness and pressure (Fig. 10). The high-energy tail dropped off quickly with increasing sheath thickness and pressure due to an increased number of charge exchange collisions.

## IV. CONCLUSIONS

Parametric models for the sheath voltage and thickness and a Monte Carlo particle simulation were used to compute the arrival phase and energy of ions striking the electrodes in low pressure rf discharges. When the rf frequency is below the ion response frequency, the ions arrive at the electrode in phase with the applied rf voltage. As the rf frequency increases, the phase of the highest ion arrival probability shifts towards higher phase and the ion energy decreases. The optical emission from the plasma was also observed to peak approximately in phase with the applied rf voltage at low frequencies. At higher frequencies, the peak optical emission moves to higher phase. The transition from a highly peaked ion distribution at low frequencies to a uniform distribution at higher frequencies required at least an order of magnitude change in rf frequency. Increasing the ion mass or decreasing $\omega_I$ decreased the ion energy and reduced the frequency at which the phase distribution tends towards uniform. Increasing the rf voltage linearly increased the average ion energy, while the sheath thickness and pressure are approximately linearly related to the reciprocal of the average energy. Imposing a dc bias on the electrode produced a superposition of a peaked (rf) distribution and a more uniform (dc) ion distribution with little change in average ion energy. Changing the rf voltage, sheath thickness and pressure had only a small effect on the shape of the ion phase distribution.

## ACKNOWLEDGMENTS

This work was partially supported by the Materials Science Division of the Army Research Office under the direction of Dr. Andrew Crowson, DAAG29-85-C-0031. One of us (G.A.H.) would like to acknowledge a research fellowship provided by the Army Advanced Construction Technology Center. The authors would like to thank Dr. Joseph Verdeyen for his comments.

[1]D. J. Flamm, V. M. Donnelly, and D. E. Ibbotson, J. Vac. Sci. Technol. B 1, 23 (1983).
[2]B. Chapman, *Glow Discharge Processes* (Wiley, New York, 1980).
[3]M. J. Kushner, J. Appl. Phys. 54, 4958 (1983).
[4]D. B. Graves and K. F. Jensen, IEEE Trans. Plasma Sci. PS-14, 78 (1986).
[5]A. Garscadden, Mater. Res. Soc. Symp. Proc. 68, 127 (1986).
[6]G. A. Hebner and J. T. Verdeyen, IEEE Trans. Plasma Sci. PS-14, 132 (1986).
[7]D. L. Flamm and V. M. Donnelly, J. Appl. Phys. 59, 1052 (1986).
[8]R. A. Gottscho, R. H. Burton, D. L. Flamm, V. M. Donnelly, and G. P. Davis, J. Appl. Phys. 55, 2707 (1984).
[9]B. F. Thompson, K. D. Allen, A. D. Richards, and H. H. Sawin, J. Appl. Phys. 59, 1890 (1986).
[10]K. Kohler, J. W. Coburn, D. E. Horne, E. Kay, and J. H. Keller, J. Appl. Phys. 57, 59 (1985).
[11]V. A. Godyak and A. S. Khanneh, IEEE Trans. Plasma Sci. PS-14, 112 (1986).
[12]V. M. Donnelly, D. L. Flamm, and R. H. Bruce, J. Appl. Phys. 58, 2135 (1985).
[13]M. J. Kushner, J. Appl. Phys. 58, 4024 (1985).
[14]S. L. Lin and J. N. Bardsley, J. Chem. Phys. 66, 435 (1977).
[15]J. Lucas, Int. J. Electron. 32, 393 (1972).

# A phenomenological model for surface deposition kinetics during plasma and sputter deposition of amorphous hydrogenated silicon

Mark J. Kushner
*University of Illinois, Department of Electrical and Computer Engineering, Gaseous Electronics Laboratory, 607 East Healey Street, Champaign, Illinois 61820*

(Received 1 July 1987; accepted for publication 1 September 1987)

The surface processes during the plasma-enhanced chemical vapor deposition and reactive sputter deposition of amorphous hydrogenated silicon (*a*-Si:H) are investigated by use of a phenomenological model. The model consists of an accounting, in rate equation form, of adsorption of radicals from the plasma onto the surface, surface diffusion, incorporation into the lattice, interconnection of bonds in the lattice, and burial of species on the surface, thereby constituting film growth. By accounting for the coordination partners of Si atoms in the film, the atomic fraction of hydrogen in the film is computed for the lattice and for hydrogen in polymeric or isolated configurations. Results from the model are discussed while parametrizing the probability for hydrogen elimination during incorporation and the probability for saturation of dangling bonds by gas phase species. We find that the mode of hydrogen elimination during incorporation distinguishes films grown dominantly from $SiH_2$ or $SiH_3$ radicals. Characteristics of films grown by sputter deposition are investigated as a function of the composition of the radical flux. We find that films grown from hydrogen-rich fluxes are composed dominantly of dihydride ($=Si<^{H}_{H}$) configurations, whereas hydrogen-lean mixtures are composed of dominantly hydride ($\equiv$Si–H) configurations.

## I. INTRODUCTION

Thin films of amorphous hydrogenated silicon (*a*-Si:H) are produced by a variety of means, including thermal chemical vapor deposition (CVD),[1] homogeneous chemical vapor deposition (HOMOCVD),[2] plasma-enhanced chemical vapor deposition (PECVD),[3] and reactive sputter deposition (RSD).[4] The films thus produced typically have atomic hydrogen fractions of 5%–20%, and thicknesses of $\simeq 0.5\,\mu$m for use in electronic devices and 10–15 $\mu$m for use as photoreceptor material.[5] Of the methods of fabrication listed above, the former two rely upon thermal pyrolysis of gaseous silane compounds (e.g., $SiH_4$, $Si_2H_6$) to generate the radicals from which the film is grown; the latter two methods generate the radicals by electron or ion impact processes. The purpose of this paper is to theoretically investigate the property of *a*-Si:H films produced by the latter two methods.

The apparatus typically used for PECVD is a parallel-plate capacitively coupled radio-frequency discharge sustained in mixtures of silane (or disilane), hydrogen, and noble gases at pressures $\lesssim$ 0.5 Torr.[6,7] The substrate temperature is typically 400–700 K. Silicon-containing radicals (e.g., $SiH_2$, $SiH_3$) are generated by electron impact dissociation of the feed stock at discharge power levels of tens to hundreds of mW cm$^{-3}$. The radicals then diffuse out of the plasma to the substrate where they are incorporated into the growing film. The apparatus typically used for RSD is functionally similar to that for PECVD, except that one of the electrodes (the target) is covered by a silicon plate, and the gas pressure is lower ($\ll$0.1 Torr).[8] Noble gas ions from the discharge impact into the target, thereby sputtering Si atoms, which then drift to, and deposit on, the substrate, typically the opposite electrode. By flowing controlled amounts of hydrogen through the sputter chamber, the fraction of hydrogen incorporated into the film can be controlled.[5] Additional control of the amount of incorporated hydrogen in the film is obtained in both methods by regulating the substrate temperature; the higher the substrate temperature, the lower the hydrogen fraction.

The processes through which radicals generated by the plasma during PECVD and RSD are adsorbed onto the surface and incorporated into the film are complex, and the study of those processes are current topics of research.[2,5,9–15] The processes can be divided into the following general categories: adsorption, incorporation, hydrogen elimination, interconnection, etching, sputtering, and burial. Adsorption is the process whereby radicals from the plasma stick to the surface and become available for bonding to the film. Incorporation is the process whereby a radical on the surface covalently bonds to another silicon atom in the film. We call this bonding to the lattice, although the use of the term lattice does not claim any long-term order. Incorporation can be direct, in which a radical attaches to the lattice at the site of a dangling bond; or indirect, in which the radical displaces hydrogen from saturated bonds (i.e., Si–H), thereby eliminating hydrogen from the surface. Etching is the process whereby radicals remove atoms from the lattice or remove adsorbed species by colliding and bonding to those species but not sticking on the surface. Sputtering is the analogous process performed by energetic ions colliding with the surface. Burial is the process during which interconnection and incorporation cover over atoms previously on the surface and exposed to the plasma, and confine them to the lattice.

The fraction of hydrogen in *a*-Si:H films, 5%–20%, is small compared to the ratio of hydrogen to silicon atoms in the flux of radicals which adsorb or collide with the growing film. The manner in which the excess hydrogen is eliminated

 0021-8979/87/244763-10$02.40  

is therefore an important consideration. Heuristic models for growth of *a*-Si:H films by PECVD have been suggested by Kampas,[9] Scott, Reimer, and Longeway,[11] Longeway,[14] Gallagher,[15] and others. These models differ qualitatively in the manner in which hydrogen is eliminated from the film. Kampas[9] suggests that cross linking between adjacent Si–H bonds on the surface resulting in elimination and desorption of $H_2$ is the dominant mechanism. Scott[11] also suggests that hydrogen atoms are removed from Si–H bonds on the surface via etching reactions by radicals from the plasma. Another suggested method is that radicals (e.g., $SiH_3$) bond to the lattice as activated silyl groups, which spontaneously eliminate $H_2$ as a method of relaxation. Gleason *et al.*[16] have recently published a Monto Carlo simulation for thin-film growth of *a*-Si:H. In their model the initiating step (called the addition reaction) proceeds by incorporation of $SiH_4$ directly into the film with the simultaneous elimination of $H_2$. This step resembles heterogeneous pyrolysis, and therefore the model is most directly applicable to CVD (as opposed to PECVD). In their model, though, hydrogen is eliminated from the film by cross linking between adjacent ≡Si–H bonds, in a manner similar to that suggested by Kampas.[9]

In this paper a phenomenological model for the surface deposition kinetics during PECVD and RSD of *a*-Si:H is presented, and results from the model are discussed for a variety of plasma conditions. The model consists of a set of rate equations describing the major processes of adsorption, surface diffusion, incorporation, interconnection, hydrogen elimination, and burial. From the results of the model, one obtains the fraction of hydrogen in the film, and the distribution of hydride (≡Si–H) and dihydride ($=Si\lesssim^{H}_{H}$) bonds in the film. The model is described in Sec. II after which rate constants used in the model are discussed in Sec. III. Results from the model are presented in Sec. IV in the subtopics of hydrogen elimination during incorporation, the burial effect, saturation and etching, temperature effects, reactive sputter deposition, and deposition in the absence of $SiH_3$ insertion. Concluding remarks are in Sec. V.

## II. DESCRIPTION OF THE MODEL

A model for gas phase chemical kinetics can be formulated by defining a set of species and rates, and expressing them as a set of rate equations. The rate equations have the general form

$$\frac{dN_i}{dt} = \sum_{l,m} N_l N_m k^i_{lm} - N_i \sum_{l,m} N_l k^m_{il}, \qquad (1)$$

where $k^i_{lm}$ is the rate constant for formation of species $N_i$ by collisions between species $N_l$ and $N_m$. The terms on the right-hand side of Eq. (1) simply represent the sources and sinks for species $N_i$. The surface deposition model (SDM) described in this paper consists of a set of rate equations similar to that which one would write for gas phase chemistry. There are six classes of species in the model. Allowing $X$ to denote some specific species, the six classes are the following: $X(F)$, the flux of radicals incident onto the surface; $X(A)$, adsorbed nonmobile radicals; $X(M)$, adsorbed mobile radicals; $X(G)$, desorbed gas phase molecules; $X(L)$, a silicon atom bounded to the lattice in the film but residing on the surface; and $X(B)$, a silicon atom bonded to the lattice in the film and buried beneath the surface.

The individual species in each class described above are listed in Table I. The species $X(L)$ and $X(B)$ represent silicon atoms on and below the surface. The relative densities of species in class $X(B)$ contain the information from which the fractions of hydrogen and silicon in the film are obtained and the types of bonds in the film are calculated. This information is obtained by tagging the silicon atoms $X(L)$ and $X(B)$ with their coordination partners. For example, SSSH($B$) represents a silicon atom that is part of the lattice and buried beneath the surface. It is bonded to three other silicon atoms (SSS) and a hydrogen atom (H). SSHD($L$) represents a silicon atom on the surface bonded to two silicon atoms (SS), one hydrogen atom (H) and having one dangling bond (D). The atomic fractions of hydrogen and silicon in the film are obtained by summing the silicon and hydrogen bonds of the buried silicon atoms and taking the appropriate ratios.

The following conceptual sequence of events is simulated by the SDM. Radicals are generated in the gas phase by electron impact and molecular reactions, and diffuse towards the surface. The composition of the radical flux is either specified as part of a parametric study or obtained from the results of a companion plasma chemistry model for rf discharges in silane gas mixtures.[17] The radicals then adsorb on the surface as mobile adsorbates [$X(M)$], or etch or saturate the surface (see below). As energetically allowed, sputtering by ions directed towards the surface may also occur. Adsorbed mobile radicals diffuse on the surface. These radicals thermally desorb from an immobile state and readsorb to the immobile state desorbing many times before colliding with a bonding site in the lattice on the surface [e.g., SSSD($L$)]. At that time it is incorporated into the lattice, and hydrogen may be eliminated from the surface in the manner described below. Mobile radicals which collide and react with other mobile radicals may desorb from the surface as saturated molecules [e.g., $SiH_3(M) + SiH_3(M) \rightarrow Si_2H_6(G)$]. Heterogeneous production of saturated molecules in this fashion is believed to be an important contribution to the density of gas phase species.[10,15] Once a member of the lattice, further reactions, such as interconnection, may take place between adjacent silicon atoms. The silicon atoms on the surface are gradually buried [i.e., SSSH($L$) → SSSH($B$)] at a rate determined by the magnitude of the

TABLE I. Species included in the surface deposition model.

| Surface and lattice species [$X(L)$, $X(B)$] | Radical flux, adsorbed, and buried isolated species [$X(F)$, $X(M)$, $X(A)$, $X(B)$] |
|---|---|
| SSSS | H Si SiH $SiH_2$ $SiH_3$ |
| SSSD SSSH | $Si_2H_2$ $Si_2H_3$ $Si_2H_4$ $Si_2H_5$ |
| SSDD SSHD SSHH | |
| SDDD SHDD SHHD SHHH | |
| Saturated gas phase species [$X(G)$] | |
| $H_2$ $SiH_4$ $Si_2H_6$ | |

flux of radicals incident onto the surface and by the requirement that the total density of surface species remains a constant. Burial is distinct from interconnection. Radicals on the surface may interconnect; however, they are not buried beneath the surface unless there is a flux of radicals to cover them.

There are two types of surface sites. The first site is the location at which a silicon atom bonds to the lattice; the second site is a location at which a radical is immobily adsorbed. The density of bonding sites, $\rho_0$ is $a^{-2}$, where $a$ is the average bond length, taken to be 2.75 Å. The density of adsorption sites was assumed to be $0.5\rho_0$. The distinction between mobile and immobile adsorbed radicals is that mobile radicals are free to diffuse along the surface. Immobile adsorbed radicals are confined to their adsorptions sites, but they may thermally desorb and become mobile. Mobile and immobile adsorbed radicals were invoked to account for the observation that hydrogen in $a$-Si:H films produced by PECVD is contained in both the lattice and in isolated polymeric configurations, $(SiH_2)_n$.[7,12] We attribute the isolated configurations to clusters of adsorbed $SiH_n$ molecules which the film has grown over and buried, but which are not incorporated (i.e., bonded) to the lattice.

Rate equations were formulated for the processes described above using the coordination partner notation to account for bond densities. For example, the interconnection of dangling bonds of two adjacent silicon atoms on the surface is represented schematically as

$$\mathrm{SSHD}(L) + \mathrm{SSSD}(L) \rightarrow \mathrm{SSSH}(L) + \mathrm{SSSS}(L). \quad (2)$$

The contribution of this process to the rate equations is simply $[\mathrm{SSHD}(L)][\mathrm{SSSD}(L)]k$, where $[X]$ is the surface density of the species and $k$ is the reaction rate constant. A set of sample reactions appear in Table II. All energetically allowed combinations of reactants from Table I for the sample reactions were included in the model.

## III. REACTION RATE CONSTANTS

Reaction rate constants are required for all the processes described above; adsorption, desorption, surface diffusion, lattice building, interconnection, and burial. Although some of these rates are known for crystalline silicon, such as the adsorption probability,[18] they are generally not known for amorphous silicon, particularly when dangling bonds on the surface may be passivated by hydrogen. Therefore, the rate constants must be estimated in an internally consistent fashion, as described below.

### A. Adsorption, passivation, and etching

This category of reactions includes processes involving the flux of radicals or molecules from the plasma. These reactions are represented schematically, or by example, by

$$X(F) \rightarrow X(M) \quad \text{(adsorption)}, \quad (3)$$

$$X\mathrm{H}(F) + \mathrm{SSSD}(L) \rightarrow \mathrm{SSSH}(L) + X(F) \quad \text{(passivation)}, \quad (4)$$

$$X(F) + \mathrm{SSSH}(L) \rightarrow \mathrm{SSSD}(L) + X\mathrm{H}(F) \quad \text{(etching)}. \quad (5)$$

Since the values of $X(F)$ in the SDM are specified parameters and are nearly independent of the surface processes (see below), their densities are constants in the expressions above. The time rate of change of the density of a surface species, $X(L)$, expressed as $\mathrm{cm}^{-2}\,\mathrm{s}^{-1}$, for process $j$ involving $X(F)$ is therefore $[X(F)]p_j[X(L)]/\rho_0$, where $p_j$ is the probability of the process and $[X(L)]/\rho_0$ is the fractional surface coverage of the reactant surface species. For adsorption, the fractional surface coverage is set to unity so that the rate of adsorption depends only on the probability $p_j$. We treat $p_j$ as a parameter in the model.

### B. Mobile and immobile adsorbed radicals

Mobile radicals $X(M)$ are immobilized by "colliding" with an active adsorption site. Since the adsorption site can be considered equivalent to a lattice site, the rate of immobile adsorption is as given in the next section. The rate of desorption for $X(A) \rightarrow X(M)$ is $\nu_d e^{-(\Delta\epsilon_a/kT_s)}$, where $\nu_d$ is the desorption frequency, $T_s$ is the substrate temperature, and $\Delta\epsilon_a$ is the adsorption energy. By parametrizing the results of the model for the hydrogen fraction in isolated configurations as a function of surface temperature (see below), and comparing to experiment,[7] we estimated that $\nu_d = 10^5\,\mathrm{s}^{-1}$ and $\Delta\epsilon_a = 0.2$ eV.

TABLE II. Examplary reactions included in the model (see text for rates).[a]

| | |
|---|---|
| $SiH_2(F) \rightarrow SiH_2(M)$ | Adsorption to mobile state |
| $SiH_2(M) \rightleftharpoons SiH_2(A)$ | Mobile adsorption⇌Immobile desorption |
| $SiH_2(F) + \mathrm{SSSH}(L) \rightarrow SiH_1(F) + \mathrm{SSSD}(L)$ | Etching |
| $M^*(F) + \mathrm{SSSH}(L) \rightarrow M(F) + \mathrm{SSSD}(L) + \mathrm{H}(G)$ | Sputtering[b] |
| $SiH_1(F) + \mathrm{SSSD}(L) \rightarrow SiH_2(F) + \mathrm{SSSH}(L)$ | Saturation |
| $SiH_1(M) + SiH_1(M) \rightarrow Si_2H_n(G)$ | Surface clustering and desorption |
| $SiH_2(M) + \mathrm{SSSD}(L) \rightarrow \mathrm{SSSS}(L) + \mathrm{SSHH}(L)$ | Incorporation |
| $SiH_1(M) + \mathrm{SSSH}(L) \rightarrow \mathrm{SSSS}(L) + \mathrm{SHHD}(L) + H_2(G)$ | Incorporation with $H_2$ elimination |
| $\mathrm{SSSD}(L) + \mathrm{SSSD}(L) \rightarrow \mathrm{SSSS}(L) + \mathrm{SSSS}(L)$ | Interconnection |
| $\mathrm{SSSH}(L) + \mathrm{SSSH}(L) \rightarrow \mathrm{SSSS}(L) + \mathrm{SSSS}(L) + H_2(G)$ | Interconnection with $H_2$ elimination |
| $\mathrm{SSSH}(L) \rightarrow \mathrm{SSSH}(B)$ | Burial (lattice species) |
| $SiH_2(A) \rightarrow SiH_2(B)$ | Burial (isolated configurations) |

[a] All allowed permutations of exemplary reactions for the species listed in Table I are included in the model.
[b] $M^*$ denotes any energetic ion incident onto the surface.

### C. Surface clustering, lattice building, and interconnection

The reactions in this category have the general or examplary form of

$$X(M) + Y(M) \rightarrow XY(M) \quad \text{(surface clustering)}, \quad (6)$$

$$X(M) + Y(L) \rightarrow XY(L) \quad \text{(lattice building)}, \quad (7)$$

$$\text{SSSD}(L) + \text{SSHD}(L) \rightarrow \text{SSSS}(L) + \text{SSSH}(L) \quad \text{(interconnection)}. \quad (8)$$

The time rate of change of a surface species resulting from process $j$ in this category is $[X][Y]k_j p_j e^{-(\Delta\epsilon_j/kT_s)}$, where $[X]$ and $[Y]$ are the densities of the reactants ($\text{cm}^{-2}$), $k_j$ is the rate constant ($\text{cm}^2\,\text{s}^{-1}$), $\Delta\epsilon_j$ is an activation energy, and $p_j$ is a relative probability of the process. For processes involving reactants that are both lattice species, $p_j = 1$. For processing where one of the reactions is a mobile species, and therefore diffusing on the surface, $p_j = \{(T_s/500\,K) \times [M/(2\mu)]\}^{1/2}$, where $M$ is the molecular weight of $SiH_3(M)$ and $\mu$ is the reduced mass of the reactants. This scaling parameter merely accounts for lighter adsorbates having a higher thermal velocity and therefore a higher probability for reaction per unit time. Unless otherwise noted, for reactions between adsorbed species, or adsorbed species and the lattice, $k_j$ ($T_s = 500$ K) $= 1.5\times10^{-12}\,\text{cm}^2\,\text{s}^{-1}$ and $\Delta\epsilon = 0$ (see below). For interconnection reactions between saturated lattice species [i.e., SSSH($L$)], $k_j = 3.0\times10^{-8}\,\text{cm}^2\,\text{s}^{-1}$, and $\Delta\epsilon$ is either 1.5 or 10 kcal/mol (see below).

For unity coverage of reactants, the reaction frequency is approximately $2000\,\text{s}^{-1}$. The average time a radical is immobily adsorbed ($T_s = 500$ K) is 0.75 ms. Therefore, radicals spend little time in the mobile state, but rather move from immobile site to immobile site or to an incorporation site. The results of the model are relatively insensitive to the choice of $k_j$ provided that the reaction frequency is comparable to or larger than the desorption frequency. The values for rate constants were obtained by parametrically comparing the results of this model to the experimental results of Ross and Jaklik.[7] The values derived are not unique and are merely intended to represent general reaction probabilities.

The activation energies $\Delta\epsilon$ were estimated for each reaction by assigning bond energies and computing the change in total energy going from reactants to products. Exothermic reactions were assigned zero activation energies; endothermic reactions were assigned an activation energy equal to the endothermicity. The bond energies for surface configurations were estimated from the work of Ho *et al.*[19] who calculated a correction factor for Si–Si and Si–H bond energies in higher silane molecules. In general, all clustering, insertion, and lattice building reactions involving species having dangling bonds are exothermic to the degree of approximation of this method. The endothermic reactions have energies on the order of a few to 10 kcal/mol. These reactions are primarily lattice interconnection with molecular hydrogen elimination. The activation energy associated with these reactions is responsible, in part, for the observed reduction in the $f_H$ with increasing substrate temperature.[7,11,20,21] We assigned an activation energy of 1.5 kcal/mol for interconnection reactions involving the lattice species SSSH($L$); and 10 kcal/mol for reactions involving SSHH($L$) and SHHH($L$). This difference in activation energies will be discussed in Sec. IV D.

The rate of interconnection between dangling bonds [e.g., SSSD($L$) + SSSD($L$) → SSSS($L$) + SSSS($L$)] is calculated during execution of the model. The instantaneous rate is chosen so that upon burial, the fractional density of dangling bonds is $< 1\%$. The rate so derived varies from case to case, but is generally close to $2\text{–}5\times10^{-12}\,\text{cm}^2\,\text{s}^{-1}$. Although the spin density in $a$-Si:H is usually much less than 0.01, we found that requiring a smaller density than this *upon burial*, that is, having a higher rate of interconnection, resulted in unphysically small hydrogen fractions. The implication of this observation is that interconnection between dangling bonds continues in the film after burial.[11]

### C. Burial

Burial is the process whereby species residing on the surface are incorporated into the film. For lattice species, this is schematically shown, for example, as

$$\text{SSSH}(L) \rightarrow \text{SSSH}(B). \quad (9)$$

The rate of burial for surface specie $X_j(L)$ is $(X_j(L)/\rho_0) \times (\rho_L - \rho_0)/\tau$ for $\rho_L > \rho_0$, and zero otherwise, where $\rho_L = \Sigma_j X_j(L)$ is the sum of all lattice species and $\tau$ is the burial equilibration time. This rate "clamps" the density of surface lattice species at $\rho_0$. The model is not sensitive to the choice of $\tau$ as long as $\tau \ll \rho_0/[\Sigma_j n_j X_j(F)]$, where $X_j(F)$ is the net flux of radical specie $j$ that sticks on the surface and $n_j$ is the number of silicon atoms contained in the radical. For very high deposition rates ($> 1000$ Å/min) the limiting value for $\tau$ is $\approx 150$ ms; therefore, we used $\tau = 10$ ms for all cases.

### D. Initial conditions

The initial conditions used for the model are that the surface is covered with dangling bonds [i.e., SSSD($L$)] having density $\rho_0$, and unoccupied adsorption sites having density $0.5\rho_0$. The fluxes are turned on and the rate equations are integrated until steady-state conditions are reached. We found that for constant fluxes, final surface conditions were obtained in 1–3 s of real time, corresponding to only 5–10 "monolayers" of film, and that the hydrogen content decreased to its steady-state value. These observations agree well with the results of Gleason *et al.*,[16] who calculated that steady-state conditions are obtained after depositing a similar number of monolayers, and hydrogen content decreases towards its steady-state value. We have also started with a prepared surface [e.g., a partial covering of SSSH($L$)]; and found little or no change in the steady-state results when compared to starting with a fresh surface.

## IV. RESULTS

In the plasmas of interest, the dominant radicals are thought to be $SiH_2$ and $SiH_3$.[22,23] The ratio of hydrogen atoms to silicon atoms in silicon-containing radicals incident onto the surface, $[H]/[Si] = F_H$, is therefore approximately 2–3. The electron impact dissociation of saturated silanes which generated the radicals also generate a nearly equal

density of atomic hydrogen. The flux of hydrogen atoms incident onto the surface is therefore larger (6–8) than the value given by the silicon-containing radicals alone. Additional hydrogen is deposited on the surface by hydrogen-containing molecules from the gas phase which saturate dangling bonds, as discussed below. The fraction of hydrogen incorporated into the film, $f_H$, though, is usually $<0.20$. Therefore, hydrogen must be eliminated from the surface some time between the processes of adsorption and burial; or once buried, hydrogen must be eliminated from the lattice. In this work we examine the former process. We assumed that hydrogen, once buried beneath the surface, is permanently part of the film.

In the results discussed below, we either specify the radical flux as part of a parametric survey or use the flux computed with the plasma chemistry model. By specifying a flux, we ignore the effect of surface chemistry on the radical flux. Since the majority of the desorbed products of the surface chemistry are saturated molecules, this effect is small.

### A. Hydrogen elimination during incorporation

When adsorbed molecules are incorporated into the lattice, they attach to either dangling bonds [e.g., SSSD($L$)] or insert into saturated bonds [e.g., SSSH($L$)]. Any adsorbed radical may incorporate directly into a site occupied by a dangling [e.g., $SiH_3(M) + SSSD(L) \rightarrow SSSS(L) + SHHH(L)$]. Incorporation by insertion into a saturated bond, though, may necessarily require elimination of hydrogen. For purposes of identification, we label the adsorbed radical by its ratio of hydrogen to silicon atoms, $F_H = [H]/[Si]$. For $F_H < 2$, adsorbed radicals may insert directly into saturated SSSH($L$) bonds without eliminating hydrogen; for example,

$$SiH_2(M) + SSSH(L) \rightarrow SHHH(L) + SSSS(L). \quad (10)$$

For adsorbed radicals having $F_H > 2$, the insertion reaction requires elimination or displacement of hydrogen. Elimination may proceed by displacing atomic or molecular hydrogen. This method of incorporation of radicals having $F_H > 2$ is the analogy of the gas phase reaction $SiH_3 + SiH_4 \rightarrow Si_2H_5 + H_2$ which, at typical substrate temperatures, proceeds with a rate constant of $\approx 10^{-13}$ cm$^3$ s$^{-1}$.[24] If radicals having a single dangling bond [e.g., $SiH_3(M)$] are unable to insert into a saturated surface site [e.g., SSSH($L$)], then incorporation can only proceed by generating dangling bonds on the surface by sputtering or etching mechanisms.[15] In this section we investigate surface deposition while allowing insertion of $SiH_3(M)$ into saturated surface sites. In Sec. V F we examine some of the consequences of requiring a dangling bond for incorporation of $SiH_3(M)$ into the lattice.

For the incorporation of $SiH_3(M)$ while allowing insertion into saturated surface sites, we may have either of[9,15]

$$SiH_3(M) + SSSH(L) \rightarrow SHHD(L) + SSSS(L) + H_2(G) \quad (11)$$

$$\rightarrow SHHH(L) + SSSS(L) + H(G). \quad (12)$$

The former reaction is thermodynamically favored. If it is more likely to occur, the elimination of molecular hydrogen during incorporation of $SiH_3(M)$ into films grown from plasmas whose predominant radical is $SiH_3(F)$ may result in less hydrogen remaining on the surface than incorporation of $SiH_2(M)$, a radical having a smaller value of $F_H$.

Before examining the results of the model for actual discharge conditions, it is instructive to examine the characteristics of $a$-Si:H films grown from specific fluxes of radicals. We will examine the fraction of incorporated hydrogen, $f_H$, as a function of the hydrogen-to-silicon ratio $F_H$ of the individual radicals incident on to the surface. This is accomplished by specifying that the radical flux is composed of only a single specie having a given $F_H$. These results are shown in Fig. 1 where $f_H$ is plotted as a function of $F_H$ while allowing adsorbed radicals with a single dangling bond to insert into a saturated surface site. The flux of silicon atoms incident on the surface was kept constant at $2 \times 10^{15}$/cm$^2$ s, typical of moderately power discharges of tens to 100 mW/cm$^3$ sustained in a few hundred mTorr of $SiH_4$ and corresponding to a deposition rate of $a$-Si:H of $\approx 250$ Å/min. As expected, $f_H$ increases with increasing $F_H$, but only to a ratio of $F_H \approx 2$ (as shown by the triangles in the figure), after which $f_H$ decreases. This trend is a result of having $H_2$ (as opposed to H) being eliminated during incorporation of adsorbed radicals, that is, using the insertion step shown in Eq. (11) as opposed to that shown in Eq. (12). If we instead specify that H atoms are eliminated during incorporation (dashed line in Fig. 1), $f_H$ differs little from the cases for elimination of $H_2$ for $F_H < 2$, but is larger than the previous cases for $F_H > 2$. For these conditions, $f_H$ is equally determined by hydrogen elimination during interconnection of adjacent Si–H($L$) bonds after incorporation, and hydrogen elimination during incorporation. The latter process can have a significant effect on $f_H$ for plasmas dominated by radicals having $F_H > 2$.

The sensitivity of $f_H$ on the mode of hydrogen elimination during incorporation is further illustrated in Fig. 2 where $f_H$ is plotted for films grown from $SiH_2(F)$ and $SiH_3(F)$ as a function of the probability of eliminating $H_2$.

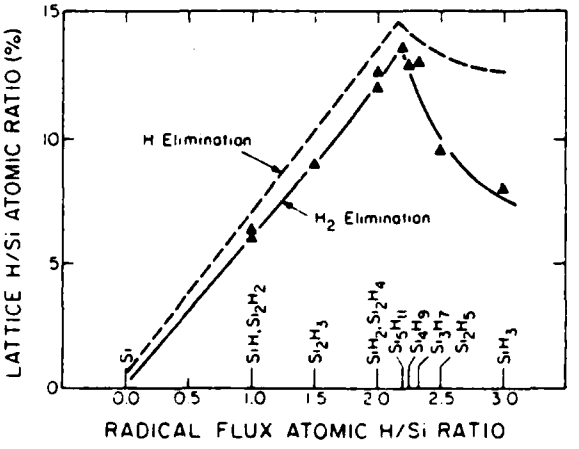


FIG. 1. Atomic fraction of hydrogen in $a$-Si:H films, $f_H$, as computed with the surface deposition model as a function of the H/Si ratio of individual radicals incident onto the surface. For these results, adsorbed radicals having a single dangling bond may insert into saturated surface sites. The triangles are for $H_2$ elimination during incorporation; the dashed line is for H atom elimination during incorporation.

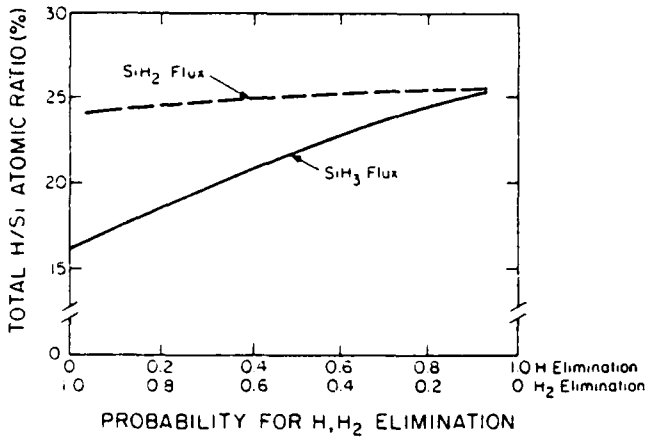


FIG. 2. Total hydrogen fraction (lattice and isolated) as a function of the probability of eliminating $H_2$ or H for incident fluxes of $SiH_2(F)$ and $SiH_3(F)$. A high probability for eliminating $H_2$ distinguishes between *a*-Si:H films grown from $SiH_2(F)$ and $SiH_3(F)$ when $SiH_3(M)$ insert into saturated surface sites.

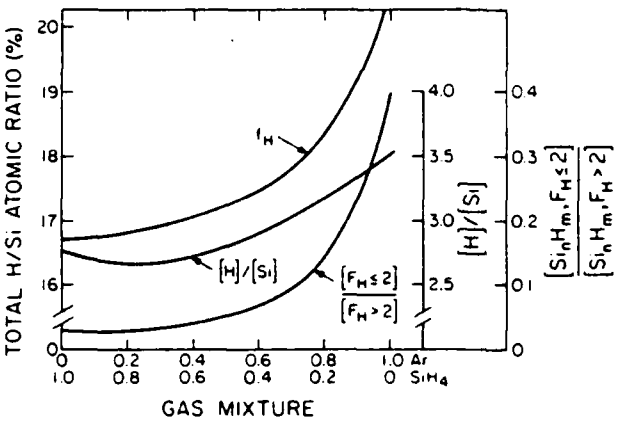


FIG. 3. Computed hydrogen fraction $f_H$ and H/Si ratios in the incident flux as a function of gas mixture. [H]/[Si] is the ratio of all hydrogen atoms to silicon atoms incident onto the surface; $[Si_nH_m, F_H \leq 2]/[Si_nH_m, F_H > 2]$ is the ratio of radicals that have $F_H = H/Si \leq 2$ and $F_H > 2$.

The value of $f_H$ for films grown from $SiH_2(F)$ is relatively insensitive to this probability, and when H atoms are eliminated there is little distinction between films grown from $SiH_2(F)$ and $SiH_3(F)$. As the probability of $H_2$ elimination increases, though, $f_H$ decreases for films grown from $SiH_3(F)$.

Computed atomic hydrogen fractions in *a*-Si:H films for films grown in $Ar/SiH_4$ rf discharges are shown in Fig. 3. The discharge conditions were simulated with the plasma chemistry model described in Ref. 17. The plasma conditions for these examples are as follows: gas pressure, 0.5 Torr; substrate temperature, 500 K; and power deposition, $\approx 25$ mW cm$^{-3}$. Cases are shown for varying the fraction of $SiH_4$ in Ar. To eliminate the burial effect (see next section) the power for each case was varied to obtain the same deposition rate. Since the total atomic hydrogen fraction increases with decreasing fraction of $SiH_4$ while the deposition rate is constant, the change in $f_H$ is a result of a change in the composition of the radical flux. Also plotted in Fig. 3 are the ratios of the total flux of H atoms to Si atoms incident on the surface, $[H/(F)]/[Si/(F)]$; and the ratio of radicals which have $F_H \leq 2$ to those having $F_H > 2$, $[Si_mH_n, n/m \leq 2]/[Si_mH_n, n/m > 2]$. Both ratios increase with decreasing fraction of silane. This trend is a consequence of silane radicals and hydrogen atoms, once generated by electron impact of silane, having a smaller probability of colliding with other silane molecules before striking the substrate as the silane fraction decreases. Of the two ratios, the latter, that comparing radicals having $F_H$ greater than and less than 2, correlates better with $f_H$. The increase in $f_H$ may therefore be caused, in part, by the effect shown in Fig. 1; radicals with $F_H > 2$ eliminate hydrogen during incorporation at a higher rate than those radicals having $F_H < 2$.

### C. The burial effect

It has been generally observed that for a given gas mixture, $f_H$ increases with increasing rate of deposition of *a*-Si:H.[7,25,26] The deposition rate is usually increased by increasing discharge power. Therefore, the increase in $f_H$ can result from either a change in the composition of the radicals incident on the surface or from what we call the burial effect. The burial effect is a physical, as opposed to a chemical, effect. The results of our model are consistent with lattice interconnection with molecular hydrogen elimination being a major method of removing hydrogen from the surface. To the extent that the rate of interconnection and hydrogen elimination is finite, the rate of hydrogen elimination is proportional to the residence time of adjacent Si–H($L$) bonds on the surface. The higher the rate of deposition, the shorter the residence time of Si–H($L$) bonds on the surface prior to burial and the smaller the probability that hydrogen is eliminated from the surface.

The burial effect is illustrated in Fig. 4, where we have plotted $f_H$ as a function of deposition rate. Figure 4(a) shows results for idealized cases of the flux of radicals being composed of a single species. Figure 4(b) shows simulated results for and the experimental results of Ross and Jaklik.[7] The simulated fluxes were generated with the model described in Ref. 17. In both cases $f_H$ increases with increasing deposition rate. For these cases we allow insertion of $SiH_3(M)$ into Si–H($L$) with $H_2$ elimination. The lattice $f_H$ for $SiH_3(F)$ is therefore less than that for $SiH_2(F)$ due to $H_2$ elimination during incorporation; $f_H$ in isolated configurations is greater for $SiH_3(F)$ in the absence of this effect. Over the indicated range of power deposition, in the simulated results [Fig. 4(b)] the fractional composition of the radical flux changes by only a few percent. The dominant effect responsible for increasing $f_H$ is the burial effect. For the results in Fig. 4, gas phase molecules did not saturate the surface. That effect will be discussed in the next section.

### D. Saturation and etching of lattice bonds by gas phase molecules

The reaction of radicals and molecules from the plasma which collide with but do not adsorb on the surface are important because they can either remove hydrogen from (etch) the surface by removing a hydrogen atom from a Si–

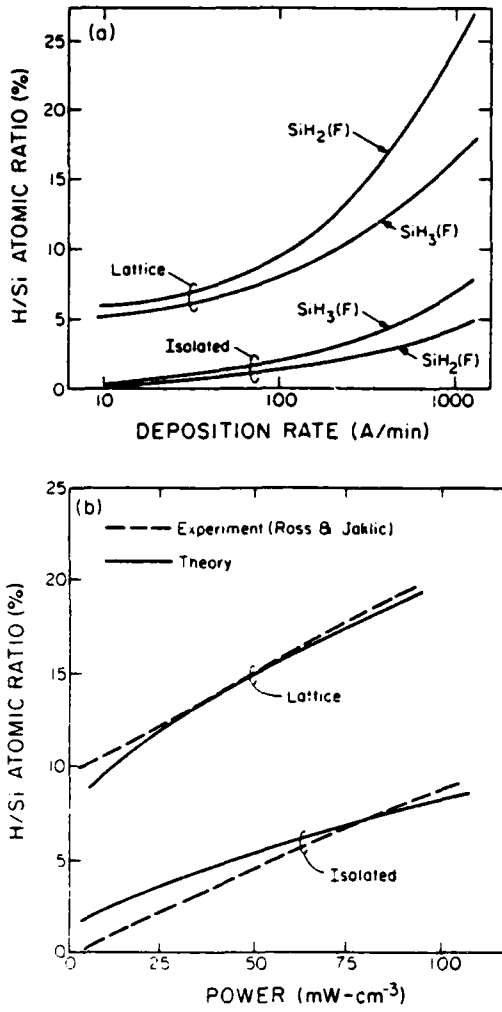


FIG. 4. Hydrogen atomic ratio in $a$-Si:H films as a function of discharge power, demonstrating the burial effect. (a) $f_{iH}$ for individual radical species, (b) this model's results and experimental values (Ref. 7) for deposition of $a$-Si:H from an rf discharge in $SiH_4$.

$H(L)$ bond, or deposit hydrogen on (saturate) the surface by inserting a hydrogen atom into a Si–$D(L)$ bond.[15] An example of these two processes are the forward (etching) and reverse (saturation) reactions

$$SiH_2(F) + SSSH(L) \rightleftharpoons SiH_3(F) + SSSD(L). \quad (13)$$

Since a Si–$H(L)$ bond on the surface is exchanged for a Si–$H(F)$ bond in the gas phase radical, the exothermicity of the class of reactions with radicals is determined by the difference in bond energies for $SiH_nH(F)$ and SSS–$H(L)$. Robertson and Gallagher assigned a bond energy of $\approx$80 kcal/mol to SSS–H(L).[10] The $SiH_2$–$H(F)$ bond energy is approximately 75 kcal/mol. To the level of accuracy of the approximations, this class of reactions involving radicals can be considered thermoneutral. The equilibrium ratio of saturated bonds to dangling bonds, $[SSSH(L)]/[SSSD(L)]$, resulting from these processes involving radicals is therefore $[SiH_n(F)]/[SiH_{(n-1)}(F)]$. For typical plasma conditions[23] this ratio is $> 10$, so that the equilibrium density of saturated to dangling bonds resulting from these radical reactions is $[SSSH(L)]/[SSSD(L)] > 10$. Therefore, surface bonds are more likely to be saturated than etched by radicals via this process. Even though the steady-state density of dangling bonds made available by this process is likely to be small, the process may be an important source of dangling bonds for the case where adsorbed radicals as $SiH_3(M)$ cannot insert into saturated surface sites [e.g., $SSSH(L)$].[15]

Analogous etching and saturation reactions can also occur by collisions of saturated molecules with the lattice. Examples of these reactions are

$$SiH_4(F) + SSSH(L) \rightarrow SiH_3(F) + H_2(G) + SSSD(L) \quad \text{(etching)}, \quad (14)$$

$$SiH_4(F) + SSSD(L) \rightarrow SiH_3(F) + SSSH(L) \quad \text{(saturation)}. \quad (15)$$

The etching reaction in Eq. (14) is endothermic, since two Si–H bonds are exchanged for the single H–H bond. The saturation reaction in Eq. (15), though, is approximately thermoneutral in the same manner as for the analogous reaction involving radicals in Eq. (13). Since $SiH_4$ is the feed stock, the large ratio of densities of $[SiH_4(F)]/[SiH_3(F)]$ insures that the equilibrium density of saturated bonds compared to dangling bonds resulting from this process is large; the relative etching probability is small, although the contribution may be an important source of dangling bonds (see above). From this discussion, one can conclude that nonadsorbing gas phase radicals and molecules colliding with the growing film are more likely to contribute hydrogen to the surface than remove it.

The saturation of dangling bonds on the surface of the lattice by gas phase, nonadsorbing molecules clearly has the potential of being an important source of hydrogen to the film. We investigated this process by assigning a probability of saturating Si–$D(L)$ bonds with hydrogen resulting from collisions of $SiH_4(F)$ and $H_2(F)$, the saturated molecules having the largest flux striking the surface. The rate of saturation of dangling bond $X_j(L)$ was specified to be $p_s([SiH_4(F)] + [H_2])[X_j(L)]/\rho_0$, where $p_s$ is the saturation probability. The effect on $f_H$ of varying $p_s$ is shown in Fig. 5. The case shown is the same as in Fig. 4(b) for Ar/

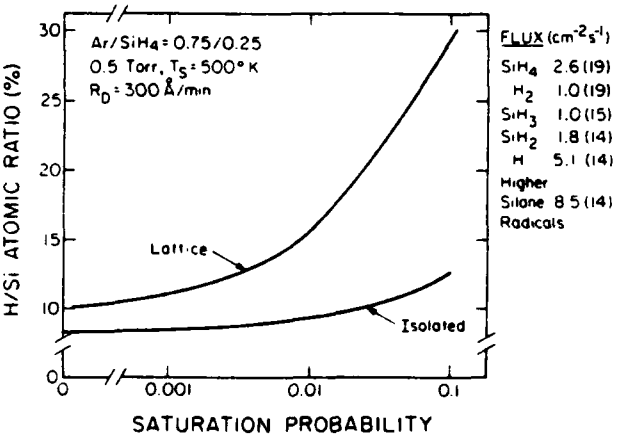


FIG. 5. Computed hydrogen atomic fraction as a function of the saturation probability of dangling bonds [e.g., $SSSD(L)$] by nonadsorbing molecules form the plasma ($H_2$, $SiH_4$). The plasma conditions are the same as for Fig. 3. The partial composition of the radical and molecular flux to the surface is shown at right.

$SiH_4 = 0.75/0.25$. The composition of the flux is also shown in the figure. The fraction of incorporated hydrogen, $f_H$, increases significantly when the probability for saturation is $> 10^{-3}$.

The fraction of hydrogen in isolated configurations also increases with increasing lattice saturation probability, although to a lesser degree than $f_H$ of the lattice. The increase of $f_H$ in isolated configurations is due to the adsorbed mobile radicals $[X(M)]$ having a smaller probability of encountering a lattice site having a dangling bond when the saturation probability is high. Since incorporation of $X(M)$ into a saturated bond has a smaller rate constant, the residence time and density of $X(M)$ on the surface increases, thereby increasing the probability of being buried as an isolated configuration.

### D. Substrate temperature

Computed hydrogen fraction $f_H$ as a function of substrate temperature $T_s$ for the experimental conditions of Ross and Jaklik[7] appear in Fig. 6. $f_H$ decreases with increasing substrate temperature due to the activation energy for interconnection and hydrogen elimination of Si–H($L$) bonds. The activation energy derived here, 1.5 kcal/mol, is approximately equal to that empirically derived by measuring $f_H$ as a function of $T_s$, 1.35 kcal/mol.[11] The decrease of hydrogen in isolated or polymeric configurations results from a decrease in the residence time of $SiH_x$ ($A$) as immobile adsorbates; a consequence of the activation energy for desorption.

The relative densities of hydrides and dihydrides is also a function of substrate temperature, as shown in Fig. 7. In this figure the experimental results of Luvcosky, Nemanich, and Knights[12] and results from the model for [SSSH($B$)]/[SSHH($B$)] are plotted as a function of $T_s$ and rf power (deposition rate).[27] The relative hydride density increases with increasing $T_s$ and is nearly constant for discharge power greater than 5 W (deposition rate of 150 Å/min). To obtain these results, it was necessary to invoke a higher activation energy (10 kcal/mol) for interconnection and hydrogen elimination between di- and trihydride [SSHH($L$), SHHH ($L$)] configurations than between hydride [SSSH ($L$)] configurations (1.5 kcal/mol). If the method of hydrogen incorporation is a weak function of temperature, then a uniform activation energy for interconnection between all hydride configurations nets only a weak temperature dependence for their relative densities. It is possible that the difference in activation energies between hydrides and dihydrides lies not in the interconnection process but in the incorporation step. We assumed, though, that the latter process had no activation energy. The suggestion that activation energies for mono- and polyhydrides are different is consistent with the observation that above a substrate temperature of 575 K, hydrogen evolves from HOMOCVD films with a higher activation energy (30 kcal/mol) than below that temperature.[11]

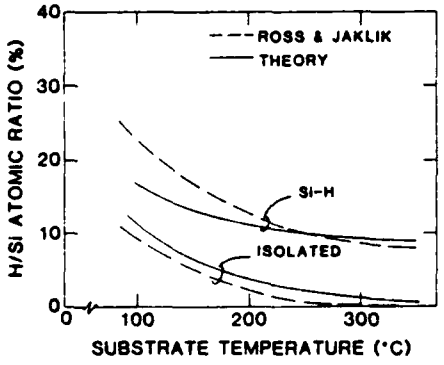


FIG. 6. Hydrogen atomic fraction as a function of substrate temperature as computed with the surface deposition model and the experimental results of Ross and Jaklik (Ref. 7).

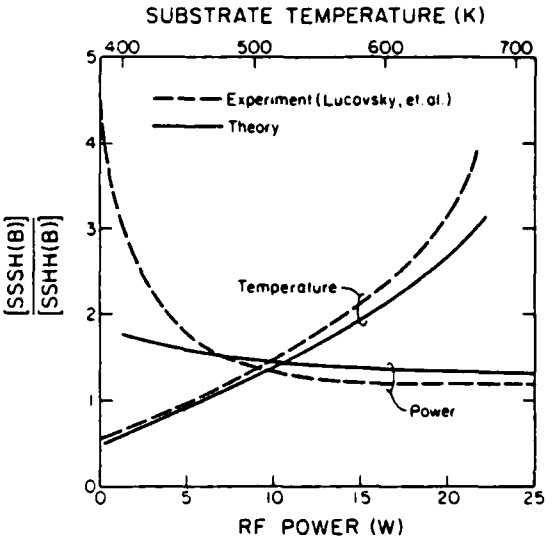


FIG. 7. The ratio of hydride [SSSH($B$)] and dihydride [SSHH($B$)] configurations in $a$-Si:H films as calculated with the surface deposition model compared to the experimental results of Lucovsky *et al.* (Ref. 12). The two cases are for varying the rf power (deposition rate) and substrate temperature $T_s$. The relative hydride density increases with increasing $T_s$. To obtain agreement with experiment for the temperature dependence, two activation energies were invoked; for interconnection between hydrides, and for interconnection between di- and trihydrides.

### E. Reactive sputter deposition

Sputter deposition of $a$-Si:H differs qualitatively from plasma deposition of $a$-Si:H in that the operator, by adjusting target voltage and hydrogen flowrate, has finer control of the composition of radicals incident onto the substrate. Unlike PECVD, where a large fraction of the hydrogen incident onto the surface is contained in silane radicals, in reactive sputter deposition the hydrogen and silicon fluxes to the surface are dominantly atomic. For sputter deposition, the scaling parameter to characterize the incident flux is $F_H^a$, the ratio of atomic H($F$) to atomic Si($F$). The computed atomic hydrogen content of sputter deposited $a$-Si:H is plotted in Fig. 8 as a function of $F_H^a$ for three different substrate temperatures. The silicon flux is constant at $2.4 \times 10^{15}$ cm$^{-2}$ s$^{-1}$ corresponding to a deposition rate of 300 Å/min. As expected, the fraction of hydrogen in both the lattice and in isolated configurations increases with increasing $F_H^a$. At higher substrate temperatures, though, $f_H$ for the lattice reaches a

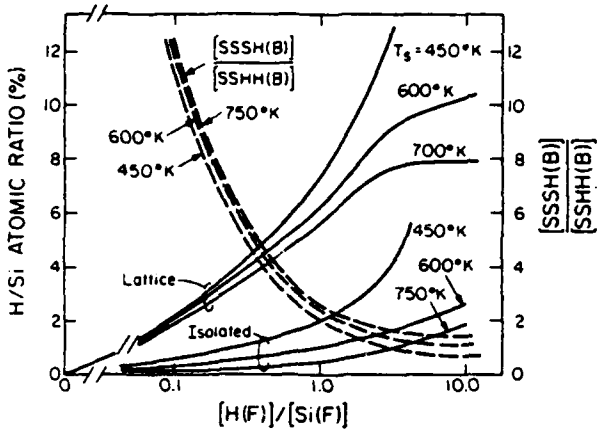


FIG. 8. Computed hydrogen atomic fraction and hydride/dihydride density for *a*-Si:H films grown by reactive sputter deposition as a function of the atomic hydrogen flux. The Si flux is constant at $2.4\times10^{15}$ cm$^{-2}$ s$^{-1}$, corresponding to a deposition rate of 300 Å/min.

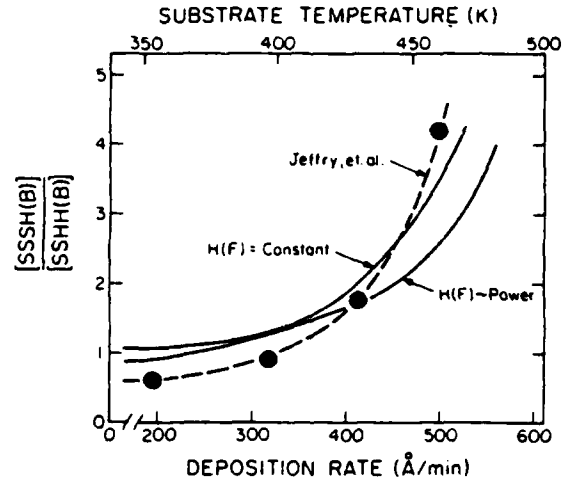


FIG. 9. Computed and experimental results for the ratio of hydride [SSSH(*B*)] to dihydride [SSHH(*B*)] density in *a*-Si:H films grown by reactive sputter deposition. The experimental results are from Jeffrey *et al.* (Ref. 8). The ratio of atomic H/Si of the radical flux for the model was obtained by normalizing to the experimental results at a desposition rate of 330 Å/min. Two case are shown, scaling H/Si with deposition rate (discharge power) and holding the hydrogen flux constant.

nearly constant value at $F^a_H \simeq 2$, whereas $f_H$ for isolated configurations continues to increase. The saturation of $f_H$ is due in part, to an equilibration between adsorption and desorption of $H_2(G)$ resulting from collisions between $H(M)$ radicals; a process proportional to $[H(F)]^2$ and which increases with increasing $T_s$.

The relative densities of hydride and dihydride configurations [i.e., SSSH(*B*)and SSHH(*B*)] in the sputtered *a*-Si:H films are also plotted in Fig. 8. At low values of $F^a_H$, the films are composed of dominantly hydride [SSSH(*B*)] configurations, and with increasing $F^a_H$, a larger fraction of hydrogen is contained in the film as dihydride [SSHH(*B*)]. The cause for the increase in dihyride density with increasing $F^a_H$ (at constant deposition rate) is analogous to the burial effect. Given a finite residence time of dangling bonds on the surface prior to burial, a higher flux of hydrogen passivates a larger fraction of those bonds, thereby leading to the higher dihydride density. If so, then at higher deposition rate (shorter residence time of dangling bonds on the surface) or higher substrate temperature (larger rate of interconnection), the ratio [SSSH(*B*)]/[SSHH(*B*)] should decrease. This trend is confirmed by comparing the computed ratio [SSSH(*B*)]/[SSHH(*B*)] to the experimental results of Jeffrey, Shanks, and Danielson[8] in Fig. 9. For these results, the ratio H(*F*)/Si(*F*) was obtained by normalizing to the experiment at a deposition of $\simeq$330 Å/min [H(*F*)/Si(*F*) = 3]. Results as a function of deposition rate were then obtained both while holding H(*F*) constant and assuming H(*F*) was proportional to the change in discharge power, which is directly proportional to deposition rate.

### F. Deposition without insertion of $SiH_3(M)$ into saturated surface sites

The details of the method of incorporation of $SiH_3(M)$ into the lattice are particularly important, because $SiH_3(F)$ has the highest flux of silicon containing radicals incident onto the surface. In Sec. V A we discussed the implications of having $SiH_3(M)$ incorporate into the lattice by inserting into Si–H($L$) bonds and eliminating hydrogen, as in reactions (11) and (12). In this section we will discuss the implications of $SiH_3(M)$ incorporation in the absence of this mechanism. For these conditions, $SiH_3(M)$ can only be incorporated into the lattice at a surface site having a dangling bond, as in the reaction

$$SiH_3(M) + SSSD(L) \rightarrow SSSS(L) + SHHH(L). \quad (16)$$

The dangling bonds at surface sites are made available by etching [reactions (13) and (14)] or sputtering by bombardment of the surface with energetic ions (see Table II).

When $SiH_3(M)$ cannot insert into Si–H($L$) bonds, the rate at which $SiH_3(M)$ incorporates into the lattice is smaller since the availability of the necessary surface sites [eg., SSSD($L$)] is also smaller. For a constant $SiH_3(F)$ flux, the surface density of $SiH_3(M)$ therefore increases. Surface clustering and desorption reactions therefore also become more likely (see Table II.) The two desorption reactions which are important are

$$SiH_3(M) + SiH_3(M) \rightarrow Si_2H_6(G). \quad (17a)$$

$$SiH_3(M) + H(M) \rightarrow SiH_4(G). \quad (17b)$$

As a result of these reactions, the effective sticking coefficient for $SiH_3(M)$ is less than unity.

We investigated the characteristics of *a*-Si:H films when $SiH_3(M)$ incorporation occurs only via a dangling bond. These results are shown in Fig. 10 where the film deposition rate and effective sticking coefficient for $SiH_3(M)$ are plotted as a function of the rate of generation of dangling bonds. The flux of radicals incident onto the surface have the ratio $SiH_3/SiH_2/H = 100/5/10$ with $[SiH_3(F)] = 10^{16}$ cm$^{-2}$ s$^{-1}$. These values are typical for a low-powered plasma in a $SiH_4/H_2 = 1/1$ gas mixture at 0.25 Torr. The independent variable is the number of dangling bonds generated on the surface by sputtering or etching as a fraction of the $SiH_3(F)$ flux incident onto the surface. As the rate of generation of

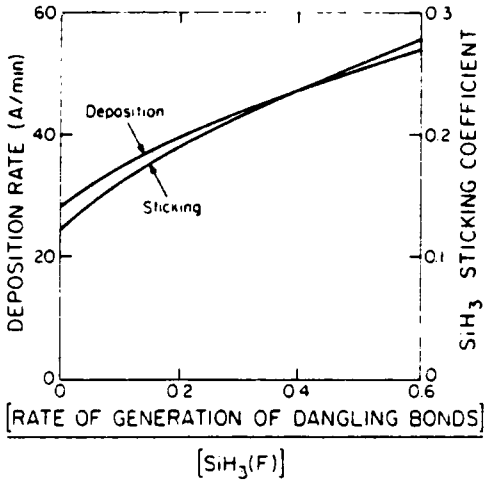


FIG. 10. Deposition rate and effective sticking coefficient for $SiH_3(M)$ as a function of the rate of generation of dangling bonds. For these results, $SiH_3(M)$ does not insert into Si–H($L$). The discharge conditions are $SiH_3/(F)/SiH_2(F)/H(F) = 100/5/10$ with $SiH_3(F) = 10^{16}\,cm^{-2}\,s^{-1}$. The rate of generation of dangling bonds is expressed as a fraction of $SiH_3(F)$.

dangling bonds increases and the number of sites available for $SiH_3(M)$ insertion increases, both the deposition rate and effective sticking coefficient of $SiH_3(F)$ also increase. Over the range investigated, though, there is little change in hydrogen fraction ($9.5\% \leqslant f_H \leqslant 10.0\%$). This last observation is explained by the fact that if a dangling bond is required for incorporation of $SiH_3(M)$, then the two reactions responsible for deposition for these conditions,

$$SiH_2(M) + SSSH(L) \rightarrow SSSS(L) + SHHH(L) \qquad (18a)$$

$$SiH_3(M) + SSSD(L) \rightarrow SSSS(L) + SHHH(L), \qquad (18b)$$

are functionally equivalent with respect to "hydrogen accounting." The $SiH_3(M)$ which does not stick is desorbed primarily as disilane, as the desorption products have the ratio $[Si_2H_6(G)]/[SiH_4(G)] = 6$.

## VI. CONCLUDING REMARKS

A phenomenological model for surface kinetics during plasma and sputter CVD of amorphous hydrogenerated silicon has been described. The model consists of an accounting, in rate equation form, of adsorption, incorporation, interconnection, and other pertinent processes. The model has successfully compared with experimental results for hydrogen fraction and distribution of bond types. We found that molecular hydrogen elimination during incorporation distinguishes between films grown from plasmas whose primary radicals $SiH_n$ have $n \leqslant$ or $n > 2$. We also found that the observed increase in hydrogen fraction with increasing deposition rate is largely a physical, as opposed to chemical, process. At higher deposition rates, the shorter residence time of Si–H($L$) bonds on the surface results in a smaller probability for interconnection and hydrogen elimination. The cause for the increase in the fraction of hydrogen contained in hydride, as opposed to dihydride, configurations with increasing substrate temperature may be a result of there being a higher activation energy of interconnection between dihydride configurations.

## ACKNOWLEDGMENT

This work was supported by the Materials Science Division of the Army Research Office under the direction of Dr. Andrew Crowson, Contract No. DAAG29-85-C-0031.

[1] M. Hirose, in *Semiconductors and Semimetals*, edited by J. I. Pankove (Academic, Orlando, 1984), Vol. 21A, p. 109.
[2] B. A. Scott, R. M. Plecenik, and E. E. Simonyi, Appl. Phys. Lett. **39**, 73 (1981).
[3] M. Hirose, in *Semiconductors and Semimetals*, edited by J. I. Pankove (Academic, Orlando, 1984), Vol. 21A, p. 9.
[4] T. D. Moustakas, in *Semiconductors and Semimetals*, edited by J. I. Pankove (Academic, Orlando, 1984), Vol. 21A, p. 55.
[5] J. A. Thornton, in *Amorphous Metals and Semiconductors*, edited by P. Maasen and R. I. Jaffee (Pergamon, New York, 1986), pp. 299–314.
[6] P. E. Vanier, J. F. Kampas, R. R. Corderman, and G. Rajeswaran, J. Appl. Phys. **56**, 1812 (1984).
[7] R. C. Ross and J. Jalik, Jr., J. Appl. Phys. **55**, 3785 (1984).
[8] F. R. Jeffery, H. R. Shanks, and G. C. Danielson, J. Appl. Phys. **50**, 7034 (1979).
[9] F. J. Kampas, in *Semiconductors and Semimetals*, edited by J. I. Pankove (Academic, Orlando, 1984), Vol. 21A, p. 153.
[10] R. Robertson and A. Gallagher, J. Chem. Phys. **85**, 3623 (1986).
[11] B. A. Scott, J. A. Reimer, and P. A. Longeway, J. Appl. Phys. **54**, 6853 (1983).
[12] G. Lucovsky, R. J. Nemanich, and J. C. Knights, Phys. Rev. B **19**, 2064 (1979).
[13] C. C. Tasi, J. C. Knights, G. Chang, and B. Wacker, J. Appl. Phys. **59**, 2998 (1986).
[14] P. A. Longeway, in *Semiconductors and Semimetals*, edited by J. I. Pankove (Academic, Orlando, 1984), Vol. 21A, p. 179.
[15] A. Gallagher, in *Materials Issues in Amorphous Semiconductor Technology*, edited by D. Adler, Y. Hamakawa, and A. Madan (Materials Research Society, Pittsburgh, PA, 1986), p. 3.
[16] K. K. Gleason, K. S. Wang, M. K. Chen, and J. A. Reimer, J. Appl. Phys. **61**, 2866 (1987).
[17] M. J. Kushner, in *Plasma Processing*, edited by J. W. Coburn, R. A. Gottscho, and D. W. Hess (Materials Research Society, Pittsburgh, PA, 1986), pp. 293–307.
[18] I. NoorBatcha, L. M. Raff, and D. L. Thompson, J. Chem. Phys. **81**, 3715 (1984).
[19] P. Ho, M. E. Coltrin, J. S. Binkley, and C. F. Melius, J. Phys. Chem. **90**, 3399 (1986).
[20] D. K. Beigelsen, R. A. Street, C. C. Tsai, and J. C. Knights, Phys. Rev. B **20**, 4839 (1979).
[21] J. Shirafuji, M. Kuwagaki, T. Sato, and Y. Inuishi, Jpn. J. Appl. Phys. **23**, 1278 (1984).
[22] R. Robertson, D. Hils, H. Chatham, and A. Gallagher, Appl. Phys. Lett. **43**, 544 (1983).
[23] R. Robertson and A. Gallagher, J. Appl. Phys. **59**, 3402 (1986).
[24] M. E. Coltrin, R. J. Kee, and J. A. Miller, J. Electrochem. Soc. **131**, 425 (1984).
[25] O. Kuboi, M. Hashimoto, and Y. Yatsurugi, Appl. Phys. Lett. **45**, 543 (1984).
[26] A. Matsuda, T. Kaga, H. Tanaka, L. Malhortra, and K. Tanaka, Jpn. J. Appl. Phys. **22**, L115 (1983).
[27] R. A. Street, J. C. Knights, and D. K. Biegelsen, Phys. Rev. B **18**, 1880 (1978).

# A model for the discharge kinetics and plasma chemistry during plasma enhanced chemical vapor deposition of amorphous silicon

Mark J. Kushner
*University of Illinois, Gaseous Electronics Laboratory, Department of Electrical and Computer Engineering, 607 E. Healey, Champaign, Illinois 61820*

(Received 12 October 1987; accepted for publication 4 December 1987)

A model for the plasma enhanced chemical vapor deposition of amorphous hydrogenated silicon (*a*-Si:H) in rf and dc discharges is presented. The model deals primarily with the plasma chemistry of discharges sustained in gas mixtures containing silane ($SiH_4$). The plasma chemistry model uses as input the electron impact rate coefficients generated in a separate simulation for the electron kinetics and therefore makes no *a priori* assumptions as to the manner of power deposition. Radical densities and contributions to film growth are discussed as a function of gas mixture, electrode separation, and locale of power deposition, and comparisons are made to experiment. A compendium of reactions and rate constants for silane neutral and ion chemistry is also presented.

## I. INTRODUCTION

Plasma enhanced chemical vapor deposition (PECVD) is a process whereby thin films of amorphous hydrogenated silicon (*a*-Si:H) are made at substrate temperatures of $\leq 500$ K, significantly below than those required for conventional chemical vapor deposition (CVD).[1-4] PECVD is usually performed in parallel plate, capacitively coupled radio frequency (rf) discharges sustained in gas mixtures containing silane ($SiH_4$) or disilane ($Si_2H_6$) (see Fig. 1). Deposition rates of 10's–100's A/min can be obtained from discharges in pure silane of few hundred mTorr with power deposition of tens to hundreds of mW $cm^{-3}$. Films so produced have atomic hydrogen fractions of 5%–20%, and are used in electronic devices (thickness $\approx 0.5$ $\mu$m), photovoltaic cells (0.2–0.5 $\mu$m), and as photoreceptors (10–15 $\mu$m). Solar cells of single junction *a*-Si:H fabricated by PECVD have demonstrated efficiencies of 11.7% in small areas (1 $cm^2$), and 7.9% in large area modules ($> 1000$ $cm^2$).[5]

The processes leading to the PECVD of *a*-Si:H begin with electron impact dissociation of silane, creating neutral and charged radicals consisting principally of silyl, $SiH_3$. The radicals undergo neutral chemical and ion-molecule reactions while they diffuse or drift to a substrate, usually one of the parallel plate electrodes. At the substrate, the radicals are adsorbed and incorporated into the lattice of the film. In principal, PECVD of *a*-Si:H is divisible into three sequential subprocesses: discharge electron kinetics, plasma chemistry, and surface deposition kinetics. Electron impact collisions from the first generate radicals which subsequently react in the second and which are finally incorporated into the film in the third. In reality, the three subprocesses are connected in a more global sense than a simple sequence of events. For example, depletion of the feedstock gases by electron impact dissociation cause changes in the electron distribution function, which results in a change in the rate of production of radicals. Surface reactions which cause saturated molecules to desorb into the gas may, in turn, modify the chain of chemical reactions.[6]

The electron kinetics, plasma chemistry, and surface kinetics for the PECVD of *a*-Si:H have been the topic of many previous investigations. In particular, discharge and chemical kinetics models have been developed with the goal of obtaining a theoretical understanding of the process. Turban, Catherine, and Grolleau[7] developed the first such model in 1979. In this model, all processes were assumed to be spatially uniform and a semi-empirical rate constant for electron impact dissociation of $SiH_4$ was used. At the time of the study, the cross section for electron impact dissociation of silane had not yet been measured. Ion chemistry and neutral chain reactions in silane discharges were analyzed by Haller[8,9] using rate equation models in 1980 and 1983. He concluded that reactions of radicals following electron impact dissociation of silane are equally if not more important in determining the characteristics of the deposited *a*-Si:H as the direct products of the dissociation. Chen,[10] also in 1983, analyzed PECVD from a mass transport viewpoint, examining various reactor geometries while not emphasizing the details of the plasma chemistry. Longeway, Estes, and Weakliem[11] analyzed the decomposition of silane in a dc glow discharge in 1984 using a steady-state rate equation model, and concluded that the primary dissociation product

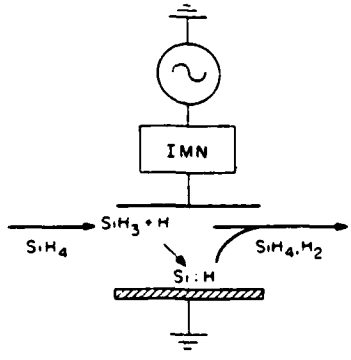


FIG. 1. Schematic of a plasma deposition reactor. A radio frequency power supply is capacitively coupled through an impedance matching network (IMN) to a set of parallel plate electrodes separated by a few to 10 cm. Reactant gas mixtures containing silane ($SiH_4$) at pressures of 10's to 100's of mTorr flow between the electrodes with residence times of 10's of ms to a second. Silane is dissociated by electron impact resulting in deposition of an *a*-Si:H film. The products and undissociated silane are pumped out of the reactor.

 0021-8979/88/082532-20$02.40  

of silane is $SiH_3$. In 1984, Tachibana[12] presented a quasi-steady-state plasma chemistry model for rf discharges in silane, including higher silane species (through $Si_5H_{12}$ and $Si_3H_6^+$). Although the neutral chemistry and ion-molecule reactions in his model are treated in a self-consistent manner, the electron density was an input parameter whose value was based on experimental electrical probe measurements. Electron impact rate constants were obtained by convolving a semi-empirical electron distribution function with cross sections. Tachibana concluded that $SiH_3$ is the most abundant gas phase radical and that $SiH_3$ is likely to directly insert into the growing film. The following year, Chang *et al.*[13] modeled positive column discharges of silane diluted by argon, helium, and neon. They assumed a Maxwellian electron distribution and, with the quasi-neutrality condition, solved for the electron temperature as a function of electron density. Values of 1–2 eV were obtained. They found that silane ions have a small density compared to neutral radicals, and excitation transfer to silane from noble gas metastables is most important for He-$SiH_4$ mixtures. Ion chemistry in the sheaths of dc discharges was studied in 1985 by Chatham and Gallagher using a one-dimensional transport model.[14] They parametrically calculated the discharge operating characteristics which yield given fractions of lower and higher silane ions.

The electron kinetics of silane discharges have also been separately theoretically studied by Garscadden, Duke, and Baily,[15] Hayashi,[16] Ohmori, Shimozuma, and Tagashima,[17] and Kushner.[18] These studies resulted in derived sets of electron impact cross sections, and the ability to generate electron impact rate constants as a function of position and time in rf discharges.

A reoccurring conclusion from previous modeling studies is that there are interdependencies between the subprocesses (electron kinetics, plasma chemistry, and surface kinetics) which put a premium on performing as self-consistent an analysis as possible. Recognizing this fact, previous investigators augmented their models by using experimental data for variables such as electron density or dissociation rates. A totally self-consistent analysis has thus far been lacking.

In this paper a model for the discharge kinetics and plasma chemistry of rf and dc discharges sustained in silane gas mixtures for the PECVD of *a*-Si:H is presented. This model differs from previous treatments in that no assumptions are made concerning parameters such as the electron distribution function, dissociation rate, reactor geometry, or reaction chain. The goal of the model is to simulate the PECVD of *a*-Si:H from discharges sustained in silane while making a minimum of *a priori* assumptions. The simulation consists of a one-and-one-half-dimensional, time-dependent plasma chemistry model whose electron impact rate constants are obtained from a Monte Carlo simulation for the electron distribution function in parallel plate rf discharges.[18,19] The plasma chemistry model includes a sufficient number and variety of species and reactions that gas mixtures of $SiH_4$ or $Si_2H_6$ diluted by Ar or $H_2$ can be simulated. Although some of the reaction rates are estimates, the model is so constructed that as new measurements of these rates become available they can be easily incorporated into the simulation.

The model uses as input gas mixture, reactor geometry, and power deposition: and produces as output the density of radicals and ions as a function of time and position between the electrodes, the flux of radicals and ions incident onto the substrates or electrodes, and the deposition rate of *a*-Si:H. The flux of radicals incident onto the electrodes can also be used as input to a separate model for surface deposition kinetics. This second model simulates characteristics of the *a*-Si:H film such as hydrogen fraction and dihydride density.[20] The three submodels for electron kinetics, plasma chemistry, and surface deposition kinetics, represent the first attempt at a totally self-consistent model for the PECVD of *a*-Si:H.[21]

In Sec. II, the plasma chemistry model is described with an accompanying discussion on the source and selection of rate constants, cross sections, and transport coefficients. The intent of the discussion and listing of reactions is to summarize the current availability of rate constants and cross sections for silane plasma chemistry. In Sec. III, a sampling of results from the model are discussed for various aspects of the PECVD of *a*-Si:H. Time and spatially dependent densities of radicals and saturated molecules are presented for rf discharges, followed by a discussion of the rate of survival of radicals. Discharge properties as a function of electrode separation and radical contributions to film growth are discussed, followed by a discussion on the formation of higher silane ions.

## II. DESCRIPTION OF THE MODEL

The plasma chemistry model consists of a set of partial differential equations (PDEs) describing the time evolution of the density of individual radical and saturated species as the input gases flow downstream in an rf glow discharge. The model principally simulates a capacitively coupled parallel plate (diode) rf glow discharge, and by modifying the boundary conditions, dc discharges are simulated. We assumed plug gas flow in the downstream direction, thus integration in time is equivalent to integrating in space along the flow direction by specifying the flowrate and dimensions of the reactor.

The PDE for each species has the general form of

$$\frac{\partial N_i(x,t)}{\partial t} = \sum_j n_e k_{ij} N_j + \sum_{j,l} \kappa_{ijl} N_j N_l - N_i\left(\sum_j n_e k_{ji} + \sum_{j,l} \kappa_{jil} N_l\right) + \nabla \cdot D_i \nabla N_i - \nabla \cdot \mu_i E N_i, \quad (1)$$

where all quantities are a function of position and time. In Eq. (1), $k_{ij}$ is the electron impact rate coefficient for production of species $i$ by electron collisions with species $j$, $\kappa_{ijl}$ is the analogous coefficient for reactions between heavy particles $j$ and $l$. $D_i$ is the diffusion coefficient for species $i$, $\mu_i$ is the mobility of charged species $i$, and $E$ is the local electric field. The first and third terms in Eq. (1) are for electron impact processes (excitation, dissociation, ionization, attachment)

resulting in generation and depletion of species $N_i$; the second and fourth terms are for generation and depletion by neutral and ion heavy particle reactions; the fifth term is for transport by diffusion for neutrals and ions; and the sixth term is for transport of ions by drift in the electric field. Using a finite difference formulation for the spatial derivatives, the set of PDEs was reduced to a set of ordinary differential equations. Initial conditions were assigned, and the system of equations was integrated in time using a third-order Runga–Kutta technique.

The diffusion approximation for gas transport is valid only for conditions where the gas flow is laminar, and the molecular mean free path is small compared to other spatial scales of interest, such as the electrode separation. For a gas density of $1.5\times10^{15}$ cm$^{-3}$ ($P = 100$ mTorr, $T_g = 650$ K), the molecular mean free path is $\simeq 0.2$ cm. The diffusion approximation is therefore valid for electrode separation $d$, obeying $d \geqslant 0.2\ [0.1/P(\text{Torr})]\ [T_g(\text{K})/650]$ cm.

### A. Species

The species included in the model are listed in Table I. The species and reactions used here are sufficient to simulate discharges sustained in gas mixtures initially consisting of $SiH_4/Si_2H_6/H_2/Ar$. The species include lower silane radicals and ions, higher silane radicals, saturated molecules, and ions, and vibrationally excited silane and disilane. Vibrationally excited silane and disilane are explicitly included in the model because a significant fraction of the power can be coupled into the discharge by vibrational excitation. The fraction of power deposited in this fashion can be $>0.2$ resulting in a fractional density of vibrationally excited silane of $<0.05$.

TABLE I. Species in the plasma chemistry model.

| Argon species | Hydrogen species |
|---|---|
| Ar | $H_2$ |
| $Ar^*(3s)$ | $H_2^*$ |
| $Ar^{**}(4p)$ | $H_2^+$ |
| $Ar^+$ | $H_3^+$ |
| $ArH^+$ | H |
| | $H^*$ |
| | $H^+$ |
| | $H^-$ |
| **Silane species** | |
| $SiH_4$ | $SiH_4(v1,3)$ |
| $SiH_4(v2,4)$ | $SiH_3$ |
| $SiH_2$ | SiH |
| Si | |
| $SiH_3^+$ | $SiH_2^+$ |
| $SiH^+$ | $Si^+$ |
| $SiH_3^-$ | $SiH_2^-$ |
| **Disilane species** | |
| $Si_2H_6$ | $Si_2H_6(v1,3)$ |
| $Si_2H_6(v2,4)$ | $Si_2H_5$ |
| $Si_2H_4$ | $Si_2H_3$ |
| $Si_2H_2$ | |
| $Si_2H_7^+$ | $Si_2H_6^+$ |
| $Si_2H_5^+$ | $Si_2H_4^+$ |
| $Si_2H_3^+$ | $Si_2H_2^+$ |
| $Si_2H^+$ | |
| **Higher silane species** | |
| $Si_3H_7$ | $Si_3H_8$ |
| $Si_4H_9$ | $Si_4H_{10}$ |
| $Si_4H_{11}$ | $Si_5H_{12}$ |
| DUST | |
| $Si_3H_6^+$ | $Si_4H_8^+$ |
| $Si_5H_{10}^+$ | |

Mass spectroscopy,[22] laser scattering measurements,[23] and qualitative observations of particulate (or dust) in silane glow discharges are evidence for the existence of higher silane radicals, molecules, and ions. These species range from higher silane molecules containing $<10$ silicon atoms to clusters exceeding many micrometers in size, thereby containing $>10^{10}$ silicon stoms. In order to investigate the clustering process, we included higher radical and saturated silane species, $Si_nH_{2n+1}$ and $Si_nH_{2(n+1)}$, respectively, for $n<5$. We also included a category labeled DUST representing molecules or clusters having greater than five silicon atoms. The polymerization chain linking the higher silanes is based on the insertion of lower silane radicals into higher saturated molecules, and the saturation of higher radicals by hydrogen. For example,

$$\begin{aligned} &SiH + Si_4H_{10} \rightarrow Si_5H_{11}, \\ &SiH_2 + Si_4H_{10} \rightarrow Si_5H_{12}, \\ &SiH_3 + Si_4H_{10} \rightarrow H_2 + Si_5H_{11}, \\ &Si_5H_{11} + H \rightarrow Si_5H_{12}. \end{aligned} \tag{2}$$

Reactions in the polymerization chain which result in molecules having more than five silicon atoms contribute to the density of DUST. The polymerization chain is propagated with a uniform rate constant, which is $k_p = 10^{-11}$ cm$^3$ s$^{-1}$ unless otherwise noted. The formation of dust is sensitive to the choice of the propagation rate constant since the density of the $n$th member in the polymerization is proportional to $(k_p)^n$. The polymerization model and its consequences will be discussed in more detail in an upcoming publication.

Higher silane ions ($n > 2$) can have large fractional densities, particularly at high silane pressures ($P>0.3$ Torr) and large electrode separations ($d>2$ cm).[22] Therefore, we included higher silane ions having $n<6$. An analogous polymerization chain to that proposed for the higher neutral silanes was included for ions and will be discussed in Sec. III E.

Although the dissociative attachment cross sections for silane and disilane producing $SiH_2^-$ and $SiH_3^-$ are not particularly large, the residence time for negative ions in the discharge can be long. These ions were therefore included in the model. For conditions typical of rf discharges, the electronegativity [$N_I/(n_e + N_I)$, $n_e$ is the electron density, $N_I$ is the negative ion density] is 0.1–0.3. For dc positive column discharges, where the electron distribution function more closely matches the dissociative attachment cross sections, the electronegativity is $>0.9$.

### B. Reactions, rate constants, and cross sections

A comprehensive set of rate constants and cross sections was compiled for the electron and heavy particle reactions

occurring in glow discharges sustained in gas mixtures of $SiH_4$, $Si_2H_6$, $H_2$, and Ar. The reactions are separated into electron-neutral, neutral-neutral, ion-molecule, electron-ion, and ion-ion. Each class of reactions will be briefly described below.

### 1. Electron impact cross sections and rate constants

The electron-neutral reactions for excitation, dissociation, and ionization included in the plasma chemistry model are listed in Table II.[16,24–42] In addition to these reactions, elastic (momentum transfer) collisions were included in the solution for the electron distribution function (see below). Cross sections for electron impact excitation, ionization, and dissociation for Ar and $H_2$ are well known and the sources for these cross sections are listed in Table II. Electron impact cross sections for silane and disilane, though, are less well known. Only a subset have been directly measured; total dissociation,[24] dissociative ionization,[29] and dissociative attachment.[30,31] Electron swarm parameters (drift velocity and net ionization coefficient), though, have been measured as a function of $E/N$ (electric field/number density).[17] With the measured cross sections, swarm parameters and knowledge of the approximate shapes of cross sections for other collisional processes, a self-consistent, though not unique, set of cross sections can be generated. In doing so, one hypothesizes a set of cross sections and uses those cross sections to compute the electron distribution function and swarm parameters. The computed swarm parameters are compared to experiment. The process is iterated until agreement is obtained.

This method for generating cross sections was used by Garscadden *et al.*[15] and Ohmori *et al.*[17] for silane, and by Hayashi[16] for silane and disilane. The cross sections so generated are not unique and depend upon the method used to solve for the electron distribution function. The cross sections obtained by Garscadden and Hayashi, for example, are quantitatively different. Both sets, though, reproduce swarm data and are therefore acceptable solutions. We repeated the process, generating self-consistent sets of cross sections for silane and disilane which are accurate for our method of solution. We used as a basis the measured dissociation, dissociative ionization, and attachment cross sections, and the momentum transfer and vibrational excitation cross sections suggested by Hayashi. We used a modified form of the Monte Carlo simulation described in Ref. 18 for solving the electron distribution function in a dc field. It was necessary to use an energy-dependent anisotropic elastic scattering cross section to obtain agreement with swarm parameters. The cross sections for silane thus derived are shown in Fig. 2.

TABLE II. Electron impact excitation, dissociation, and ionization.

| Process | Rate constant[a] | Cross-section reference |
|---|---|---|
| Collisions with silane | | |
| $e + SiH_4 \rightarrow SiH_4(v2,4) + e$ | 8.34( − 9) | 16 |
| $e + SiH_4 \rightarrow SiH_4(v1,3) + e$ | 8.74( − 9) | 16 |
| $e + SiH_4 \rightarrow SiH_3 + H + e$ | 1.59( − 10) | 24–28 |
| $e + SiH_4 \rightarrow SiH_2 + H + H + e$ | 1.87( − 11) | 24–28 |
| $e + SiH_4 \rightarrow SiH + H_2 + H + e$ | 9.34( − 12) | 24–28 |
| $e + SiH_4 \rightarrow SiH_3^+ + H + 2e$ | 5.64( − 12) | 29 |
| $e + SiH_4 \rightarrow SiH_2^+ + H_2 + 2e$ | 7.19( − 12) | 29 |
| $e + SiH_4 \rightarrow SiH^+ + H_2 + H + 2e$ | 1.39( − 12) | 29 |
| $e + SiH_4 \rightarrow Si^+ + 2H_2 + 2e$ | 1.19( − 12) | 29 |
| $e + SiH_4 \rightarrow SiH_3^- + H$ | 2.50( − 13) | 30,31 |
| $e + SiH_4 \rightarrow SiH_2^- + H_2$ | 1.50( − 13) | 30,31 |
| Collisions with disilane | | |
| $e + Si_2H_6 \rightarrow Si_2H_6(v2,4) + e$ | 1.29( − 8) | 16 |
| $e + Si_2H_6 \rightarrow Si_2H_6(v1,3) + e$ | 1.06( − 8) | 16 |
| $e + Si_2H_6 \rightarrow SiH_4 + SiH_2 + e$ | 2.86( − 10) | 24 |
| $e + Si_2H_6 \rightarrow Si_2H_4 + H_2 + e$ | 1.23( − 10) | 24 |
| $e + Si_2H_6 \rightarrow Si_2H_6^- + 2e$ | 1.44( − 11) | 29 |
| $e + Si_2H_6 \rightarrow Si_2H_4^+ + H_2 + 2e$ | 2.45( − 11) | 29 |
| $e + Si_2H_6 \rightarrow SiH_3^+ + SiH_3 + 2e$ | 1.75( − 11) | 29 |
| $e + Si_2H_6 \rightarrow Si_2H_5^+ + H + 2e$ | 1.75( − 11) | 29 |
| $e + Si_2H_6 \rightarrow Si_2H_2^+ + 2H_2 + 2e$ | 1.15( − 11) | 29 |
| $e + Si_2H_6 \rightarrow SiH_3^- + SiH_3$ | 9.45( − 14) | 16,32 |
| $e + Si_2H_6 \rightarrow SiH_2^- + SiH_4$ | 9.45( − 14) | 16,32 |
| Collisions with hydrogen | | |
| $e + H_2 \rightarrow H_2(v1) + e$ | 8.81( − 10) | 33 |
| $e + H_2 \rightarrow H_2(v2) + e$ | 3.88( − 11) | 33 |
| $e + H_2 \rightarrow H_2^* + e$ | 1.28( − 11) | 33 |
| $e + H_2 \rightarrow H_2^+ + 2e$ | 2.32( − 11) | 34 |
| $e + H_2 \rightarrow H + H + e$ | 4.49( − 12) | 35 |
| $e + H \rightarrow H^* + e$ | 9.90( − 12) | 36 |
| $e + H \rightarrow H^+ + e$ | 2.62( − 13) | 36 |
| Collisions with argon | | |
| $e + Ar \rightarrow Ar^* + e$ | 1.21( − 12) | 37,38 |
| $e + Ar \rightarrow Ar^{**} + e$ | 1.27( − 12) | 39 |
| $e + Ar \rightarrow Ar^+ + 2e$ | 1.05( − 11) | 34 |
| $e + Ar^* \rightarrow Ar^{**} + e$ | 8.07( − 8) | 40 |
| $e + Ar^* \rightarrow Ar^+ + 2e$ | 2.40( − 9) | 41 |
| $e + Ar^{**} \rightarrow Ar^+ + 2e$ | 7.02( − 9) | 42 |

[a] $1.5(-10) \equiv 1.5 \times 10^{-10}$. Rate constants have units of $cm^3\ s^{-1}$ and were obtained by convolving cross sections from the indicated references with the electron distribution function, as described in the text. Rate constants in this table are averaged over the volume of the reactor and over the rf cycle. Rate constants for electron collisions with $SiH_4$, $Si_2H_6$, and $H_2$ are for the following discharge conditions: $SiH_4/H_2 = 1/1$, 0.25 mW $cm^{-3}$, 13.56 MHz, electrode separation 2.5 cm, 0.25 Torr, and substrate temperature 500 K. The rate constants for collisions with Ar are for an $Ar/SiH_4$ gas mixture having similar discharge conditions.

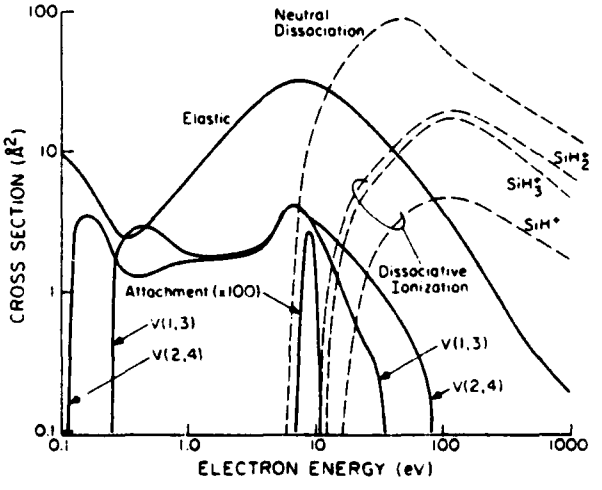


FIG. 2. Electron impact cross sections for $SiH_4$ used in the model (see Sec. II B 1 and Table II for references).

The agreement with swarm measurements is shown in Fig. 3.[43]

Electron impact rate coefficients were obtained as a function of phase during the rf cycle and position between the electrodes by parameterizing the electron kinetics simulation program RFDIS. This model is a multidimensional, time-dependent Monte Carlo particle simulation for the electron distribution function in a parallel plate capacitively coupled rf discharge, and has been described in detail in previous publications.[18] Electron impact rate coefficients were obtained by convolving the cross sections with the electron distribution generated by RFDIS. A sample of rate constants so calculated are shown in Fig. 4. High threshold energy processes, such as ionization, have rate constants which are significantly modulated during the rf cycle, a consequence of a modulation of the high-energy tail of the electron distribution function. The high-energy tail is "pumped" at the peaks of the rf cycle near the electrodes, a result of the oscillating sheaths. Processes with lower threshold energies, such as vibrational excitation, have rate constants which are more uniform as a function of position and time, as lower energy "bulk" electrons participate in these processes. Electron impact rate constants averaged over position and phase of the rf cycle appear in Table II for typical discharge conditions, as noted in the table. These rate constants are only representative; the manner of selecting the appropriate coefficients during execution of the model are described below.

For each initial gas mixture and plate separation, RFDIS was parameterized while using different values of the applied rf voltage and electric field in the bulk plasma. For each run of RFDIS, labeled $j$, we computed the quantity $\rho_j = (P/n_e)_j$, where $P$ is the spatially averaged power deposition per unit volume and $n_e$ is the spatially averaged electron density. A set of time and spatially dependent electron impact rate constants was generated and labeled, $k_i(\rho_j)$, where $i$ denotes the electron impact collision. A look-up table was constructed of these rate constants using $\rho_j$ as the parametric variable. When executing the plasma chemistry model, we used power deposition per unit volume, $P$, as a scaling parameter. Knowing the instantaneous electron density, $n_e(t)$, the electron impact rate constant $k_i$ was obtained by interpolating the table $k_i[(P/n_e)_j]$ using the parameter $P/n_e(t)$. The power includes contributions from ions which are accelerated through the sheaths and strike the electrodes. For the reference conditions presented in Sec. III ($SiH_4$ 250 mTorr, 25 mW cm$^{-3}$), <5%–10% of the power is dissipated in this fashion.

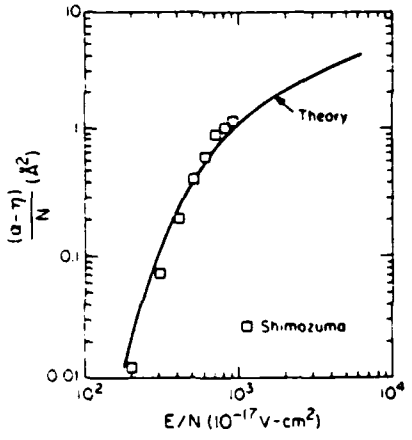


FIG. 3. Net ionization coefficient (ionization attachment) for dc discharges in silane as a function of electric field/number density. Theoretical results are as generated with the cross sections from Fig. 2. The experimental results are from Shimozuma and Tagashira (Ref. 43).

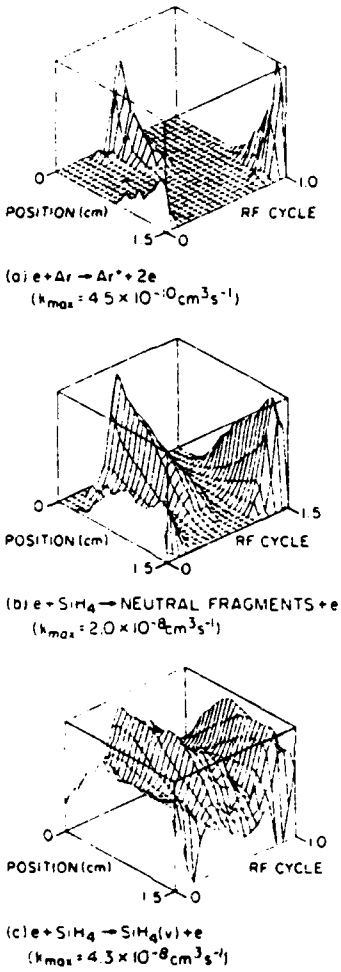


FIG. 4. Typical electron impact rate constants as used in the plasma chemistry model plotted as a function of position between parallel plate electrodes and time, expressed as fraction of the rf cycle; (a) electron impact ionization of argon, (b) neutral dissociation of silane, and (c) vibrational excitation of silane. As the threshold energy increases from vibrational excitation to ionization, the uniformity of excitation (position and time) decreases.

### 2. Neutral-neutral reactions

The neutral chemistry occurring in silane plasmas has been the topic of numerous previous investigations and is summarized in Refs. 2 and 7. We have benefited by those works and others, and have collated the suggested reaction pathways into a global set of reactions. The neutral-neutral reactions included in the model are listed in Table III.[12,25,26,28,44–62] In addition to the reactions suggested by previous investigators, we included polymerization reactions leading to the formation of higher silane radicals and molecules, and higher silane ions. These reactions are discussed in Sec. II A and III E. We also included homogeneous pyrolysis reactions of silane and disilane. The substrate temperatures typically used in PECVD are <500 K, and based on these temperatures, pyrolysis should not be important. For moderate power deposition (>25 mW cm$^3$) and

TABLE III. Neutral heavy particle reactions.

| Process | Rate constant[a] | Reference[b] |
|---|---|---|
| **Reactions with silane and disilane** | | |
| $SiH_4 + H \rightarrow SiH_3 + H_2$ | 2.68( − 12) | 26,44–46 |
| $SiH_4 + Si \rightarrow SiH_2 + SiH_2$ | 5.33( − 13) | 47 |
| $SiH_4 + SiH \rightarrow Si_2H_5$ | 2.50( − 12) | 25,46,48 |
| $SiH_4 + SiH \rightarrow Si_2H_3 + H_2$ | 1.70( − 12) | 25,46,48 |
| $SiH_4 + SiH_2 \rightarrow Si_2H_6^*$ | 1.00( − 11) | 12,25,26,47,49–51 |
| $SiH_4 + SiH_3 \rightarrow Si_2H_5 + H_2$ | 1.78( − 15) | 47 |
| $SiH_4 + Si_2H_4 \rightarrow Si_3H_8$ | 1.00( − 11) | est. (52) |
| $SiH_4 + Si_2H_5 \rightarrow Si_2H_6 + SiH_3$ | 5.00( − 13) | est. |
| $Si_2H_6 + SiH_3 \rightarrow SiH_4 + Si_2H_5$ | 1.00( − 12) | est. (53) |
| $Si_2H_6 + SiH_2 \rightarrow Si_3H_8$ | 1.20( − 10) | 12,50–52 |
| $Si_2H_6 + SiH \rightarrow Si_3H_7$ | 1.00( − 11) | PC |
| $Si_2H_6 + H \rightarrow SiH_3 + SiH_4$ | 1.11( − 12) | 53 |
| $Si_2H_6 + H \rightarrow H_2 + Si_2H_5$ | 2.16( − 12) | 49,53 |
| $Si_2H_6^* \rightarrow Si_2H_4 + H_2$ | 5.00(6)$s^{-1}$ | est. (28) |
| $Si_2H_6^* + M \rightarrow Si_2H_6 + M$ | 1.00( − 10) | est. (54) |
| $Si_2H_6^{**} \rightarrow H_2 + Si_2H_4$ | 2.30(7) $s^{-1}$ | est. (28) |
| $Si_2H_6^{**} \rightarrow SiH_4 + SiH_2$ | 2.30(7) $s^{-1}$ | est. (28) |
| $Si_2H_6^{**} + M \rightarrow Si_2H_6 + M$ | 2.00( − 10) | est. (54) |
| **Reactions of radicals with radicals, higher silanes, and hydrogen** | | |
| $SiH_3 + H \rightarrow SiH_2 + H_2$ | 1.00( − 10) | est. (44) |
| $SiH_3 + SiH_2 \rightarrow Si_2H_5$ | 3.77( − 13) | 46 |
| $SiH_3 + SiH_3 \rightarrow SiH_2 + SiH_4$ | 7.00( − 12) | 12,26–28,44 |
| $SiH_3 + SiH_3 \rightarrow Si_2H_6^{**}$ | 1.00( − 11) | 12,26,44 |
| $SiH_3 + Si_2H_5 \rightarrow Si_3H_8$ | 1.00( − 11) | est. (52) |
| $SiH_2 + Si \rightarrow Si_2H_2$ | 4.53( − 13) | 47 |
| $SiH_2 + SiH \rightarrow Si_2H_3$ | 7.22( − 13) | 47 |
| $SiH_2 + H_2 \rightarrow SiH_4$ | 2.00( − 13) | 50–52,55 |
| $SiH_2 + Si_3H_8 \rightarrow Si_4H_{10}$ | 1.00( − 11) | PC |
| $SiH_2 + H \rightarrow SiH + H_2$ | 7.96( − 13) | 46 |
| $SiH_2 + H \rightarrow SiH_3$ | 1.11( − 12) | 46 |
| $SiH + H_2 \rightarrow SiH_3$ | 1.98( − 12) | 47 |
| $Si + H_2 \rightarrow SiH_2$ | 6.59( − 12) | 47 |
| $Si_2H_4 + H_2 \rightarrow Si_2H_6$ | 5.33( − 13) | 47 |
| $Si_2H_4 + H_2 \rightarrow SiH_4 + SiH_2$ | 3.56( − 9) | 47 |
| $Si_2H_3 + H_2 \rightarrow Si_2H_5$ | 1.70( − 12) | 47 |
| $Si_2H_2 + H_2 \rightarrow Si_2H_4$ | 1.40( − 11) | 47 |
| $Si_2H_2 + H \rightarrow Si_2H_3$ | 4.94( − 11) | 47 |
| $Si_2H_5 + Si_2H_5 \rightarrow Si_4H_{10}$ | 1.00( − 11) | PC |
| $Si_2H_4 + Si_2H_6 \rightarrow Si_4H_{10}$ | 1.00( − 11) | PC |
| $SiH + Si_2H_6 \rightarrow Si_3H_7$ | 1.00( − 11) | PC |
| $Si_3H_7 + H \rightarrow Si_3H_8$ | 1.00( − 11) | PC |
| $SiH + Si_3H_8 \rightarrow Si_4H_9$ | 1.00( − 11) | PC |
| $SiH_3 + Si_3H_7 \rightarrow Si_4H_9 + H_2$ | 1.00( − 11) | PC |
| $Si_4H_9 + H \rightarrow Si_4H_{10}$ | 1.00( − 11) | PC |
| $SiH + Si_4H_{10} \rightarrow Si_5H_{11}$ | 1.00( − 11) | PC |
| $SiH_2 + Si_4H_{10} \rightarrow Si_5H_{12}$ | 1.00( − 11) | PC |
| $SiH_3 + Si_4H_{10} \rightarrow Si_5H_{11} + H_2$ | 1.00( − 11) | PC |
| $Si_5H_{11} + H \rightarrow Si_5H_{12}$ | 1.00( − 11) | PC |
| **Excitation transfer and radiative decay** | | |
| $[Ar^*,Ar^{**}] + H_2 \rightarrow H + H + Ar$ | 7.00( − 11) | 56 |
| $[Ar^*,Ar^{**}] + SiH_4 \rightarrow SiH_3 + H + Ar$ | 1.40( − 10) | c, 56–58 |
| $[Ar^*,Ar^{**}] + SiH_4 \rightarrow SiH_2 + H + H + Ar$ | 2.60( − 10) | c, 56–58 |
| $[Ar^*,Ar^{**}] + SiH_3 \rightarrow SiH_2 + H + Ar$ | 1.00( − 10) | c, 56–58 |
| $[Ar^*,Ar^{**}] + SiH_2 \rightarrow SiH + H + Ar$ | 1.00( − 10) | c, 56–58 |
| $[Ar^*,Ar^{**}] + SiH \rightarrow Si + H + Ar$ | 1.00( − 10) | c, 56–58 |
| $[Ar^*,Ar^{**}] + Si_2H_6 \rightarrow Si_2H_4 + H + H + Ar$ | 6.60( − 10) | c, 56–58 |
| $[Ar^*,Ar^{**}] + Si_2H_4 \rightarrow Si_2H_2 + H + H + Ar$ | 6.60( − 10) | c, 56–58 |
| $H_2^* + H_2^* \rightarrow H_2^+ + H_2 + e$ | 1.00( − 11) | est. |
| $Ar^{**} \rightarrow Ar^*$ | 1.00(7) $s^{-1}$ | est. |
| $H_2^* \rightarrow H_2$ | 1.00(7) $s^{-1}$ | est. |
| $H^* \rightarrow H$ | 2.00(7) $s^{-1}$ | est. |

TABLE III. (*continued*).

| Process | Rate constant[a] | Reference[b] |
|---|---|---|
| Vibrational relaxation (see text) | | |
| $SiH_4(v2,4) + SiH_4 \rightarrow SiH_4 + SiH_4$ | 1.92( − 13) | 59,60 |
| $SiH_4(v2,4) + Ar \rightarrow Ar + SiH_4$ | 1.86( − 14) | 60,61 |
| $SiH_4(v2,4) + H_2 \rightarrow H_2 + SiH_4$ | 3.05( − 12) | 60–62 |
| $SiH_4(v2,4) + Si_2H_6 \rightarrow Si_2H_6 + SiH_4$ | 5.71( − 11) | 60–62 |
| $SiH_4(v1,3) + SiH_4 \rightarrow SiH_4 + SiH_4(v2,4)$ | 6.08( − 11) | 60–62 |
| $SiH_4(v1,3) + Ar \rightarrow Ar + SiH_4(v2,4)$ | 5.37( − 12) | 60–62 |
| $SiH_4(v1,3) + H_2 \rightarrow H_2 + SiH_4(v2,4)$ | 1.53( − 10) | 60–62 |
| $SiH_4(v1,3) + Si_2H_6 \rightarrow Si_2H_6 + SiH_4(v2,4)$ | 3.00( − 10) | 60–62 |
| $Si_2H_6(v2,4) + SiH_4 \rightarrow SiH_4 + Si_2H_6$ | 6.40( − 12) | 60–62 |
| $Si_2H_6(v2,4) + Ar \rightarrow Ar + Si_2H_6$ | 1.09( − 12) | 60–62 |
| $Si_2H_6(v2,4) + H_2 \rightarrow H_2 + Si_2H_6$ | 1.80( − 10) | 60–62 |
| $Si_2H_6(v2,4) + Si_2H_6 \rightarrow Si_2H_6 + Si_2H_6$ | 1.13( − 11) | 60–62 |
| $Si_2H_6(v1,3) + SiH_4 \rightarrow SiH_4 + Si_2H_6(v2,4)$ | 3.00( − 10) | 60–62 |
| $Si_2H_6(v1,3) + Ar \rightarrow Ar + Si_2H_6(v2,4)$ | 3.00( − 10) | 60–62 |
| $Si_2H_6(v1,3) + H_2 \rightarrow H_2 + Si_2H_6(v2,4)$ | 3.00( − 10) | 60–62 |
| $Si_2H_6(v1,3) + Si_2H_6 \rightarrow Si_2H_6 + Si_2H_6(v2,4)$ | 3.00( − 10) | 60–62 |
| $SiH_4(v2,4) \rightarrow SiH_4$ | 2.50(00) | est. (62) |
| $Si_2H_6(v2,4) \rightarrow Si_2H_6$ | 2.50(00) | est. (62) |
| Homogeneous pyrolysis | | |
| $SiH_4 \rightarrow SiH_2 + H_2$ | 5.0(12)exp( − 52.2 kcal/$kT$) $s^{-1}$ | 47 |
| $SiH_4 \rightarrow SiH_3 + H$ | 3.7(15)exp( − 93.0 kcal/$kT$) $s^{-1}$ | 47 |
| $Si_2H_6 \rightarrow Si_2H_4 + H_2$ | 2.5(14)exp( − 52.2 kcal/$kT$) $s^{-1}$ | 47 |
| Reactions leading to formation of DUST ($X + Y \rightarrow$ DUST). [Uniform rate constant 1.0( − 11) $cm^3 s^{-1}$. See text] | | |
| $SiH_n + [Si_3H_{11}, Si_5H_{12}]$ | $Si_4H_9 + [Si_4H_9, Si_4H_{10}]$ | |
| $SiH_n + DUST$ | $Si_4H_9 + [Si_5H_{11}, Si_5H_{12}]$ | |
| $Si_2H_n + [Si_4H_9, Si_4H_{10}]$ | $Si_4H_9 + DUST$ | |
| $Si_2H_n + [Si_5H_{11}, Si_5H_{12}]$ | $Si_5H_{11} + [Si_5H_{11}, Si_5H_{12}]$ | |
| $Si_2H_n + DUST$ | $Si_5H_{11} + DUST$ | |
| $Si_3H_7 + [Si_3H_7, Si_3H_8]$ | | |
| $Si_3H_7 + [Si_4H_9, Si_4H_{10}]$ | | |
| $Si_3H_7 + [Si_5H_{11}, Si_5H_{12}]$ | | |
| $Si_3H_7 + DUST$ | | |

[a] $1.50(-10) \equiv 1.50 \times 10^{-10}$. Rate constants have units of $cm^3 s^{-1}$ unless otherwise noted.

[b] PC denotes that the reaction is hypothesized as being part of the polymerization chain leading to formation of DUST and has an estimated rate constant (see text).

[c] Rate constant estimated by analogy to $CH_4$, $C_2H_6$, and their radicals.

electrode separations ($d > 3$ cm), though, the centerline gas temperature can exceed the substrate temperature by many hundreds of degrees (see Sec. II C). For these conditions, pyrolysis will occur in the bulk plasma. Rates for homogeneous pyrolysis of silane and disilane were obtained from Coltrin, Kee, and Miller.[47]

A subset of the rate constants listed in Table III was estimated and they are so noted in the table. The major classes of rate constants that were estimated are those for the polymerization chain (see above), Penning reactions of electronically excited argon with silane and disilane, and collisional deactivation of $SiH_4(v1,3; v2,4)$ and $Si_2H_6(v1,3; v2,4)$. For the Penning reactions, (e.g., $Ar^* + SiH_4 \rightarrow SiH_3 + H + Ar$), we used the analogous rates for Penning reactions of argon with methane ($CH_4$).[56–58] Rate constants for vibrational relaxation of silane and disilane were also obtained by analogy to methane. In methane, rapid vibrational relaxation proceeds by

$$CH_4(v1,3) \xrightarrow{M} CH_4(v2,4) \xrightarrow{M} CH_4(v0,0). \quad (3)$$

Rate constants for the vibrational relaxation of $CH_4$ by Ar, $H_2$, $CH_4$, and other molecules are available, as well as for the vibrational relaxation of silane by silane.[59–62] By comparing the rate of self-relaxation of silane to that of methane, one obtains a scaling parameter representing the ratio of the average mutual interaction potential, approximately 8.9. This value was used to scale the vibrational relaxation rates of methane with various collision partners to silane. The results are shown in Table III.

Rate constants were also estimated when quoted or measured values varied over a large range. In this class of reactions are the important processes:

$$H + SiH_4 \rightarrow SiH_3 + H_2, \quad (4)$$

$$SiH_2 + SiH_4 \rightarrow Si_2H_6^{**} + M \rightarrow Si_2H_6 \quad (5a)$$
$$\downarrow$$
$$Si_2H_4 + H_2$$
$$\uparrow$$
$$SiH_3 + SiH_3 \rightarrow Si_2H_6^{**} + M \rightarrow Si_2H_6 \quad (5b)$$
$$\rightarrow SiH_2 + SiH_4. \quad (5c)$$

Reactions (4) and (5a) are important because they are first-order reactions of the dissociation products of silane with silane. The former hydrogen abstraction reaction is effectively a radical multiplication reaction. A radical which does not directly contribute to film growth, H, is exchanged for a radical that will be incorporated into the film, $SiH_3$. The latter reaction is important for the opposite effect; a radical which can be directly incorporated in the film, $SiH_2$, is exchanged for either a saturated molecule ($Si_2H_6$) which is not incorporated into the film, or a molecule ($Si_2H_4$) which likely has a lower sticking coefficient. Although reactions (5c) and (5d) are second order, they are important because the most probable branches reduce by at least half the number of radicals which can contribute to film growth. Observations that film growth increases less than linearly with increasing discharge power could be attributed to this reaction, whose rate scales as the square of the rate of dissociation of silane.[63] The rate constants for these reactions were studied parametrically, as reported in Ref. 26. The values for the rate constants listed inTable III are those resulting from this study.

### 3. Ion-neutral

The ion-molecule reactions included in the model are listed in Table IV.[14,65–73] Rate constants or cross sections have been measured for $Si_nH_m^+$,[65–69] $H_n^+$,[69] and $Ar^+$[64,70] collisions with silane and disilane as a function of ion energy. Ion-molecule reactions were placed in endothermic and exothermic categories based on the average gas temperature. The endothermic reactions typically have energy defects of a few eV. Those reactions classed as exothermic were included in the model at all locations in the discharge. Those reactions classed as endothermic were included only in the sheaths. Positive ions in the sheaths are accelerated to energies in excess of the energy defect, thereby allowing reactions which are endothermic in the bulk plasma to occur in the sheaths. The endothermic ion-molecule reactions for which this applies are labeled by "E" in Table IV.

Ion molecule reactions between $Si_nH_m^+$ ions and silane or disilane generally add silicon atoms to the ions for $n \leq 5$–6. For example, the major branches for reactions of $Si_2H_2^+$ with silane and disilane are[14,67,68]

$$Si_2H_2^+ + SiH_4 \rightarrow Si_3H_6^+, \quad (6a)$$
$$Si_2H_2^+ + Si_2H_6 \rightarrow Si_4H_8^+. \quad (6b)$$

Such addition reactions have nearly gas kinetic rate constants ($\simeq 10^{-10}$ cm$^3$ s$^{-1}$). As a result, higher silane ions can be generated quickly in silane plasmas from the products of the dissociative ionization of silane, primarily $SiH_3^+$ and $SiH_2^+$.

In analogy to the neutral polymerization model described in Sec. II A, we hypothesized a "clustering" chain for higher silane ions. The clustering reaction of lower silane ions with higher silane saturated molecules has the form of

$$SiH^+ + Si_mH_{2(m+1)} \rightarrow Si_{m+1}H_{2(m+1)}^+ + H, \quad (7a)$$
$$SiH_2^+ + Si_mH_{2(m+1)} \rightarrow Si_{m+1}H_{2(m+1)}^+ + H_2, \quad (7b)$$
$$SiH_3^+ + Si_mH_{2(m+1)} \rightarrow Si_{m+1}H_{2(m+1)}^+ + H_2 + H. \quad (7c)$$

Rate constants for reactions in the clustering chain were estimated to be $10^{-11}$ cm$^3$ s$^{-1}$, if not otherwise available.

Recent work by Mandich, Reents, and Jarrold[74] has shown that ion-molecule reactions of the form of

$$Si_nD_m^+ + SiD_4 \rightarrow Si_{n+1}D_{m+2}^+ + D_2 \quad (8)$$

form a chain which may terminate with $n = 4$ due to an activation energy barrier. In a plasma, a significant activation energy is available in the form of excited states of the reactants and which may aid in breaching any activation energy barrier in the chain. Since silane, as the feedstock, has the highest number density of any reactant, sequential ion-molecule reactions with silane could potentially and rapidly lead to higher silane ions if the chain propagates. This topic will be discussed further in Sec. III E.

Ion-molecule reactions of $H_2^+$ and $Ar^+$ with silane (and disilane) usually result in charge exchange to silane and reduce the number of H atoms in the product ions. (The $SiH_4^+$ ion has only been observed under near collisionless conditions and is believed to be unstable in typical discharges.) The differences in the ionization potentials of hydrogen (15.4 eV) and argon (15.8 eV) with the appearance potentials of ions from silane (11.6 eV) and disilane (9.9 eV) are a reservoir of energy for dissociative branches. Typical reactions are[64,69,70]

$$H_2^+ + SiH_4 \rightarrow SiH_3^+ + H_2 + H, \quad (9a)$$
$$Ar^+ + Si_2H_6 \rightarrow Si_2H^+ + 2H_2 + H. \quad (9b)$$

Ion-molecule reactions of $Ar^+$ with silane have unusually small rate constants ($1–4 \times 10^{-12}$ cm$^3$ s$^{-1}$) when compared to the same reactions for $H_2^+$, $Ne^+$, and $He^+$.[64,70] The fraction of $Ar^+$ ions in $Ar/SiH_4$ gas mixtures will therefore be larger than the analogous fractions in gas mixtures containing hydrogen, neon, or helium.

### 4. Ion-ion and electron-ion reactions

The ion-ion and electron-ion reactions and rate constants included in the model are listed in Table V.[75–79] Negative ions are formed in silane plasmas by the dissociative attachment reactions

$$e + SiH_4 \rightarrow SiH_3^- + H \quad (10a)$$
$$\rightarrow SiH_2^- + H_2. \quad (10b)$$

The cross sections for dissociative attachment to silane and disilane are small ($\lesssim 2 \times 10^{-18}$ cm$^2$),[30,31] as are the rate constants ($10^{-13}$–$10^{-12}$ cm$^3$ s$^{-1}$). Negative ions, though, are not lost rapidly to the walls due to the negative space charge there. They are lost dominantly by electron impact detachment and ion–ion neutralization reactions. The electronegativity (fraction of negative ions compared to the total density

TABLE IV. Ion-molecule reactions.

| Process | Rate constant[a] | Reference[b] |
|---|---|---|
| $SiH_3^+ + SiH_4 \rightarrow Si_2H^+ + H_2 + H_2 + H_2$ | 0.13( − 10) E | 14,65 |
| $SiH_3^+ + SiH_4 \rightarrow Si_2H_2^+ + H_2 + H_2 + H$ | 0.25( − 10) E | 14,65 |
| $SiH_3^+ + SiH_4 \rightarrow Si_2H_3^+ + H_2 + H_2$ | 0.07( − 10) | 66 |
| $SiH_3^+ + SiH_4 + Si_2H_3^+ + H_2$ | 0.25( − 10) | 14,66 |
| $SiH_3^+ + SiH_4 + M \rightarrow Si_2H_7^+ + M$ | 1.80( − 26) $cm^6\ s^{-1}$ | 67 |
| $SiH_3^+ + Si_2H_6 \rightarrow Si_2H_5^+ + SiH_4$ | 5.20( − 10) | 68 |
| $SiH_3^+ + Si_2H_6 \rightarrow Si_3H_6^+ + H_2 + H$ | 3.50( − 10) | 68 |
| $SiH_3^+ + Si_3H_8 \rightarrow Si_4H_8^+ + H_2 + H$ | 1.00( − 11) | PC |
| $SiH_3^+ + Si_4H_{10} \rightarrow Si_5H_{10}^+ + H_2 + H$ | 1.00( − 11) | PC |
| $SiH_2^+ + SiH_4 \rightarrow SiH_3^+ + SiH_3$ | 1.07( − 9) | 66 |
| $SiH_2^+ + SiH_4 \rightarrow Si_2H^+ + H_2 + H_2 + H$ | 0.13( − 10) E | 65 |
| $SiH_2^+ + SiH_4 \rightarrow Si_2H_2^+ + H_2 + H_2$ | 0.55( − 10) | 66 |
| $SiH_2^+ + SiH_4 \rightarrow Si_2H_2^+ + H_2 + H + H$ | 0.70( − 10) E | 65 |
| $SiH_2^+ + SiH_4 \rightarrow Si_2H_3^+ + H_2 + H$ | 0.12( − 10) E | 14,65 |
| $SiH_2^+ + SiH_4 \rightarrow Si_2H_4^+ + H_2$ | 2.50( − 10) | 14,65 |
| $SiH_2^+ + SiH_4 \rightarrow Si_2H_5^+ + H$ | 0.08( − 10) E | 65 |
| $SiH_2^+ + H_2 \rightarrow SiH_3^+ + H$ | 1.01( − 10) E | 69 |
| $SiH_2^+ + Si_2H_6 \rightarrow Si_2H_2^+ + SiH_4 + H_2$ | 1.40( − 10) | 68 |
| $SiH_2^+ + Si_2H_6 \rightarrow Si_2H_2^+ + SiH_4 + H_2$ | 3.10( − 10) | 68 |
| $SiH_2^+ + Si_2H_6 \rightarrow Si_2H_5^+ + SiH_3$ | 3.60( − 10) | 68 |
| $SiH_2^+ + Si_2H_6 \rightarrow Si_3H_6^+ + H_2$ | 5.62( − 10) | 68 |
| $SiH_2^+ + Si_3H_8 \rightarrow Si_4H_8^+ + H_2$ | 1.00( − 11) | PC |
| $SiH_2^+ + Si_4H_{10} \rightarrow Si_5H_{10}^+ + H_2$ | 1.00( − 11) | PC |
| $SiH^+ + SiH_4 \rightarrow SiH_3^+ + SiH_2$ | 0.60( − 10) E | 14,65 |
| $SiH^+ + SiH_4 \rightarrow Si_2H^+ + H_2 + H + H$ | 1.20( − 10) E | 65 |
| $SiH^+ + SiH_4 \rightarrow Si_2H^+ + H_2 + H_2$ | 0.70( − 10) | 14,66 |
| $SiH(v)^+ + Si_2H^+ + H_2 + H_2$ | 1.20( − 9) | 90d,e |
| $SiH^+ + SiH_4 \rightarrow Si_2H_2^+ + H_2 + H$ | 0.52( − 10) E | 65 |
| $SiH^+ + SiH_4 \rightarrow Si_2H_3^+ + H_2$ | 2.80( − 10) | 66 |
| | 5.20( − 10) | 90d |
| $SiH^+ + SiH_4 + M \rightarrow Si_2H_5^+ + M$ | 1.30( − 26) | 67 |
| $SiH^+ + H_2 \rightarrow SiH_2^+ + H$ | 1.84( − 11) E | 69 |
| $SiH^+ + Si_2H_6 \rightarrow Si_2H^+ + SiH_4 + H_2$ | 1.10( − 10) | 68 |
| $SiH^+ + Si_2H_6 \rightarrow Si_2H_3^+ + SiH_4$ | 3.30( − 10) | 68 |
| $SiH^+ + Si_2H_6 \rightarrow Si_3H_6^+ + H$ | 5.50( − 10) | 68 |
| $SiH^+ + Si_3H_8 \rightarrow Si_4H_8^+ + H$ | 1.00( − 11) | PC |
| $SiH^+ + Si_4H_{10} \rightarrow Si_5H_{10}^+ + H$ | 1.00( − 11) | PC |
| $Si^+ + SiH_4 \rightarrow Si_2H_2^+ + H_2$ | 4.80( − 10) | 66 |
| | 6.90( − 10) | 79d |
| $Si^+ + SiH_4 \rightarrow Si_2H_3^+ + H$ | 0.15( − 10) E | 14,65 |
| $Si^+ + SiH_4 \rightarrow Si_2H^+ + H_2 + H$ | 0.15( − 10) E | 14,65 |
| $Si^+ + SiH_4 + M \rightarrow Si_2H_4^+ + M$ | 1.40( − 26) $cm^6\ s^{-1}$ | 67 |
| $Si^+ + Si_2H_6 \rightarrow Si_2H_2^+ + SiH_4$ | 7.80( − 10) | 68 |
| $Si^+ + Si_2H_6 \rightarrow Si_3H_6^+$ | 2.40( − 10) | 68 |
| $Si_2H_7^+ + SiH_4 \rightarrow Si_3H_6^+ + H_2 + H_2 + H$ | 5.00( − 11) | 14 |
| $Si_2H_6^+ + SiH_4 \rightarrow Si_3H_6^+ + H_2 + H_2$ | 5.00( − 11) | 14 |
| $Si_2H_5^+ + SiH_4 \rightarrow Si_3H_6^+ + H_2 + H$ | 5.00( − 11) | 14 |
| $Si_2H_4^+ + SiH_4 \rightarrow Si_3H_6^+ + H_2$ | 5.20( − 11) | 14,67 |
| $Si_2H_3^+ + SiH_4 \rightarrow Si_3H_6^+ + H$ | 5.00( − 11) | 14,67 |
| $Si_2H_2^+ + SiH_4 \rightarrow Si_3H_6^+$ | 3.76( − 11) | 14,67 |
| $Si_2H_2^+ + SiH_4 \rightarrow Si_3H_4^+ + H_2$ | 3.20( − 11) | 79d,e |
| $Si_2H^+ + SiH_4 \rightarrow Si_2H_2^+ + H_2 + H_2$ | 3.10( − 10) | 90d,e |
| $Si_2H^+ + SiH_4 \rightarrow Si_3H_6^+$ | 1.08( − 10) | 14,67 |
| $Si_2H_6^+ + Si_2H_6 \rightarrow Si_2H_7^+ + Si_2H_5$ | 5.80( − 10) | 68 |
| $Si_2H_5^+ + Si_2H_6 \rightarrow Si_3H_6^+ + SiH_4 + H$ | 0.86( − 10) | 68 |
| $Si_2H_4^+ + Si_2H_6 \rightarrow Si_3H_6^+ + SiH_4$ | 0.65( − 10) | 68 |
| $Si_2H_4^+ + Si_2H_6 \rightarrow Si_4H_8^+ + H_2$ | 1.40( − 10) | 68 |
| $Si_2H_3^+ + Si_2H_6 \rightarrow Si_3H_6^+ + SiH_3$ | 1.87( − 10) | 68 |
| $Si_2H_3^+ + Si_2H_6 \rightarrow Si_4H_8^+ + H$ | 3.34( − 10) | 68 |
| $Si_2H_2^+ + Si_2H_6 \rightarrow Si_3H_6^+ + SiH_2$ | 1.10( − 10) | 68 |
| $Si_2H_2^+ + Si_2H_6 \rightarrow Si_4H_8^+$ | 2.95( − 10) | 68 |
| $Si_2H^+ + Si_2H_6 \rightarrow Si_3H_6^+ + SiH$ | 0.50( − 10) | 68 |

TABLE IV. (*continued*).

| Process | Rate constant[a] | Reference[b] |
|---|---|---|
| $Si_2H^+ + Si_2H_6 \rightarrow Si_4H_8^+$ | 4.90( − 10) | 68 |
| $Si_mH_n^+ + SiH_4 \rightarrow Si_{m+1}H_{n+2} + H_2$ | 1.00( − 11) | PC,c |
| $Si_3H_4^+ + SiH_4 \rightarrow Si_4H_6^+ + H_2$ | 1.70( − 10) | 79d,e |
| $Si_4H_6^+ + SiH_4 \rightarrow Si_5H_{10}^+$ | 1.00( − 13) | 79d,e |
| $Si_4H_2^+ + SiH_4 \rightarrow Si_5H_4^+ + H_2$ | 1.30( − 10) | 90d,e,f |
| $H^+ + SiH_4 \rightarrow SiH_3^+ + H_2$ | 5.00( − 10) | est. |
| $H_2^+ + SiH_4 \rightarrow Si^+ + H_2 + H_2 + H_2$ | 3.66( − 11) | 69 |
| $H_2^+ + SiH_4 \rightarrow SiH^+ + H_2 + H_2 + H$ | 3.66( − 11) | 69 |
| $H_2^+ + SiH_4 \rightarrow SiH_2^+ + H_2 + H_2$ | 6.59( − 11) | 69 |
| $H_2^+ + SiH_4 \rightarrow SiH_3^+ + H_2 + H$ | 6.23( − 10) | 69 |
| $H_2^+ + SiH_4 \rightarrow SiH_3 + H_2^+$ | 1.83( − 11) | 69 |
| $H_3^+ + SiH_4 \rightarrow SiH_3^+ + H_2 + H_2$ | 5.16( − 10) | 69 |
| $Ar^+ + SiH_4 \rightarrow Si^+ + H_2 + H_2 + Ar$ | 1.18( − 11) | 64,70 |
| $Ar^+ + SiH_4 \rightarrow SiH^+ + H + H_2 + Ar$ | 4.20( − 12) | 64,70 |
| $Ar^+ + SiH_4 \rightarrow SiH_2^+ + H_2 + Ar$ | 1.66( − 12) | 64,70 |
| $Ar^+ + SiH_4 \rightarrow SiH_3^+ + H + Ar$ | 2.40( − 12) | 64,70 |
| $Ar^+ + Si_2H_6 \rightarrow Si_2H^+ + H_2 + H_2 + H + Ar$ | 1.80( − 10) | 64,70 |
| $Ar^+ + Si_2H_6 \rightarrow Si_2H_2^+ + H_2 + H_2 + Ar$ | 6.50( − 11) | 64,70 |
| $Ar^+ + Si_2H_6 \rightarrow Si_2H_3^+ + H_2 + H + Ar$ | 5.50( − 11) | 64,70 |
| $H_2^+ + H_2 \rightarrow H_3^+ + H$ | 2.10( − 9) | 71 |
| $Ar^+ + H_2 \rightarrow ArH^+ + H$ | 7.40( − 10) | 72 |
| $H_3^+ + Ar \rightarrow ArH^+ + H_2$ | 1.00( − 11) | 73 |
| $ArH^+ + H_2 \rightarrow H_3^+ + Ar$ | 1.50( − 9) | 73 |

[a] $1.5(-10) \equiv 1.5\times10^{-10}$. Rate constants have units of $cm^3\,s^{-1}$ unless otherwise noted. The notation "E" by the rate constant specifies that this reaction is endothermic in the bulk plasma and occurs only in the sheaths (see Sec. II B 3).
[b] PC denotes that the reaction is hypothesized as being part of an ion clustering chain and has an estimated rate constant (see Sec. II B 3).
[c] See Sec. III E.
[d] This most recent value of reaction rate constant for analogous deuterated species was not available at the time of formulation of the model. The rate constant is listed for reference.
[e] This reaction was not explicitly included in the model.
[f] Structural isomeric reactant ion, estimated abundance 0.75.

TABLE V. Charged particle-charge particle reactions.

| Reaction | Rate constant[a] | Reference |
|---|---|---|
| Electron-ion recombination[b] | | |
| $e + SiH_2^+ \rightarrow SiH + H$ | 1.69( − 7) | 75 |
| $e + SiH_3^+ \rightarrow SiH_2 + H$ | 1.69( − 7) | 75 |
| $e + SiH^+ \rightarrow Si + H$ | 1.69( − 7) | 75 |
| $e + Si_2H^+ \rightarrow Si + H + H$ | 1.69( − 7) | 75 |
| $e + Si_2H_2^+ \rightarrow Si + Si + H_2$ | 1.69( − 7) | 75 |
| $e + Si_2H_m^+ (m>3) \rightarrow Si_2H_{(m-1)} + H$ | 1.69( − 7) | 75 |
| $e + Si_4H_6^+ \rightarrow Si_2H_4 + SiH_2$ | 1.69( − 7) | 75 |
| $e + Si_4H_8^+ \rightarrow Si_2H_6 + Si_2H_2$ | 1.69( − 7) | 75 |
| $e + Si_5H_{10}^+ \rightarrow Si_3H_8 + Si_2H_2$ | 1.69( − 7) | 75 |
| $e + H_2^+ \rightarrow H^* + H$ | 5.66( − 8) | 76 |
| $e + H_3^+ \rightarrow H_2^* + H$ | 9.75( − 8) | 76 |
| $e + H^+ \rightarrow H^*$ | 2.62( − 13) | 76 |
| $e + Ar^+ \rightarrow Ar^{**}$ | 8.15( − 13) | 77 |
| Ion-ion neutralization | | |
| $SiH_n^- + Si_lH_m \rightarrow SiH_n + Si_lH_m$ | 5.00( − 7) | est. (78,79) |
| $SiH_n^- + M^+ \rightarrow M + SiH_n$ | 1.00( − 7) | est. (78,79) |

[a] $1.5(-10) \equiv 1.5\times10^{-10}$. Rate constants have units of $cm^3\,s^{-1}$ unless otherwise noted.
[b] Rate constants for dissociative recombination of $Si_lH_m^+$ were estimated by analogy to methane.

of negative ions and electrons) of silane plasmas can therefore be many tenths to near unity. We estimated that ion-ion neutralization reactions between silane ions (e.g., $SiH_3^- + SiH_3^+ \rightarrow 2\,SiH_3$) have uniform rate constants of $5\times10^{-7}$ $cm^3\,s^{-1}$, whereas neutralization between unlike ions (e.g., $SiH_3^- + Ar^+ \rightarrow SiH_3 + Ar$) have rate constants of $1\times10^{-7}$ $cm^3\,s^{-1}$.[78,79]

Electron-ion recombination in the bulk plasma of glow discharges typically occurs by radiative recombination (e.g., $e + A^+ \rightarrow A^*$), collisional radiative recombination (e.g., $e + e + A^+ \rightarrow A^* + e$), or dissociative recombination of molecular ions [e.g., $e + H_2^+ \rightarrow H + H(v)$]. Typical rate constants for these processes are $10^{-13}/T_e^{1/2}$ $cm^3\,s^{-1}$, $10^{-27}/T_e^{9/2}$ $cm^6\,s^{-1}$, and $10^{-7}/T_e^{1/2}$ $cm^3\,s^{-1}$, respectively, where the electron temperature $T_e$ has units of eV. For typical bulk electron temperatures of 1–2 eV and ion densities of $10^9$–$10^{10}$ $cm^{-3}$, only dissociative recombination is a significant electron/ion loss mechanism when compared to diffusion to the walls, attachment, and ion-ion neutralization.

The products for dissociative recombination of silane ions, as well as the rate constants, have not been measured. The rate of dissociative recombination of $CH_4^+$, though, has been obtained by Kline.[75] By analogy, the cross section cor-

responding to this rate was used for the dissociative recombination of all silane ions in the model. These reactions have the general form

$$e + Si_nH_m^+ \rightarrow Si_nH_m^* \rightarrow Si_nH_{(m-1)} + H. \quad (11)$$

The actual product distribution depends upon the details of the curve crossing of the potential surfaces for the intermediate excited state and products. There would though, be sufficient energy in the intermediate state to break any multiple bond and therefore result in a variety of products. In the absence of knowledge of the actual product distribution, we chose the indicated products for all dissociative recombinations.

### C. Gas heating

Heating of the gas by power deposition is important in at least two respects. First, since the deposition reactor is isobaric, the reactant gas density is inversely proportional to the local gas temperature. Second, for sufficiently high temperatures ($T_g \geqslant 800$ K) gas phase pyrolysis will occur.

Heat transfer within the plasma can be described by Ficks law provided the molecular mean free path is much less than the electrode separation (see Sec. II A); and $\Lambda^2/\alpha \ll \Delta t$, where $\alpha$ is the thermal diffusivity, $\Lambda$ is the reactor diffusion length, and $\Delta t$ is the gas residence time between the electrodes. The thermal diffusivity is $\alpha = \nu/(\mathrm{Pr}\rho)$, where $\nu$ is the viscosity, Pr is the Prandtl number, and $\rho$ is the gas mass density (see Sec. II D). For our conditions in pure silane, $\alpha \simeq 2\times10^3$ cm$^2$ s$^{-1}$. Thermal diffusion is therefore a good description for heat transfer provided that $\Delta t \gg 0.05\,d^2$ ms, where the electrode spacing $d$ is in cm. This condition is met for all electrode spacings and residence times of interest. The gas temperature is therefore in quasiequilibrium with discharge power deposition and the gas temperature in a symmetric parallel plate geometry is approximately

$$T_g(x) \simeq T_s + \left(\frac{d^2P}{\pi^2\kappa}\right)\cos\left(\frac{x\pi}{d}\right). \quad (12)$$

$T_s$ is the substrate temperature, $\kappa$ is the thermal conductivity ($\simeq 8\times10^{-5}$ W cm$^{-1}$ K$^{-1}$ for pure silane), $P$ is power deposition excluding that dissipated by ions striking the electrodes, and $x$ is measured from the midplane of the reactor. In this expression, we have assumed that power deposition by electron collisions is uniform throughout the discharge. The average gas temperature is $\overline{T} = T_s + (2d^2P)/(\pi^3\kappa)$. For example, with an electrode separation of 2.5 cm and power deposition of 25 mW cm$^{-3}$, the centerline gas temperature $T_s$ + 200 K and the average gas temperature is $T_s$ + 130 K.

### D. Transport coefficients and thermodynamic properties

Diffusion coefficients for neutral species were obtained by assuming diffusion through the feedstock gases. Coefficients were computed using Lennard–Jones parameters in the manner described in Ref. 80. Lennard–Jones parameters for silane species were assumed to be the same as their methane counterparts, when available, and estimated when not. The parameters as used in the model are listed in Table VI. These parameters were also estimated, with qualitatively different results in Ref. 46.

The heat capacities of the input gases (Ar, $H_2$, $SiH_4$, and $Si_2H_6$) were obtained as a function of temperature from a various sources during model development. They are now summarized in a thermodynamic data base published as Ref. 81. In that compilation, the heat capacity is expressed as the sum

$$c_p/R = \sum_{i=0,5} a_i T^i.$$

The coefficients for silane ($i = 0,5$) are: 2.475 1668, $9.003\,721\,18\times10^{-3}$, $2.185\,394\,35\times10^{-6}$, $-2.681\,423\,08\times10^{-9}$, $-6.621\,080\,64\times10^{-13}$.

The thermal conductivity, $\kappa$, of the gas mixture was obtained from $\kappa = \nu c_p/\mathrm{Pr}$[82] where $\nu$ is the viscosity and Pr is the Prandtl number. The viscosity of the mixture was computed from Lennard–Jones parameters as described in Ref. 80. The Prandtl number is $\mathrm{Pr} = 4\gamma/(9\gamma - 5)$ where the specific heat ratio $\gamma = (c_p/R)/(c_p/R - 1)$.

The mobility of ions in the gas mixture were calculated from $\mu = 1/\Sigma_i(1/\mu_i)$, where $\mu_i$ is the mobility of the ion in gas $i$. Mobilities of silane ions, $Si_nH_m^+$, in silane were obtained from Chatham and Gallagher,[14] having low-field limits of 1180 and 675 cm$^2$ Torr/V s for $n = 1$ and $n = 2$. The mobilities of $Ar^+$ in Ar, $H^+$ in $H_2$, and $H_3^+$ in $H_2$ were obtained from the compilations of Ellis and co-workers.[83] The mobilities of other ions were calculated from $\mu_0 = 2.46\times10^4/[(M/m^{0.5})T_g^{0.5}\sigma]$ cm$^2$/V s, where $\mu_0$ is the mobility at standard temperature and pressure, $M$ is the molecular weight (amu), $m$ is the reduced mass with the collision partner (amu), $T_g$ is the gas temperature (K), and $\sigma$ is the sum of the elastic and charge exchange cross sections (A$^2$). The charge exchange cross sections were obtained from the charge exchange rate constants listed in Table IV. The elastic cross section was assumed to be 10 A$^2$ for all species.

### E. Boundary and initial conditions, and deposition rate

The simulation begins with the density of all radicals being zero, and the density of the feedstocks being determined by the absolute pressure, gas temperature, and their

TABLE VI. Estimated Lennard–Jones parameters for neutral species.

| Species | $\sigma$(A) | $\epsilon$(K) |
|---|---|---|
| Ar | 3.44 | 120 |
| $H_2$ | 2.94 | 36 |
| H | 2.50 | 30 |
| Si | 3.84 | 100 |
| $SiH_4$ | 3.84 | 140 |
| $Si_2H_2$ | 4.22 | 185 |
| $Si_2H_4$ | 4.23 | 195 |
| $Si_2H_4$ | 4.23 | 205 |
| $Si_2H_5$ | 4.33 | 217 |
| $Si_2H_6$ | 4.42 | 230 |
| $Si_3H_6$ | 5.08 | 254 |
| $Si_4H_8$ | 5.80 | 254 |
| $Si_5H_{10}$ | 6.50 | 254 |

mole fractions. The electron and ion densities are set to small initial values ($\simeq 10^7\ cm^{-3}$). All positive ions are assumed to be neutralized at the boundaries by either electrons or negative ions, with the products returning to the plasma. The fraction of negative ions which are neutralized at the wall is determined by the appropriate ratio of fluxes between electrons and negative ions.

Molecules which do not stick to the surface have the boundary condition $\partial N/\partial x(x = \pm d/2) = 0$. Radicals with unity sticking coefficient have the boundary condition of $N(x = \pm d/2) = 0$. Those radicals with a nonunity sticking coefficient $s$ are treated as having a net flux "sink" at the wall of magnitude $sD(\partial N/\partial x)$. The sticking coefficients of saturated molecules is zero, whereas those for $Si_nH_m$, $m \leq 2n$ are unity. The sticking coefficient of radicals with $m = 2n + 1$ (e.g., $SiH_3$) is 0.15, in accordance with recent measurements.[63] The initial transient in gas temperature, which lasts for a ms or less, is usually ignored and the initial gas temperature is set equal to the values as given in Sec. II C.

The deposition rates of amorphous silicon on the substrates at $x = \pm d/2$ are given by

$$R_d = \Sigma_i b^3 n_i s_i D_i \nabla N_i \left(x = \pm \frac{d}{2}\right),$$

where $b$ is the average bond length (2.8 Å) between silicon atoms in the film, $n_i$ is the number of silicon atoms in radical $i$, $s_i$ is the sticking coefficient, $D_i$ is the diffusion coefficient, and number density of the radical is $N_i$.

## III. RESULTS

In this section, results from the plasma deposition model will be discussed for discharges in mixtures of silane and argon or hydrogen. In each case, we have assumed that the parallel plate reactor is symmetric; therefore results are plotted as a function of position only from the left electrode to the center line. Power deposition is cited as W $cm^{-3}$ averaged over the volume of the reactor. The substrate temperature is 500 K. Species densities presented as a function of position between the electrodes are for a time after the input species have flowed downstream and reached their quasi-steady-state conditions. These conditions are defined as when mono- and di-silane radicals and ions have reached an equilibrium, and the silane has been depleted by $\leq 0.1$. This value corresponds roughly to 20 mJ/Torr $cm^{-3}$ of silane. Higher silane radicals, saturated molecules, and DUST may continue to increase in density beyond the equilibration time for lower radicals.

### A. Typical results

Species densities for a discharge sustained in 250 mTorr of silane between electrodes with 2.5-cm separation with a power deposition of 25 mW $cm^{-3}$ are shown in Figs. 5–8. The computed deposition rate of $a$-Si:H for these conditions is $\simeq 250$ A/min, which agrees well with experimental values for similar conditions.[3] The time evolution of the density of saturated molecules is shown in Fig. 5(a). At the end point, silane has been depleted by 8%. The stable product with the highest density is $H_2$ representing a net deposition reaction of $SiH_4(g) \rightarrow Si{:}H(s) + H_2(g)$, where $(g)$ and $(s)$ denote gas phase and solid species, respectively. Based only on volumetric processes, the next most abundant saturated product is initially $Si_3H_8$, but after a short flow downstream is replaced by $Si_2H_6$. This condition is likely a result of the rapid reaction sequence

$$SiH_2 + SiH_4 \rightarrow Si_2H_6^{**} \rightarrow Si_2H_4 + H_2 \xrightarrow{SiH_4} Si_3H_8 + H_2 \quad (13a)$$

$$\qquad\qquad\quad \rightarrow + M \rightarrow Si_2H_6 \xrightarrow[SiH_2]{} Si_3H_8 \quad (13b)$$

which depletes disilane. Only after a sufficient density of $H_2$ builds up does the reverse reaction $H_2 + Si_2H_4 \rightarrow Si_2H_6$ become frequent enough to reduce the relative importance of reaction (13a). Operating at a higher pressure also reduces the relative importance of this reaction, thereby increasing the density of disilane by increasing the branching ratio of reaction (13b). This effect that can also be obtained by diluting with $H_2$. In fact, in a $SiH_4/H_2 = 1/1$ gas mixture for the same discharge conditions, the density of disilane is always at least twice that for trisilane. Higher silanes having more

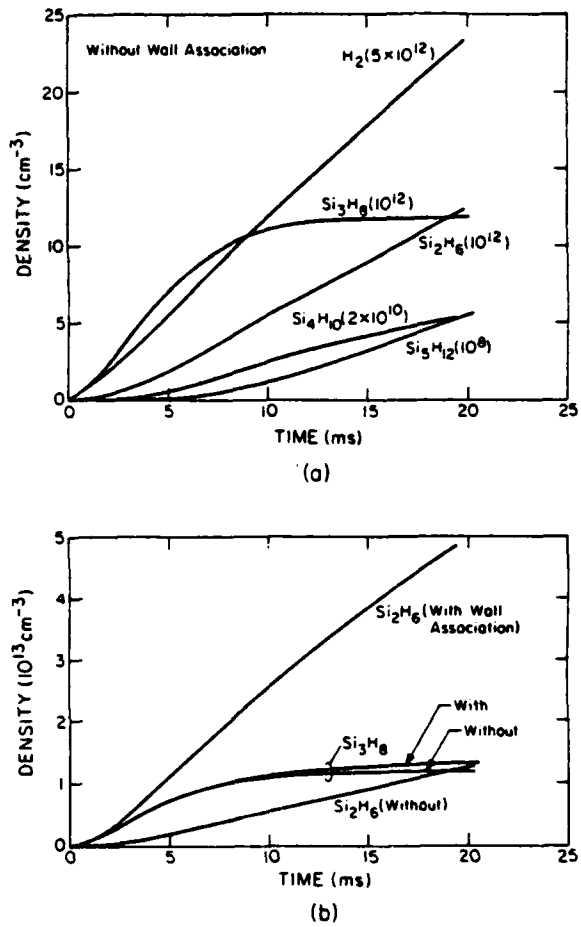


FIG. 5. Volume averaged densities of saturated molecules in an rf discharge sustained in silane as a function of flow time: (a) without the wall association reaction $2 \cdot SiH_3(g) \rightarrow 2 \cdot SiH_3(a) \rightarrow Si_2H_6(g)$, (b) with the wall association reaction. The gas pressure is 250 mTorr with power deposition of 25 mW $cm^{-3}$ and substrate temperature of 500 K. The electrode separation is 2.5 cm. Hydrogen is the most abundant saturated product, but only with the wall association reaction is disilane the most abundant higher silane.

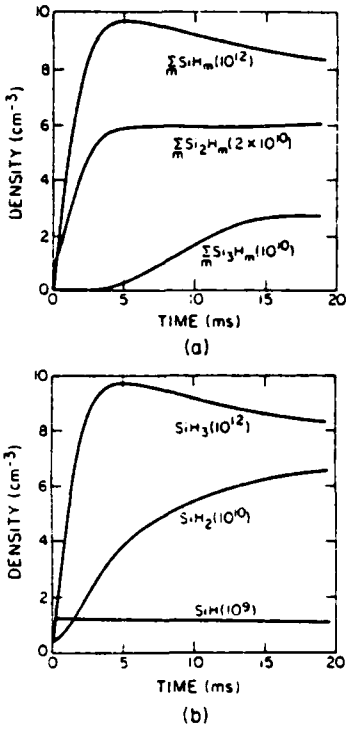


FIG. 6. Volume averaged radical densities for the conditions of Fig. 5; (a) the sums of monomer, dimer, and trimer radical densities, (b) the individual monomer radical densities. The monomer radicals are the most abundant, however only the dimer radicals come quickly into equilibrium.

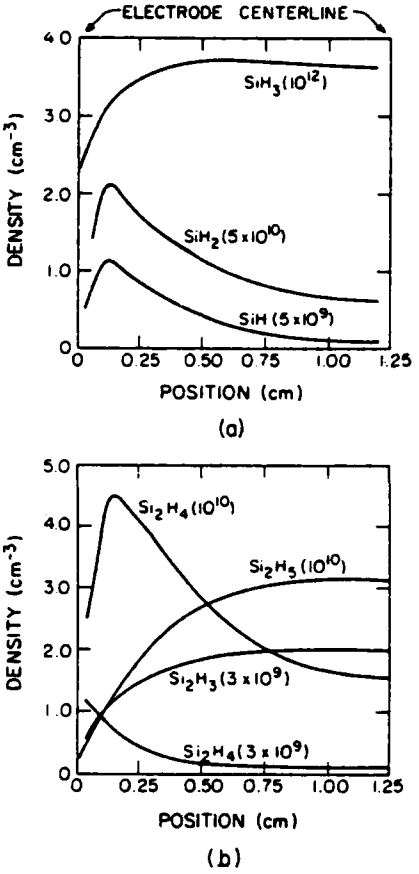


FIG. 7. The density of monomer [(a) top] and dimer radicals [(b) bottom] as a function of position between the electrodes for the discharge conditions of Fig. 5. The discharge is symmetric. The electrode is at the left boundary, and the discharge centerline is at the right. $SiH_2$ and SiH are peaked near the electrode as electron impact dissociation of silane are their dominant source and they rapidly react with silane. $SiH_3$ is nearly uniform as a function of position due to its more distributed production and low sticking coefficient. $Si_2H_4$ is peaked near the electrode due to its source being insertion of $SiH_2$ into silane. [Note: The label on the lowest curve in 7(b) is incorrect. It should be $Si_2H_2$.]

than four silicon atoms obtain only modest densities for these conditions. The density of the higher silanes, though, depends critically on the choice of the chain propagating rate constant, which is $1.0\times10^{-11}\ cm^{-3}\ s^{-1}$ in this example.

It appears that at low pressures (<200 mTorr) gas phase reactions do not favor formation of disilane. Large mole fractions of disilane, though, have been observed for similar discharge conditions by Chatham and Gallagher.[14] They attributed the high density to the heterogeneous wall association reaction

$$2\cdot SiH_3(g)\rightarrow 2\cdot SiH_3(a)\rightarrow Si_2H_6(g), \qquad (14)$$

where $(a)$ denotes adsorbed species. This reaction was included in the model for the nonsticking silyl flux striking the electrodes. The density of $Si_2H_6$ increased as shown in Fig. 5(b). For these results, half of the nonsticking silyl flux striking the electrodes participates in reaction 14. The wall association reaction results in disilane becoming the most abundant higher silane molecule, consistent with Chatham and Gallagher's observations.

The time evolution of $SiH_m$, $Si_2H_m$, and $Si_3H_m$ radicals are shown in Fig. 6(a). The dimer radicals quickly come into equilibrium and the trimer radicals do so at a later time. The monomer radicals display an extremum, due primarily to the density of $SiH_3$. This behavior is shown in more detail in Fig. 6(b), where the densities of the individual $SiH_m$ radicals are plotted. The density of SiH quickly comes into equilibrium between its production by electron impact dissociation of silane and its subsequent insertion into silane. Although the production rate of $SiH_3$ is relatively constant, the density of $SiH_3$ initially peaks then settles to a near equilibrium value. (The production of $SiH_3$ by hydrogen abstraction from $SiH_4$ exceeds that by electron impact dissociation of silane in the ratio of $\approx 1.5/1$.) The decrease in $SiH_3$ density is due to the increase in density of other radicals and saturated molecules with which $SiH_3$ reacts. These species are principally H, $SiH_2$, $Si_2H_5$, and higher silanes. The

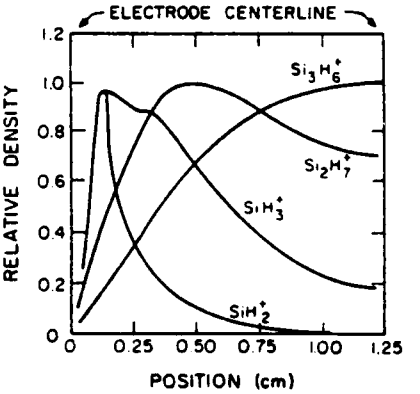


FIG. 8. Silane ion densities as a function of position between the electrodes for the conditions of Fig. 7. The progressively more uniform densities going from $SiH_2^+$ to $Si_3H_6^+$ indicate that the source of the ion is further displaced from the originating step in the chain, electron impact ionization of silane.

density of $SiH_2$ increases monotonically towards an equilibrium value as its dominant destruction mechanism, insertion into silane, does not appreciably change its rate.

The spatially dependent densities of $SiH_m$ radicals at the terminal time shown in the previous figures are in Fig. 7(a). The spatial distribution of $SiH_3$ is fairly uniform whereas those for $SiH_2$ and SiH are maximum near the electrode at the location of the peak in the production rate by electron impact dissociation. The density of $SiH_3$ near the electrode is about two-thirds that of the maximum, a consequence of its nonunity sticking coefficient (0.15); the densities of $SiH_2$ and SiH are negligible at the electrode due to their unity sticking coefficient. The spatially dependent densities of the dimer radicals are shown in Fig. 7(b). The density of $Si_2H_2$ is largest near the electrode because neutralization of $Si_2H_2^+$ at the surface is an important source for the radical. The density of $Si_2H_4$ has an extremum near the electrode at the site of production of $SiH_2$, as the insertion of that radical into silane is the major source of $Si_2H_4$. The densities of $Si_2H_3$ and $Si_2H_5$ have the characteristic profiles of radicals having volumetric sources and edge sinks. Initially, the major source of $Si_2H_5$ is insertion of SiH into silane; downstream after the density of disilane increases, the major source is hydrogen abstraction of disilane.

The spatially dependent densities of $SiH_2^+$, $SiH_3^+$, $Si_2H_7^+$, and $Si_3H_6^+$ are shown in Fig. 8 for the same conditions. This sequence of ions represents species which result from 1, 1 or 2, 2, and three collisions, respectively, where the first collision is electron impact ionization of silane. The density of $SiH_2^+$ closely mirrors the source function. The $SiH_3^+$ ion is produced either directly by electron impact dissociation or by the ion-molecule reaction of $SiH_2^+$ with silane. The $Si_2H_7^+$ ion results from reaction of $SiH_3^+$ with silane; and the trimer ion results from collisions of dimer ions with silane. As more collisions are required to form the species by ion-molecule reactions, the ion appears to have a more uniform rate of production. This issue is further discussed in the following section.

### B. Rate coefficient versus production rate versus survival rate

The local electron impact rate coefficient $k$ is a function of phase during the rf cycle and position between the electrodes. The rate of production $R$ of a radical by electron impact, though, is the product $R = n_e kN$, where $N$ is the heavy particle reactant density. The rate constant is maximum near the electrodes, whereas the electron density is maximum near the center of the discharge due to the loss by diffusion to the walls. The heavy particle density is a minimum at the center line because of gas heating. The result is that the production rate has a maximum displaced from the electrodes. The displacement of the rate of production away from the electrodes has important implications with respect to the flux of radicals incident onto the substrates.

Film properties are a function of the composition of the flux of radicals incident on, and sticking to, the substrate. The composition of the flux which strikes the substrate is different from that which results from electron impact dissociation of silane. This discrepancy results from reactions which occur between the site of production of radicals by electron impact and their arrival at the substrate. In this respect, we define the survival ratio as

$$\beta = sD/\Lambda^2 \Big/ \sum_i \kappa_i N_i, \tag{15}$$

where $D$ is the diffusion coefficient, $s$ is the sticking coefficient, $\Lambda$ is the diffusion length and $\kappa_i$ is the rate of reaction with heavy particle $i$ having density $N_i$. If $\beta \gg 1$, the rate of diffusion is large compared to the rate of chemical reaction and the radical survives to reach the surface as produced by electron impact dissociation. The spatially dependent density of a sticking radical then resembles that having a uniform volume source and edge sink. If $\beta \ll 1$, the radical reacts soon after production and its spatially dependent density mirrors that of the production rate. A comparison of the spatial distribution of production and density of a radical is therefore an indication of its survivability and contribution to growth of the film.

To illustrate these points, we examine the spatial distributions of $SiH_2$ and $SiH_3$ as a function of silane mole fraction in hydrogen. These radicals are the major products of electron impact dissociation of silane. $SiH_3$ is not particularly reactive with silane ($\kappa \approx 10^{-15}$ cm$^3$ s$^{-1}$) and has a low sticking coefficient, while $SiH_2$ is reactive with silane ($\kappa \approx 10^{-12}$ cm$^3$ s$^{-1}$) and has a unity sticking coefficient. The densities of $SiH_2$ and $SiH_3$ as a function of position and dilution of silane by hydrogen are shown in Fig. 9. The distributions of $SiH_3$ do not appreciably change as silane is diluted with hydrogen. The distribution for the $SiH_4/H_2 = 1/1$ mixture, though, is displaced from the electrode. This motion reflects the fact that the production of $SiH_3$ is more dominantly by hydrogen abstraction from silane in the 1/1 mixture as opposed to electron impact dissociation of silane (a ratio of $\approx 10/1$ compared to $\approx 1.5/1$ for a pure silane). The production rate by electron impact dissociation is maximum near the electrodes, whereas that by hydrogen abstraction is maximum in the bulk, as shown in the figure. The distributions of $SiH_2$ are highly peaked near the electrode in a pure silane and maximum in the bulk for a $SiH_4/H_2 = 1/1$ mixture. This trend indicates production occurs near the electrodes and the primary reactant is silane. The survival ratio for $SiH_2$ analogously increases with dilution with $H_2$, as shown in Fig. 9(c).

Similar trends will occur if the location of production of radicals is displaced from the electrodes. This is best illustrated in a negative glow dc discharge where the production rate of radicals by electron impact is maximum at the edge of the cathode fall. The cathode fall thickness is a function of many parameters, but generally increases with increasing cathode fall voltage. Therefore, operating at larger cathode fall voltages moves the production of silane radicals by electron impact away from the cathode, thereby changing the probability that a particular radical survives to reach the substrate (cathode). We modified the plasma chemistry model to simulate a dc negative glow discharge and computed the ratio of the fluxes of $SiH_3$ to $SiH_2$, $\varphi(SiH_3)/\varphi(SiH_2)$, incident on the cathode. Typical $SiH_3$ and $SiH_2$ densities are

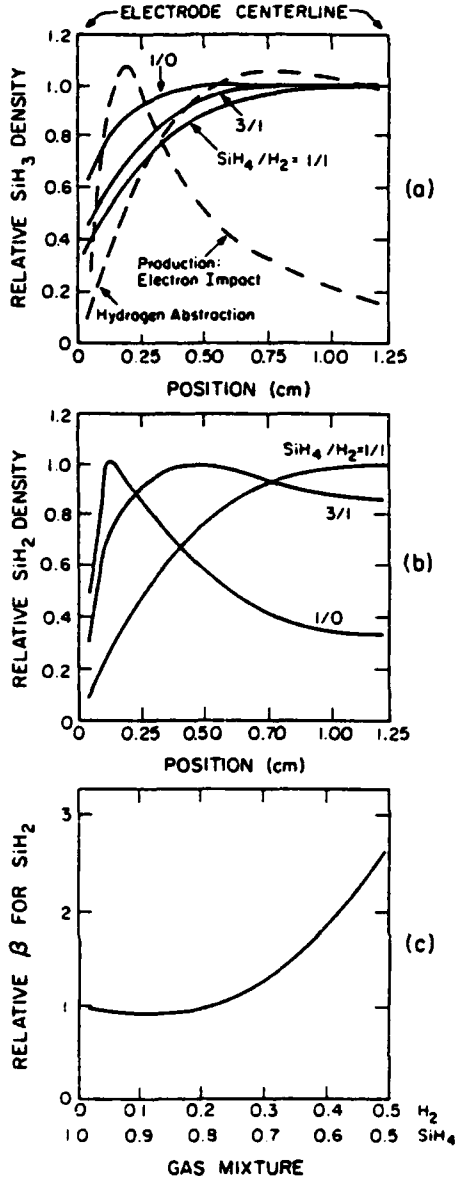


FIG. 9. Radical densities for rf discharges in mixtures of silane and hydrogen; (a) $SiH_3$ and (b) $SiH_2$. The densities of the radicals for each mixture are normalized to their maximum value to emphasize the difference in their spatial distributions. The density of $SiH_3$ is always fairly uniform, reflecting its low reaction rate and low sticking coefficient. The density of $SiH_2$ is uniform only with low mole fractions of silane. The relative probability of survival of $SiH_2$ radicals to reach the substrate increases with decreasing silane mole fraction, as shown in (c).

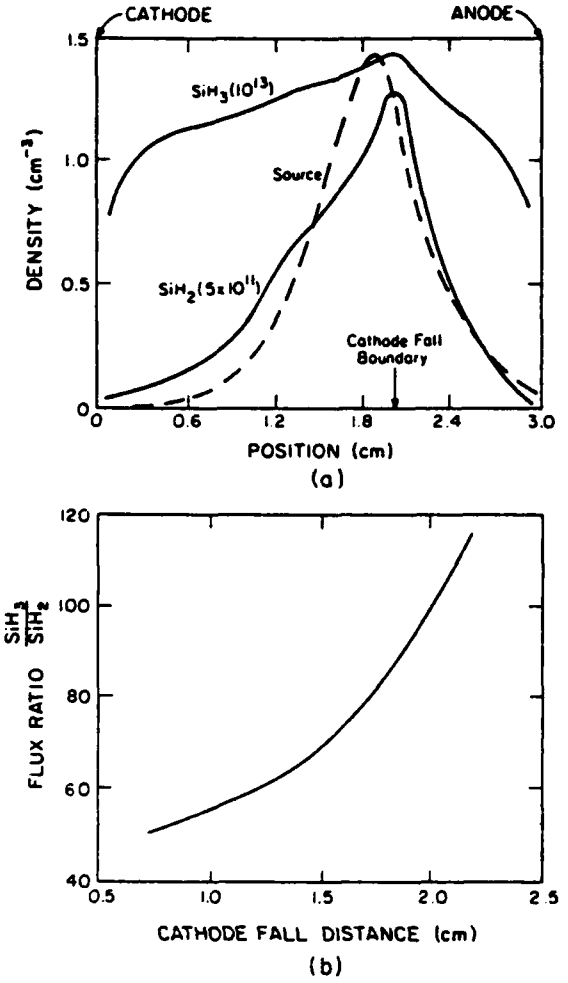


FIG. 10. Radical densities and flux ratios for a dc discharge in 150 mTorr of silane sustained between two parallel electrodes (cathode at left, anode at right): (a) $SiH_3$ and $SiH_2$ density for a cathode fall distance of 2 cm with the distribution of production of radicals by electron impact dissociation, (b) The ratio of the flux of $SiH_3$ to $SiH_2$ incident on the cathode as a function of cathode fall distance. The ratio increases with increasing cathode fall distance due to the increased residence time for $SiH_2$.

shown in Fig. 10(a) for a cathode fall length of 2.0 cm. The survival probability for $SiH_2$ to reach the cathode is low due to the long residence time of $SiH_2$ radicals to diffuse to the cathode, and the high probability of reaction before reaching it. As a result, the flux ratio $\varphi(SiH_3)/\varphi(SiH_2)$ is large, $> 100$. As the cathode fall distance decreases, this ratio increases, a result of the increased probability of survival for $SiH_2$ [see Fig. 10(b)] as its residence time decreases. Since the quality of *a*-Si:H films depends on this ratio (see Sec. III D), the thickness of the cathode fall directly effects the properties of the film.

### C. Electrode separation

A common measure of power deposition in parallel plate discharges is W $cm^{-2}$ based on electrode area. This scaling parameter implies that the deposition rate of *a*-Si:H should be independent of electrode separation. This deposition rate, though, has generally been observed to decrease with increasing electrode separation.[3,6] One would predict that if specific power deposition (W $cm^{-3}$) is held constant, the deposition rate should increase with increasing electrode separation since the area to volume ratio scales as $d$. This trend is also not always observed. There must therefore be other processes which effect deposition rate when the electrode separation is changed. In this section, we will discuss some of these processes.

Changes in the geometry of the reactor (that is, electrode separation) can affect the manner of power deposition, residence time for radicals and ions, and, as a result, the composition of the flux incident onto the substrate. Power

deposition by electrons occurs in two distinct regions; by higher energy electrons in and near the sheaths and by lower energy electrons in the bulk plasma which resembles a positive column. The power deposition associated with the sheaths can more easily access processes with higher threshold energies. The power deposition in the bulk typically accesses lower threshold processes. Since the sheaths occupy a fixed volume near the electrodes, the fraction of power deposited by processes associated with the sheaths decreases as the electrode separation increases, and that deposited in the bulk by lower energy electrons fractionally increases. The fractional amount of power dissipated by ions striking the electrodes also changes, usually decreasing as the electrode separation increases. The contribution for our conditions therefore remains small, $< 10\%$.

Consequences of this change in the manner of power deposition are shown in Fig. 11 where the densities of $SiH_3$ radicals and vibrationally excited silane ($[SiH_4(v1,3)] + [SiH_4(v2,4)]$) are plotted as function of position in the discharge for three different electrode separations. The discharge conditions are $SiH_4/H_2 = 1/1$, 250 mTorr, with power deposition constant at 25 mW $cm^{-3}$. As the electrode separation $d$ increases, the density of $SiH_3$ decreases while the density of $SiH_4(v)$ increases. This trend indicates that as $d$ increases, a larger fraction of power deposition occurs through lower energy processes, such as vibrational excitation, resulting in less dissociation. The discharge appears more like a positive column. Less dissociation leads to a smaller radical density and hence lower deposition rate of $a$-Si:H. The predicted deposition rate of $a$-Si:H as a function of electrode spacing appears in Fig. 12 and decreases with increasing $d$. For comparison, experimental results from Ross and Jaklik[3] and Ishihara *et al.*[6] are also shown.

A second consequence of increasing $d$ is that the average residence time for radicals also increases, thereby increasing the probability of chemical reactions after the initial electron impact dissociation of silane. The change in residence will result in a change in the composition of the flux incident onto the electrodes. An example is shown in Fig. 13 where the ratio of fluxes incident on the electrodes for $SiH_3$ and $SiH_2$, $\varphi(SiH_3)/\varphi(SiH_2)$, is plotted as a function of $d$. This ratio increases with increasing electrode separation as the probability for reaction of, and consumption of, $SiH_2$ by insertion into silane increases with increasing residence time. The depletion of $SiH_3$ increases at a lower rate. Also shown in Fig. 13 is the density of DUST, which decreases with increasing separation. Both of these trends coincide with film quality increasing with large electrode separation, trading off against lower deposition rates. Further parametric tradeoffs for film quality are discussed in the following section.

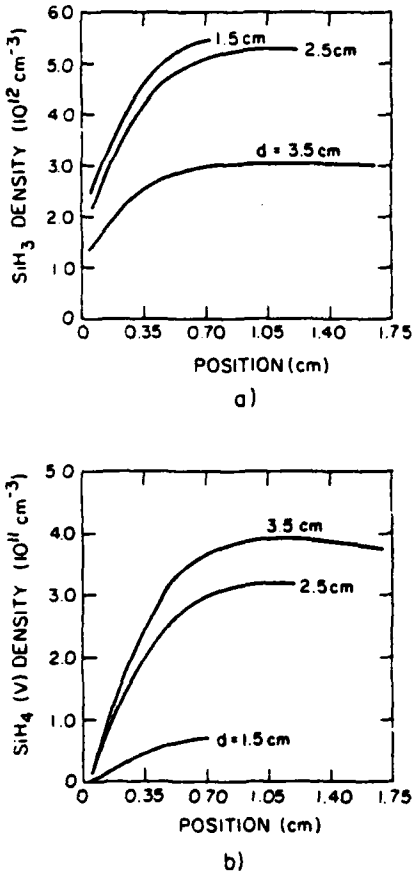


FIG. 11. The density of $SiH_3$ [(a), top] and vibrationally excited silane, $SiH_4(v)$, [(b), bottom] as a function of position between the electrodes in an rf discharge for different electrode separations. The discharge conditions are otherwise the same as for Fig. 5. Relative rates of high threshold processes such as dissociation decrease with increasing electrode separation as the discharge becomes dominated by the positive column.

### D. Contributions to deposition

Conditions for which the $a$-Si:H film grown from silane discharges is judged "device quality" are empirically known. Generally, one operates where gas phase polymerization and particulate formation is not likely to occur (i.e., low power and low partial pressures of silane), and conditions where the ion flux is a small fraction of the radical flux. The latter criteria insure that the process is dominantly chemical vapor deposition, as opposed to physical vapor deposition[84] and minimizes the formation of columnar structures.[85] High-quality films have also been correlated with conditions

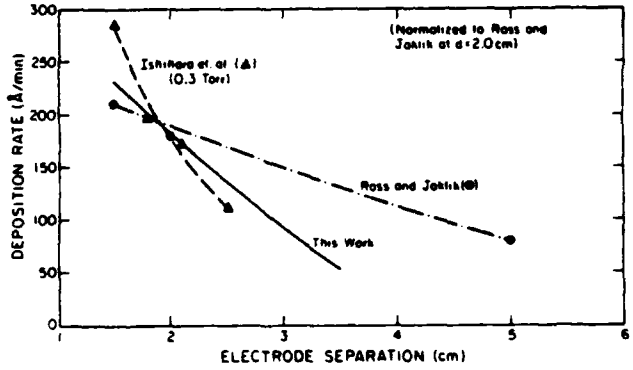


FIG. 12. Computed deposition rate of $a$-Si:H as a function of electrode separation compared to the results of Ross and Jaklik (Ref. 3) and Ishihara *et al.* (Ref. 6) for similar conditions. The results have been normalized to Ross and Jaklik at $d = 2$ cm.

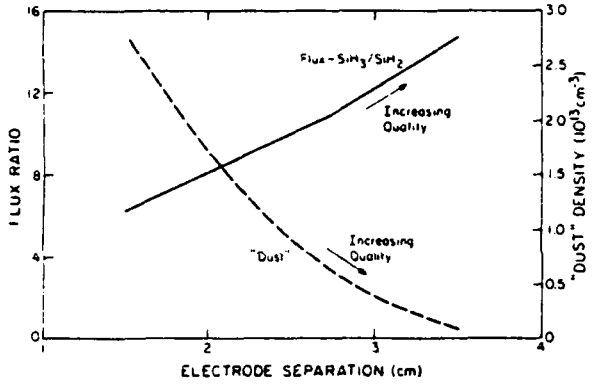


FIG. 13. The ratio of the flux of $SiH_3$ to $SiH_2$ incident on the substrate and the density of DUST as a function of electrode separation. The increase in this ratio, and decrease in the density of DUST, with increasing electrode separation, are indications of increasing quality of the *a*-Si:H films deposited.

where the ratio of $SiH_3$ to $SiH_2$ incident on the surface is high. $SiH_3$ has a high surface mobility compared to $SiH_2$.[86] Films grown from primarily $SiH_3$ radicals therefore will resemble the preferred chemical vapor deposition, as opposed to physical vapor deposition. In this respect, we quantify three measures of film quality; a large fraction of deposition resulting from lower silanes ($Si_nH_m$, $n<2$), a large ratio of deposition from $SiH_3$ as compared to $SiH_2$, and large ratio of the flux of radicals containing Si atoms compared to the flux of ions of any type incident onto the substrate.

Discharges were simulated for gas mixtures of silane diluted in argon and hydrogen. The argon diluted gas mixtures are at a total pressure of 0.5 Torr and power deposition of 50 mW cm$^{-3}$; the hydrogen diluted mixtures are at a total pressure of 0.25 Torr and power deposition of 25 mW cm$^{-3}$, each case being the same specific power loading. The results are shown in Fig. 14 as a function of the ratio of $[SiH_4]/([SiH_4]+[Ar \text{ or } H_2])$.

For both dilutions, the fraction of deposition due to lower silanes decreases with increasing silane mole fraction as the probability of radicals colliding with other silane species before being incorporated into the film increases with increasing silane mole fraction. The fraction of deposition from lower silanes decreases from $\approx$0.9 to $\approx$0.6 (see Fig. 14), and by this measure, film quality should decrease with increasing silane mole fraction. By other measures, though, film quality should increase with increasing silane mole fraction. For example, the ratio of $SiH_3/SiH_2$ incorporated into the film increase from about 2 to 20 as the mole fraction of silane in hydrogen increases, as shown in Fig. 14(a). This trend is a consequence of the higher probability of $SiH_2$ inserting into silane before the radical reaches the surface.

Our other measure of film quality, the ratio of the silicon radical flux to the total ion flux, also increases with increasing silane mole fraction, as shown in Fig. 14(b). This ratio increases by a factor of 4 from a 5% mixture of silane in argon to pure silane. The increase is a result of a larger fraction of discharge power being coupled through the neutral dissociative modes of silane, and a decrease in the average electron energy with increasing silane fraction, which favors neutral dissociation over dissociative ionization.

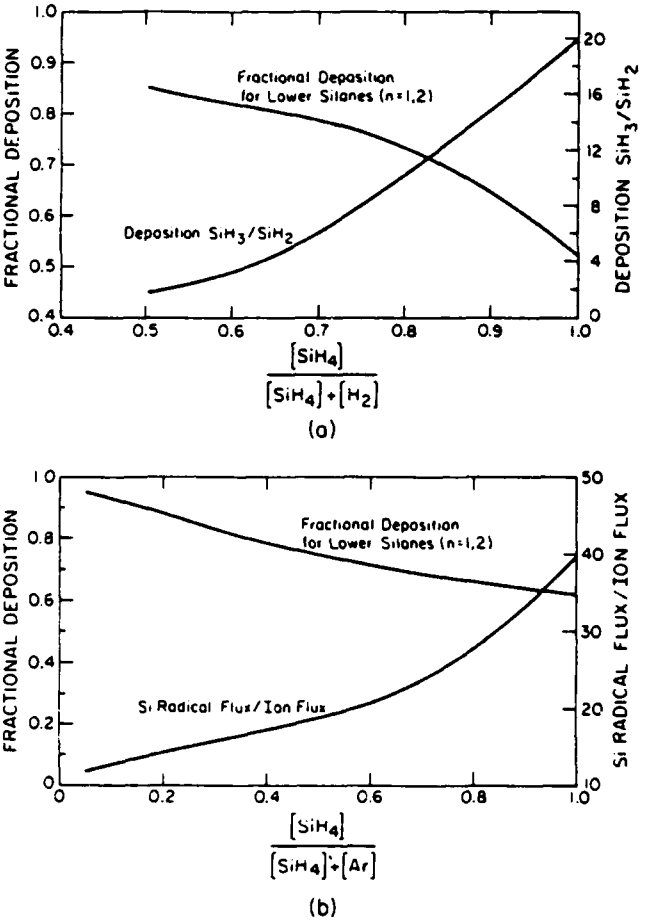


FIG. 14. Measures of film quality for discharges sustained in mixtures of silane diluted by hydrogen [(a), top] and silane diluted by argon [(b), bottom]. Quality increases with an increasing fraction of the deposition from $SiH_3$ compared to $SiH_2$, increasing Si radical flux compared to ion flux, and increasing deposition by lower silanes. These measures of quality have different dependencies on silane mole fraction.

These measures of film quality have different dependencies on silane mole fraction and partial pressure. A tradeoff must be performed to optimize the quality of *a*-Si:H films when diluting silane or changing its partial pressure.

Other parameters are also important to film deposition, particularly the rate of deposition. The deposition rate does not simply scale with silane mole fraction due to the changes in the electron distribution, and hence electron impact rate constants when the mixture is diluted. For example, when diluting with argon, the average electron energy and rate constant for dissociation increases. Therefore, in spite of reducing the mole fraction of silane, the total rate of dissociation, and hence deposition rate, can increase as more net power is coupled into the dissociation of silane. This trend is illustrated in Fig. 15, where deposition rate is plotted as a function of $Ar/SiH_4$ gas mixture. Normalized experimental results of Street, Knights, and Biegelsen[87] are shown for comparison. The maximum in deposition rate at $SiH_4/Ar \approx 1/1$ is a result of the tradeoff between an increasing rate constant for dissociation and decreasing mole fraction of silane.

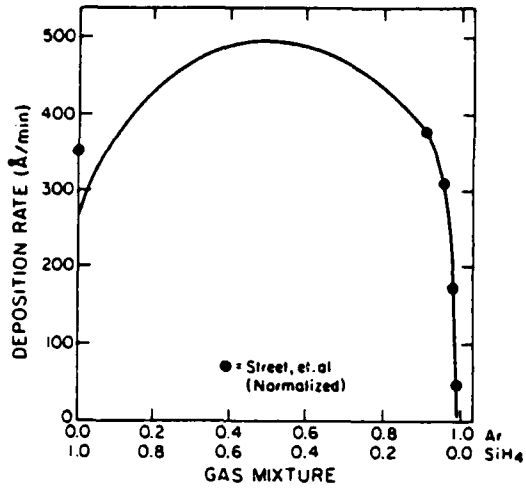


FIG. 15. Deposition rate of *a*-Si:H for silane/argon gas mixtures, compared to the normalized experimental results of Street *et al.* (Ref. 87). The deposition rate optimizes as a tradeoff between increasing electron impact dissociation rate constant and decreasing silane mole fraction.

## E. Formation of higher silane ions

The formation of particulate matter (synonomous with clusters and dust) is relevant with respect to the detrimental effect particulate matter is believed to have on the quality of films. Particulates are often observed and their spatial distributions have been measured by laser light scattering.[88] The formation of particulates is generally associated with high-power deposition and a high partial pressure of silane. Low film quality under these conditions is attributed to silicon "flakes" which are incorporated into the film as polymeric groups $(SiH_2)_n$.[89]

When quantitatively observed, particulates usually have a higher densities adjacent to the sheaths, leading one to assume that they are charged. One then requires a mechanism to explain the growth of higher silane ions, presumably the precursor to charged particulates. Silane ions having greater than 6–8 silicon ions have been observed in dc discharges by Weakliem, Estes, and Longeway.[22] Chatham and Gallagher have calculated that $Si_nH_m^+$ ions with $n>2$ are the most abundant ions in dc negative glow discharges for $j/p < 0.05$ A/cm$^2$ Torr.[14] We studied the formation of higher silane ions by comparing results from our model to the experiments of Weakliem *et al.*, an example which is reproduced in Fig. 16(a) for a silane pressure of 0.5 Torr and current density of 13 mA cm$^{-2}$. In this figure, the fractional abundances of $Si_mH_n^+$ ions having $m<6$ arriving at the anode of a dc discharge are plotted as a function of electrode separation. Note that the dominant silane ions have $\geq 4$ silicon atoms and that the least abundant ion is mono-silicon.

Pathways for the formation of higher silane ions are illustrated in Fig. 17. The rate of loss of $Si_nH_m^+$ ions by ion-ion neutralization, dissociative recombination, and diffusion have typical timescales of 2–8 ms. The formation of higher silane ions by ionization of higher silane radicals has a typical timescale of 50 ms. Clustering of ions with radicals of all description has a time scale of approximately 2 ms. For higher silane ions to be the most abundant ion, one must invoke

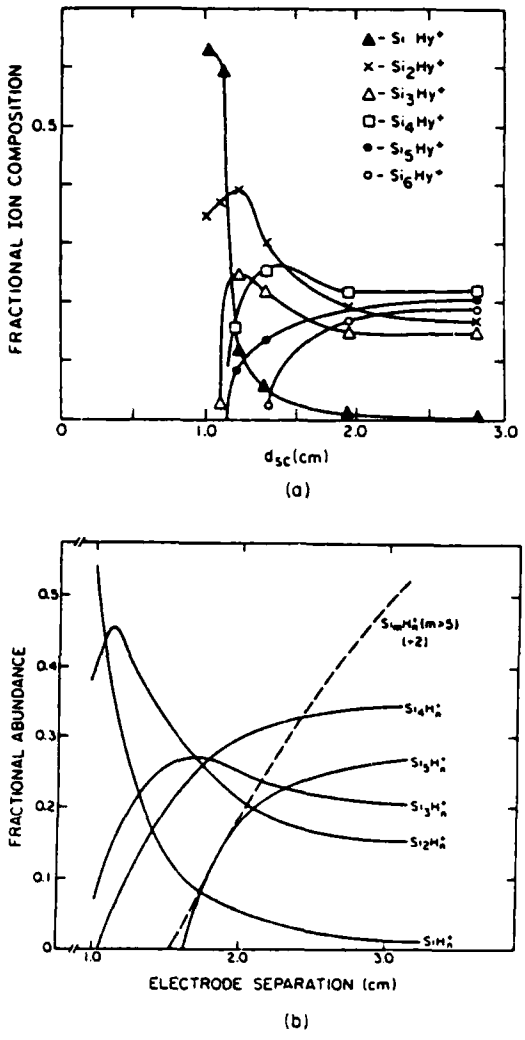


FIG. 16. Fractional densities of lower and higher silane ions incident on the anode of a dc discharge in silane as a function of distance between cathode and anode (13 mA/cm$^2$, 0.5 Torr); (a) experimental results from Weakliem *et al.* (Ref. 22), (b) results from the model.

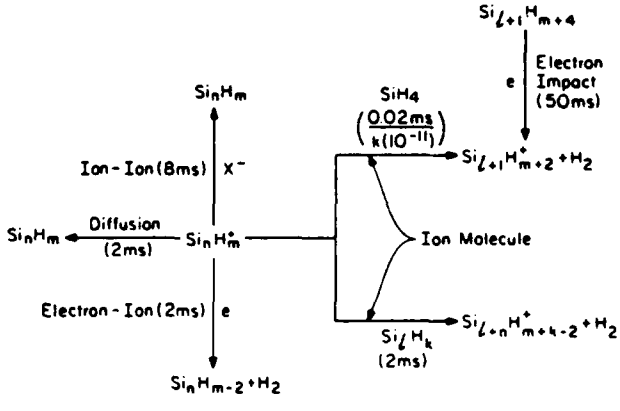


FIG. 17. Pathways and reaction times for creating higher silane ions for typical discharge conditions. The values in parenthesis are the characteristic times for the indicated loss process (ion-ion neutralization, diffusion, or recombination) or for the ion-molecule reaction leading to clustering. The entry for clustering by ion-molecule reactions with silane has a characteristic time of 0.02 ms/k, where the rate constant is expressed in $10^{-11}$ cm$^3$ s$^{-1}$.

ion-molecule reactions with silane, as only this mechanism has a typical time scale less than that for losses when a reasonable rate constant ($k \leq 10^{-10}$ cm$^3$ s$^{-1}$) is used.

The electron kinetics and plasma chemistry models were modified to simulate a dc discharge and were used to model the experiments of Weakliem *et al.* We hypothesized that higher silane ions are formed by consecutive ion molecule reactions of the form

$$Si_nH_m^+ + SiH_4 \rightarrow Si_{n+1}H_{m+2}^+ + H_2 \qquad (16)$$

and parametrized the rate constant for this class of reactions. The results of the study are shown in Fig. 16(b), which should be compared to the experimental results of Fig. 16(a). The systematic agreement is quite good, showing that for similar conditions (silane partial pressure $\geq$0.3–0.5 Torr, electrode separation 2–4 cm), the majority of ions are higher silanes. To obtain the results in Fig. 14(b), the chain propagating rate constant for reaction 16 was $1\times10^{-11}$ cm$^3$ s$^{-1}$, with the exception of the reaction with $n = 3$ where the rate constant was $2\times10^{-11}$ cm$^3$ s$^{-1}$. We also found it necessary to reduce the three-body rate constant for the reaction $SiH_3^+ + SiH_4 + M \rightarrow Si_2H_7^+ + M$ from $1.8\times10^{-26}$ cm$^6$ s$^{-1}$ to $1.0\times10^{-26}$ cm$^6$ s$^{-1}$. Note that if the reaction sequence of Eq. (16) holds beyond $n = 5$, the detection limit of Weakliem's experiments, the absolute density of all ions having greater than 6 silicon atoms exceeds that of the lesser ions for large electrode separations.

These results only qualitatively agree with the recent measurements by Mandich *et al.*[74] who obtained rate constants for the clustering chain of cold ions (300 $k$) given by

$$\begin{aligned} Si^+ + SiD_4 &\rightarrow SiD_4Si_2D_2^+ + D_2 \\ SiD_4 &\big| \\ &\rightarrow Si_3D_4^+ + D_2 \\ SiD_4 &\big| \\ &\rightarrow Si_4D_6^+ + D_2 \rightarrow \cdots \rightarrow Si_5D_8^+ + D_2. \end{aligned} \qquad (17)$$

Their measurements indicate a bottleneck in the step between $Si_4D_6^+$ and $Si_5D_8^+$, with the rate constant decreasing by a factor of $>200$ from the previous step. To reproduce experimental results, we must sidestep this bottleneck. If the bottleneck at $n = 5$ is due to an activation energy barrier, electronically and vibrationally excited species in the plasma may provide the energy reservoir required to relieve the bottleneck, a reservoir not available during Mandich's measurements. In this respect, subsequent measurements by Reents and Mandich[90] have shown that the rate constants for ion-molecule clustering reactions of $Si_nD_n^+$ with $SiD_4$ are sensitive to the internal energy of the reactant ion, as well as on its structural isomeric state. For example, structural isomeric pairs of $Si_4D_2^+$ either react rapidly with $SiD_4$ to form $Si_5D_4^+$ (rate constant $1.3\times10^{-10}$ cm$^{-3}$ s$^{-1}$) or have no measurable reaction. Reaction rates for sets of $Si_nD_m^+$ ions ($n$ fixed, $m$ variable) with $SiD_4$ were also found to have significantly different rate constants.[90] These results imply that the propagation length of an ion-molecule clustering chain may critically depend on the availability of activation energy in the plasma and on the initiating step of the chain (e.g., $SiH_n^+ + SiH_4 \rightarrow$ products, $0 \leq n \leq 3$).

There are many implications of the observation that ions in silane discharges of moderate electrode separation and pressure are dominantly higher silanes. Since the reaction chain is first order, the formation of higher silane ions depends only upon the pressure $x$ electrode separation ($pd$) product and not upon having higher power deposition. Therefore, the formation of large silane ions can be prevented only by operating at small $pd$. Since large ions are less efficient at transferring momentum to individual species when they collide with the substrate, the rate of sputtering and activation of surface sites will be lower with higher silane ions. To the extent that site activation may be required for incorporation of radicals such as $SiH_3$ into passivated surface bonds (i.e., $\equiv$Si–H), this change in the rate of surface activation will change both film growth rates and surface morphology.

## IV. CONCLUDING REMARKS

A plasma chemistry model for the deposition of amorphous silicon from rf and dc discharges sustained in gas mixtures containing silane has been described, and results from the model discussed. A compendium of rate constants for silane plasma chemistry has also been presented and important reactions discussed. We conclude that the spatial distribution of the production of radicals and the subsequent probability of survival to reach the substrate of those radicals greatly impact the characteristics of the $a$-Si:H film. Geometry will also impact the quality of the film through changes in the manner of power deposition and the formation of higher silane species. Diluting silane with either inert or active gases changes both the manner of power deposition and the reaction chain, thereby affecting film properties. The formation of higher silane ions requires first-order reactions with silane and also may affect film properties. Clearly, even small changes in discharge parameters may impact the quality of $a$-Si:H films produced.

## ACKNOWLEDGMENTS

The author would like to thank the following individuals for fruitful discussions on this topic and for sharing the results of their research before publication: Dr. W. Bottenberg (ARCO Solar), Dr. B. Stafford (SERI), Dr. A. Gallagher (JILA), Dr. J. Jasinski (IBM/Watson), Dr. M. Mandich (Bell Labs), Dr. A. Garscadden (WPAFB), Dr. R. Roth (AMOCO), and Dr. L. Kline (Westinghouse). The author would also like to acknowledge the contributions of Professor J. A. Thornton of the University of Illinois who died unexpectedly in November 1987. This work was supported by Spectra Technology, Inc., and by Army Research Office, Contract No. DAAG29-85-C-0031, under the direction of Dr. A. Crowson.

[1] J. A. Thorton, in *Amorphous Metals and Semiconductors*, edited by P. Maasen and R. I. Jaffee (Pergamon, New York, 1986), pp. 299–314.
[2] F. J. Kampas, in *Semiconductors and Semimetals*, edited by J. I. Pankove (Academic, Orlando, 1984), Vol. 21A, p. 153.

[3]R. Ross and J. Jaklik, J. Appl. Phys. 55, 3785 (1984).
[4]P. E. Vanier, F. J. Kampas, R. R. Corderman, and G. Rajeswaren, J. Appl. Phys. 56, 1812 (1984).
[5]W. Wallace, E. Sabisky, B. Stafford, and W. Luft, Proceedings of the 19th IEEE PV Specialists Conference, 1987 (to be published).
[6]S. Ishihara, M. Kitagawa, T. Hirao, K. Wasa, T. Arita, and K. Mori, J. Appl. Phys. 62, 485 (1987).
[7]G. Turban, Y. Catherine, and B. Grolleau, Thin Solid Films 60, 147 (1979).
[8]I. Haller, Appl. Phys. Lett. 37, 282 (1980).
[9]I. Haller, J. Vac. Sci. Technol. A 1, 1376 (1983).
[10]I. Chem, Thin Solid Films 101, 41 (1983).
[11]P. A. Longeway, R.D. Estes, and H. A. Weakliem, J. Phys. Chem. 88, 73 (1984).
[12]K. Tachibana, in *Proceedings of the 8th Symposium on Ion Sources and Ion-Assisted Technology*, edited by T. Takagi (Institute of Electrical Engineering, Tokyo, Japan, 1984), p. 319.
[13]J.-S. Chang, R. M. Hobson, Y. Ichikawa, S. Matsumura, K. Sakurai, and S. Teii, *Proceedings of the 8th International Conference on Gas Discharges and Applications* (Leeds University Press/Pergamon, Leeds, 1985), pp. 493–496.
[14]H. Chatham and A. Gallagher, J. Appl. Phys. 58, 159 (1985).
[15]A. Garscadden, G. L. Duke, and W. F. Baily, Appl. Phys. Lett. 43, 1012 (1983).
[16]M. Hayashi, in *Swarm Studies and Inelastic Electron-Molecule Collisions*, edited by L. C. Pitchford, B. V. McKoy, A. Chutjian, and S. Trajmar (Springer, New York, 1987), pp. 167–187.
[17]Y. Ohmori, M. Shimozuma, and H. Tagashima, J. Phys. D 19, 1029 (1986).
[18]M. J. Kushner, IEEE Trans. Plasma Sci. PS-14, 188 (1986); M. J. Kushner, J. Appl. Phys. 54, 4958 (1983).
[19]M. J. Kushner, H. M. Anderson, and P. J. Hargis, in *Plasma Synthesis and Etching of Electronic Materials*, edited by R. P. H. Chang and B. Abeles (Materials Research Society, Pittsburgh, PA, 1985), pp. 201–213.
[20]M. J. Kushner, J. Appl. Phys. 62, 4763 (1987).
[21]M. J. Kushner, in *Plasma Processing*, edited by J. W. Coburn, R. A. Gottscho, and D. W. Hess (Materials Research Society, Pittsburgh, PA, 1986), pp. 293–307.
[22]H. A. Weakliem, R. D. Estes, and P. A. Longeway, J. Vac. Sci. Technol. A 5, 29 (1987).
[23]R. M. Roth, K. G. Spears, and G. Wong, Appl. Phys. Lett. 45, 28 (1984).
[24]J. Perrin, J. P. M. Schmitt, G. DeRosny, B. Drevillon, J. Huc, and A. Llorett, Chem. Phys. 73, 383 (1982).
[25]J. P. M. Schmitt, P. Gressier, M. Krishnan, G. DeRosny, and J. Perrin, Chem. Phys. 84, 281 (1984).
[26]M. J. Kushner, J. Appl. Phys. 62, 2803 (1987).
[27]B. Rieman, A. Matthew, R. Lampert, and P. Potzinger, Ber. Bunsenges. Phys.Chem. 81, 500 (1977).
[28]G. G. A. Perkins, E. R. Austin, and F. W. Lampe, J. Am. Chem. Soc. 101, 1109 (1979).
[29]H. Chatham, D. Hils, R. Robertson, and A. Gallagher, J. Chem. Phys. 81, 1770 (1984).
[30]H. Ebinghaus, K. Kraus, W. Muller-Duysing, and H.Neuert, A. Naturforschg 19a, 732 (1964).
[31]S. K. Srivastava and O. J. Orient, Bull. Am. Phys. Soc. 31, 149 (1986).
[32]P. Potzinger and F. W. Lampe, J. Phys. Chem. 73, 3912 (1969).
[33]M. Hayashi, J. Phys. (Paris Colloq) C7 40, 45 (1979).
[34]D. Rapp and P. Englander-Golden, J. Chem. Phys. 43, 1464 (1965).
[35]S. J. B. Corrigan, J. Chem. Phys. 43, 4381 (1965).
[36]H. W. Drawin, Z. Phys. 164, 513 (1961).
[37]E. Eggarter, J. Chem. Phys. 62, 833 (1975).
[38]J. H. Jacob and J. A. Mangano, Appl. Phys. Lett. 29, 467 (1976).
[39]H. N. Kucukarpaci and J. Lucas, J. Phys. D 14, 2001 (1981).
[40]I. P. Zapesochyni and L. L. Shimon, Opt. Spectrosc. 11, 155 (1966).
[41]R. H. McFarland and J. D. Kinney, Phys. Rev. 137, A1058 (1965).
[42]L. Vriens, Phys. Lett. 8, 260 (1964).
[43]M. Shimozuma and H. Tagashira, J. Phys. D 19, L197 (1986).
[44]D. Mihelcic, V. Schubert, R. N. Schindler, and P. Potzinger, J. Phys. Chem. 81, 1543 (1977).
[45]K. Y. Choo, P. P. Gasper, and A. P. Wolf, J. Phys. Chem. 79, 1752 (1975).
[46]M. E. Coltrin, R. J. Kee, and J. A. Miller, J. Electrochem. Soc. 133, 1206 (1986).
[47]M. E. Coltrin, R. J. Kee, and J. A. Miller, J. Electrochem. Soc. 131, 425 (1984).
[48]F. J. Kampas, J. Appl. Phys. 57, 2290 (1985).
[49]P. E. Vanier, F. J. Kampas, R. R. Cordermann, and G. Rajeswaran, J. Appl. Phys. 56, 1812 (1984).
[50]G. Inoue and M. Syzuki, Chem. Phys. Lett. 122, 361 (1985).
[51]J. M. Jasinski and J. O. Chu (unpublished).
[52]P. John and J. Purnell, J. Chem. Soc. Faraday Trans. 1 69, 1455 (1973).
[53]T. L. Pollock, H. S. Sandhu, A. Jodhan, and O. P. Strauz, J. Am. Chem. Soc. 95, 1017 (1973).
[54]K. Yachibana, M. Nishida, H. Harima, and Y. Urano, J. Phys. D 17, 1727 (1984).
[55]C. D. Eley, M. C. A. Rowe, and R. Walsh, Chem. Phys. Lett. 126, 153 (1986).
[56]L. G. Piper, J. E. Velazco, and D. W. Setser, J. Chem. Phys. 59, 3323 (1973).
[57]J. Balamuta, M. F. Golde, and Y.-S. Ho, J. Chem. Phys. 79, 2822 (1983).
[58]J. E. Velazco, J. H. Kolz, and D. W. Setser, J. Chem. Phys. 69, 4357 (1978).
[59]T. L. Cottrel and A. J. Matheson, Trans. Faraday Soc. 58, 2336 (1963).
[60]C. B. Moore, J. Chem. Phys. 43, 2979 (1965).
[61]J. T. Yardley, M. N. Fertig, and C. B. Moore, J. Chem. Phys. 52, 1450 (1970).
[62]J. T. Yardley and C. B. Moore, J. Chem. Phys. 45, 106 (1960).
[63]A. Gallagher (private communication).
[64]H. Chatham, D. Hils, R. Robertson, and A. C. Gallagher, J. Chem. Phys. 79, 1301 (1983).
[65]J. M. S. Henis, G. W. Stewart, and P. P. Gaspar, J. Chem. Phys. 58, 3639 (1973).
[66]J. M. Henis, G. W. Stewart, M. K. Tripodi, and P. P. Gaspar, J. Chem. Phys. 57, 389 (1972).
[67]T.-Y. Yu, T. M. H. Cheng, V. Kenpter, and F. W. Lampe, J. Phys. Chem. 76, 3321 (1972).
[68]T. M. H. Cheng, T.-Y. Yu, and F. W. Lampe, J. Phys. Chem. 78, 1184 (1974).
[69]W. N. Allen, T. M. H. Cheng, and F. W. Lampe, J. Chem. Phys. 66, 3371 (1977).
[70]M. T. Bowers and D. Elleman, Chem. Phys. Lett. 16, 486 (1972).
[71]L. P. Theard and W. T. Huntress, Jr., J. Chem. Phys. 60, 2840 (1974).
[72]N. G. Adams, D. K. Bohme, D. B. Dunkin, and F. C. Fehsenfeld, J. Chem. Phys. 52, 1951 (1970).
[73]A. E. Roche, M. M. Sutton, D. K. Bohme, and H. I. Schiff, J. Chem. Phys. 55, 5480 (1971).
[74]M. L. Mandich, W. D. Reents, and M. F. Jarrold (unpublished).
[75]L. E. Kline, IEEE Trans. Plasma Sci. PS-10, 24 (1982).
[76]C. F. Chan, "Reaction Cross Sections and Rate Coefficients Related to the Production of Positive Ions," Lawrence Berkeley Lab Report No. LBID-632 (1983).
[77]M. Biondi, in *Principles of Laser Plasmas*, edited by G. Bekifi (Wiley, New York, 1976), pp. 125–158.
[78]J. Mosley, W. Alberth, and J. R. Peterson, Phys. Rev. Lett. 24, 435 (1970).
[79]A. P. Hickman, J. Chem. Phys. 70, 4872 (1979).
[80]J. O. Hirschfelder, C. F.Curtiss, and R. Byron Bird, *Molecular Theory of Gases and Liquids* (Wiley, New York, 1954), pp. 528–541.
[81]R. J. Kee, F. M. Rupley, and J. A. Miller, "The Chemkin Thermodynamic Data Base" (Sandia National Laboratory, Report No. SAND87-8215), 1987.
[82]P. A. Thompson, *Compressible Fluid Dynamics* (McGraw-Hill, New York, 1972), p. 110.
[83]H. W. Ellis, R. Y. Pai, and E. W. McDaniel, At. Data. Nucl. Tables 17, 177 (1976); H. W. Ellis, E. W. McDaniel, D.L.Albritton, L. A. Viehland, S. L. Lin, and E. A. Mason, At. Data Nucl. Tables 22, 179 (1978).
[84]C. C. Tsai, J. C. Knights, G. Chang, and B. Wacker, Appl. Phys. Lett. 59, 2998 (1986).
[85]J. C. Knights and R. A. Lujan, Appl. Phys. Lett. 35, 244 (1979).
[86]A. Gallagher, in *Materials Issues in Amorphous Semiconductor Technology*, edited by A. Adler, Y. Hamakawa, and A. Madan (Material Research Society, Pittsburgh, PA, 1986), p. 3.
[87]R. A. Street, J. C. Knights, and D. K. Biegelsen, Phys. Rev. B 18, 1880 (1978).
[88]K. G. Spears, T. J. Robinson, and R. M. Roth, IEEE Trans. Plasma Sci. PS-14, 179 (1986).
[89]T. Hamasaki, M. Ueda, A. Chayahara, M. Hirose, and Y. Osaka, Appl. Phys. Lett. 44, 600 (1984).
[90]W. D. Reents, Jr. and M. L. Mandich (unpublished).

# IMPORTANT CONSIDERATIONS FOR OPTIMIZING PRODUCTION RATES IN RF DISCHARGE CHEMISTRY

Mark J. Kushner* and Alan Garscadden**

*Gaseous Electronics Laboratory, University of Illinois, 607 E. Healey, Champaign, Illinois, 61820

**Air Force Wright Aeronautical Laboratory, Wright Patterson Air Force Base, Ohio 45433

## ABSTRACT

Important issues which should be considered when optimizing RF discharges for use in plasma processing are discussed using results from electron kinetics and plasma chemistry models. Mixtures of $Ar/SiH_4$ and $H_2/SiH_4$ are discussed as exemplary systems for the plasma deposition of amorphous silicon. The effect of dissociation of the feed stock gas on subsequent rates of dissociation is discussed, as is the effect of diluting silane discharges with argon.

## KEYWORDS

RF glow discharges; plasma chemistry; silane; plasma deposition; plasma processing; transport coefficients; dissociation rates; plasma simulations

## INTRODUCTION

The use of radio frequency (RF) glow discharges for plasma processing of semiconductor materials is now common practice (Coburn, 1983; Kampas, 1984). The apparatus is typically a parallel plate capacitively coupled RF discharge operating at 100's of kHz to 10's of MHz, having an electrode separation of a few to 10 cm, and gas pressure of 10's to 100's of mTorr. The typical power deposition is 10's to 100's of $mW/cm^3$ with flow rates such that the residence time of gas in the discharge is 10's to 100's of ms. In a production environment, one desires to operate with optimum discharge conditions so that one simultaneously maximizes the production rate (eg., etching or deposition), utilization of the feed stock gases, and uniformity of the product throughout the discharge chamber. These goals are unfortunately contradictory. Maintaining a uniform product throughout the reactor implies that the discharge conditions remain constant from the gas inlet to the gas outlet. Having a high utilization rate of the reactant gas means that the dissociation fraction of the feedstock is large. As the feedstock gas flows downstream, this implies that discharge conditions are changing. Often the primary reactant gas in the case of plasma deposition, is diluted with a "non-reactive" buffer gas with the intent of improving the deposition parameters (Knights, 1984; Hirafuji, 1986).

In this paper, we discuss important issues that should be considered while attempting to optimize or parameterize plasma processing. With results from discharge and plasma chemistry models, we examine discharges in gas mixtures of $Ar/SiH_4$ and $H_2/SiH_4$ as model systems. These systems are used for the plasma enhanced chemical vapor deposition (PECVD) of amorphous silicon (a-Si:H). We discuss effects that result from the dilution of silane and what we call "downstream" effects. That is, consequences of the gas having a finite residence time in the discharge region as it flows from inlet to outlet.

## THE EFFECT OF DISSOCIATION ON THE RATE OF DISSOCIATION

In silane discharges as used in PECVD, radicals such as $SiH_2$ and $SiH_3$ are generated by various processes including electron impact dissociation, after which they diffuse to the substrate and incorporate into the growing film (Kampas, 1984). The influence of dissociation of silane on plasma processing occurs not only through the effect of the dissociation products on the plasma chemistry and deposition process, but also because at high levels of dissociation, the electron energy distribution changes. Consequently rate constants for electron impact dissociation and electron transport coefficients change. These effects are relatively large in silane because the gas has a Ramsauer minimum in its momentum transfer cross section and the vibrational cross sections at low energy (<10 eV) are large, $\approx 1\ A^2$ (Garscadden, 1983). Therefore small changes in the fraction of silane in a buffer gas, or dissociation of silane, significantly change the rate of energy loss at low energy, thereby changing transport coefficients.

From mass and optical spectrometry, we have determined that a major product of the dissociation of silane in slow flow or high power density plasma deposition reactors is molecular hydrogen (DeJoseph, 1982). The effect of the build up of dissociation products as the gas flows down stream is, in this case, equivalent to starting with a diluted mixture of $H_2/SiH_4$. As will be shown below, this effective "dilution" of silane with hydrogen causes a change in drift velocity and an increase in the rate of dissociation. Cross sections for the radical species which are also products of the dissociation of silane are not available. We therefore studied the effect of dissociation on drift velocity and dissociation rates by examining the effects of diluting silane with hydrogen. These studies were performed by solving for the electron distribution function (Garscadden, 1983) and deriving transport coefficients.

Some of the effects of gas dilution on transport parameters are shown in Fig. 1 (drift velocity) and Fig. 2 (dissociation rates). Pure silane has an unusual electron drift velocity profile versus E/N (electric field/gas density), having a local maximum near E/N = 20 Td (1 Td = $10^{-17}$ V-cm$^2$). A silane plasma which is instead heavily diluted with hydrogen has a relatively constant collision frequency at moderate E/N (> 50 Td) and hence has a drift velocity that is nearly linearly proportional to E/N. At low E/N, the drift velocity is nearly a monotonically increasing function of E/N losing the Ramsauer effect with even moderate dilution. At low E/N, plasmas with large fractions of silane have the higher drift velocity; at high E/N (>60 Td), dilute plasmas have the higher drift velocity. When diluting with hydrogen, though, the electron impact rate constant for dissociation of silane monotonically increases for all E/N. Therefore, to evaluate the change in the rate of dissociation of silane resulting from dilution with hydrogen, one must consider the change in drift velocity (which at constant current density implies a change in electron density) as well as the change in the rate constant for electron impact dissociation. The operative E/N of the discharge is a function of discharge geometry and other factors. The discharge operating points in Figs. 1 and 2, and hence the behavior of the transport coefficients as silane is dissociated, are therefore dependent on local conditions and circuit controls.

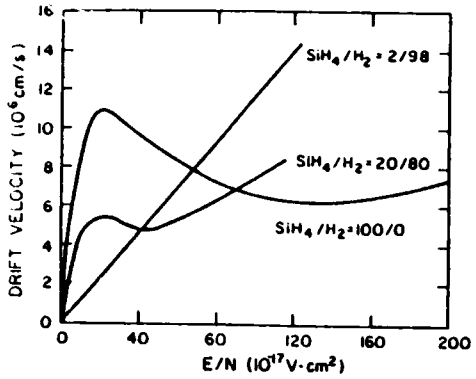


Fig. 1 . Drift velocity in mixtures of silane and hydrogen for E/N (V-cm$^2$).

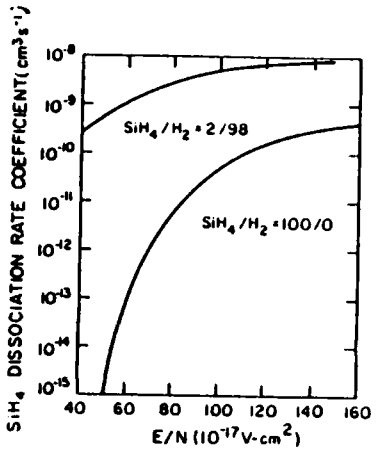


Fig. 2 . Rate coefficient for electron impact dissociation of silane.

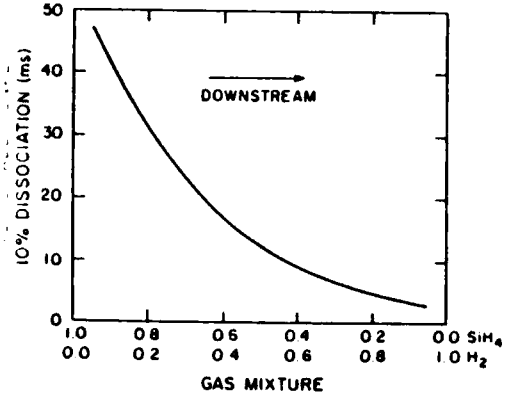


Fig. 3 . Time for 10% dissociation of remaining silane in a silane/hydrogen gas mixture.



As silane dissociates, the electron impact dissociation rate increases for all E/N due to changes in the high energy tail of the electron distribution function. This effect is unstable and could lead to "runaway" dissociation. That is, as silane dissociates, the rate constant for dissociation increases, which increases the total rate of dissociation, and so on. This effect is shown in Fig. 3 where the time required for 10% of the current density of silane to dissociate is plotted as a function of dilution with $H_2$. The conditions are a discharge power of 20 mW/cm$^3$, current density of 1 mA-cm$^2$, and E/N = 125 Td. As the silane dissociates and the hydrogen mole fraction increases, the time constant for dissociation decreases. The residence time in the reactor increases in the direction of the arrow in the figure; that is, in the direction of decreasing silane fraction.

## THE EFFECT OF DILUTION OF SILANE WITH ARGON

Silane gas mixtures for the PECVD of $\alpha$-Si:H often are diluted with a noble gas such as argon. In this section, we examine some of the effects on reaction rates, radical densities, and deposition rates of such dilution. These studies were performed with results from a model for the electron kinetics and plasma chemistry in RF discharges sustained in mixtures of Ar/$SiH_4$ (Kushner, 1986). The model utilizes a Monte Carlo particle simulation to generate electron impact rate constants, and a 1-1/2 dimensional, time dependent model for the generation and transport of radicals in the plasma.

The sequence of steps which occur in the generation of radicals and eventual growth of the film is

[Electron Impact Dissiociation] ⟶ [Additional Reactions] ⟶ [Diffusion or Drift to Substrate] ⟶ [Adsorption and Incorporation]

Any consequence of diluting the feedstock, in this case silane, which changes or interferes with any of these steps ultimately affects the characteristics of the film being deposited.

The local rate of electron impact dissociation of the feedstock is the product $R(x) = n(x)k(x)N(x)$, where x is position in the discharge, n is the electron density and k is the electron impact rate constant for collisions with reactant N. For constant power deposition, the electron density does not change dramatically with dilution, as discussed above. The electron impact rate constant, though, can significantly change, and has the most dramatic dependence both on position and on dilution. The reactant density is, of course, inversely proportional to the dilution factor.

The inter-relation of the steps in the sequence, and how they change with dilution of silane with argon is shown in Fig. 4. In this figure, reactant densities, electron impact rate constant, production rate (R = nkN), and radical densities are plotted for $SiH_2$, $SiH_3$, and $SiH_3^+$ in Ar/$SiH_4$ mixtures of 0/100 and 95/5. The power deposition and gas pressure are 50 mW/cm$^3$ and 0.5 Torr respectively (centerline temperature ≈675 K, surface temperature 500K). The sticking coefficients for $SiH_2$ and $SiH_3$ are 1.0 and 0.15 respectively. The electrode separation is 1.5 cm and the discharge is symmetric.

As silane is diluted with argon, the electric field in the bulk plasma decreases but the penetration into the bulk plasma of high energy electrons from the sheaths increases. Therefore, the value of rate constants for moderate and high threshold processes (such as electron impact dissociation and dissociative ionization)

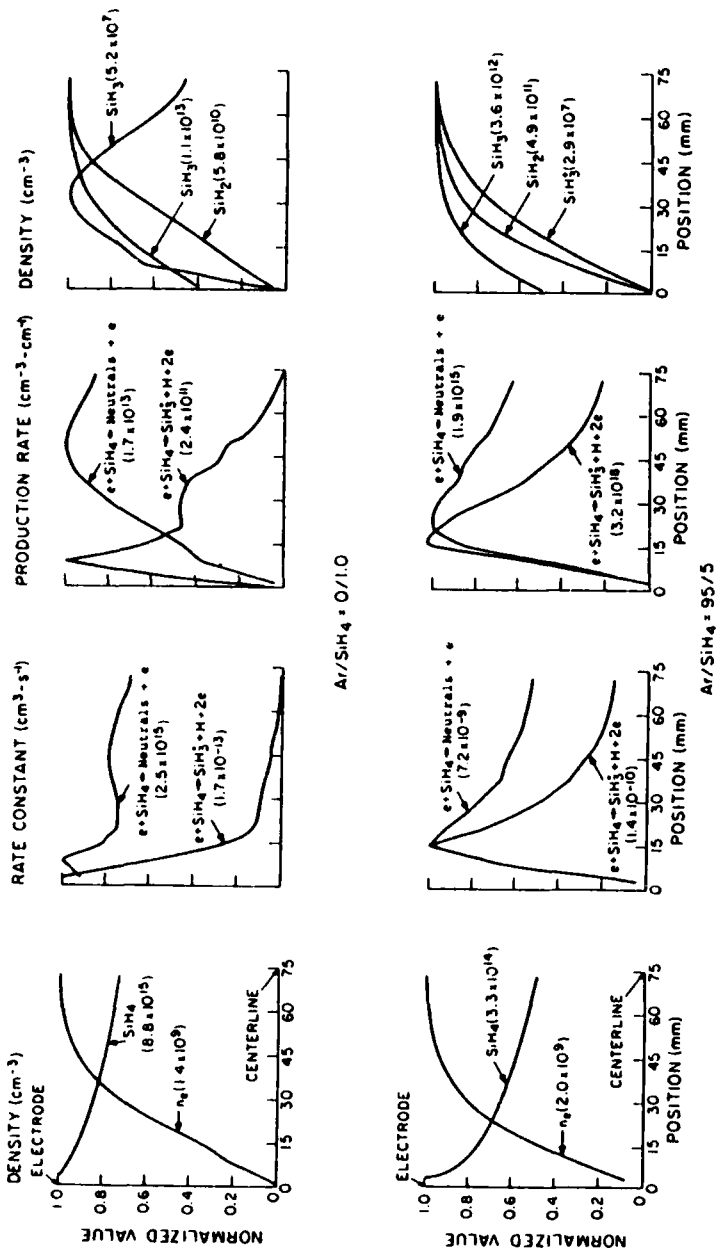


Fig. 4 - Density (silane, electrons), rate constant, production rates, and densities for production of neutrals ($SiH_2$, $SiH_3$) and ions ($SiH_3^+$) by electron impact. Results are shown for silane (top) and an argon/silane mixture (bottom).



increase in average value both near the electrodes and in the bulk, as shown in Fig. 4b. The effect is similar to that for hydrogen discussed above. When these rate constants are convolved with the reactant densities (Fig 4a) the production rates for $SiH_3^+$ and neutral dissociation are obtained (Fig. 4c). Finally, when these rates are used in the complete plasma chemistry model, the radical and ion densities shown in Fig. 4d are obtained. With large mole fractions of silane, reactions of radicals with silane (eg, $SiH_3^+ + SiH_4 + M \rightarrow Si_2H_7^+ + M$) occur rapidly. The spatial distribution of such radicals therefore resembles the distribution of their production rates. Upon dilution with argon, the spatial distribution is less dependent on the shape of the production rate since the effective mobility of the radicals increase. This topic is discussed further below.

The consequence of further plasma chemical reactions depends on the relative rate of loss by diffusion compared to loss by further reaction, principally with the feedstock. That is, when

$$\beta = \frac{D/\Lambda^2}{k[SiH_4]} \ll 1$$

(where D is the diffusion constant, $\Lambda$ the diffusion length, and k the reaction rate constant) then dilution has little effect on the disposition of the radical. In this case, the rate of reaction is sufficiently large that the location and density of the radical is determined by the balance between the rate of production by electron impact and the rate of loss by subsequent reaction. When the ratio $\beta$ is near or greater than unity, then transport is important and dilution can significantly change the density of the radical.

This effect is demonstrated in Fig. 5 where the calculated rate of production by electron impact and densities of the SiH radical are plotted as a function of position for discharges having $Ar/SiH_4$ ratios of 0/100, 25/75, and 75/25. (Production of SiH is dominated by electron impact dissociation of silane.) The rate of production differs in magnitude for the three cases however the spatial distribution is similar, peaked near the electrode where the high energy tail of the electron distribution function is important. The SiH radical reacts with silane with a rate constant of $\approx 4 \times 10^{-12}$ cm³/s, yielding a reaction time of ≈40/f μs, where f is the mole fraction of silane. For these conditions, the diffusion time is 1.5 ms, independent of f. These values yield $\beta \approx 0.03/f$. For f = 1.0 and 0.75 (as shown in the figure), $\beta \ll 1$, and the SiH radical reacts near the site of its production; its density therefore reflects the spatial distribution of the production rate. At low silane mole fractions (f = 0.05, $\beta \approx 1$), the reaction time is sufficiently long that diffusion redistributes SiH to give it the appearance of having a volumetric source and edge sink. The selective incorporation of radicals into the growing film is therefore seen to be a function of its probability of survival during transport to the substrate, and hence a function of dilution.

## BI-RADICAL DOWNSTREAM REACTIONS

As the input gases flow downstream, the cumulative densities of the products of electron impact dissociation increase. When the absolute density of radicals is small, heavy particle reactions after dissociation are dominated by those with the feedstock. As the radical density increases downstream, bi-radical reactions may become important. One such example is the reaction sequence

$$e + SiH_4 \rightarrow SiH_3 + H + e$$
$$SiH_3 + SiH_3 \rightarrow Si_2H_6^*$$

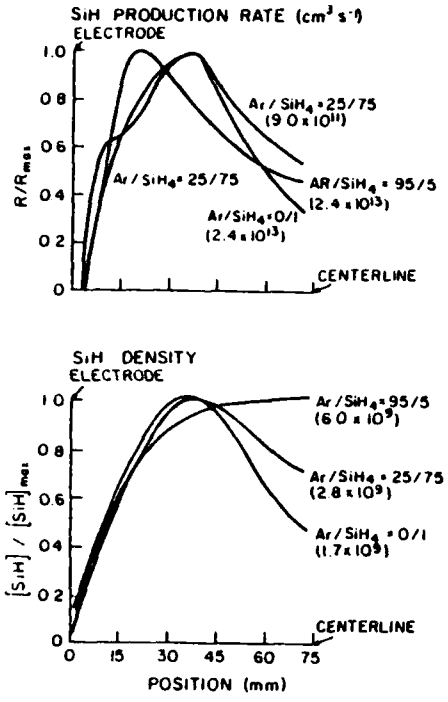


Fig. 5. Production rates and density of SiH in $Ar/SiH_4$ mixtures.

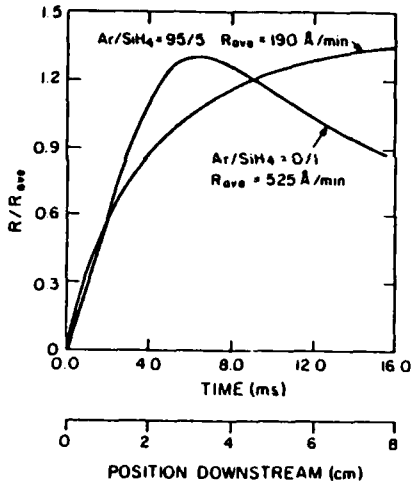


Fig. 6 . Downstream deposition rate of a-Si:H in $Ar/SiH_4$ mixtures.



where the rate constant for the biradical reaction is $\approx 2 \times 10^{-11} cm^3/s$ (Tachibana, 1984). $SiH_3$ is otherwise unreactive with silane, $k \approx 10^{-15} cm^3/s$ (Coltrin, 1984). The consumption of radicals in this manner may decrease the rate of deposition of a-Si:H. This effect is illustrated in Fig. 6 where the deposition rate is plotted as a function of downstream distance for pure silane and an argon-silane mixture of 95/5. The deposition rate in pure silane thus goes through a spatial or temporal maximum as the density of radicals becomes sufficiently large that bi-radical reactions become important. Although the deposition rate for the dilute mixture is only 35% that of the pure gas, the smaller probability of bi-radical reactions nets a more uniform deposition.

## CONCLUDING REMARKS

We have examined some issues pertaining to dilution of silane in plasma deposition of amorphous silicon that should be considered when optimizing the process. We found that dissociation rates of silane increase with decreasing mole fraction of silane, and the rates will therefore increase as the feedstock is depleted as it flows downstream. When diluting silane with noble gases, the most profound effects are on the spatial dependences of the production rates and for radicals which directly react with the feedstock. At high mole fractions, radicals react at the location of their production by electron impact. Transport to the surface can only be obtained by lowering the silane mole fraction. The uniformity of deposition is also affected by a similar process. At high silane mole fractions, which lead to high absolute radical densities bi-radical reactions become important downstream of the inlet, resulting is a less uniform deposition rate.

## ACKNOWLEDGEMENT

The work of M. J. Kushner was supported by the Materials Science Division of the Army Research Office under the direction of Dr. Andrew Crowson, Contract No. DAAG29-85-C-0031. The work of A. Garscadden was supported by the United States Air Force Systems Command.

## REFERENCES

Coburn, J. W., and H. F. Winters (1983). Ann. Rev. Mater. Sci., 13, 91-116.

Coltrin, M. E., R. J. Kee, and J. A. Miller (1984). J. Electrochem. Soc., 131, 425-433.

Dejoseph Jr., C. A., A. Garscadden, and D. R. Pond (1982). Spectroscopic Measurements in Silane Reactor Plasmas. Proceedings of the International Conference on Lasers,

Garscadden, A., G. L. Duke, and W. F. Bailey (1983). Appl. Phys. Lett., 43, 1012-1014.

Kampas, F. J. (1984). Semicond. and Semimetals, 21A, 153-177.

Knights, J. C., R. A. Lujan, M. P. Rosenblum, R. A. Street, D. K. Bieglesen, and J. A. Reimer (1984). Appl. Phys. Lett., 38, 331-333.

Kushner, M. J. (1986). in J. W. Coburn, R. A. Gottscho, and D. W. Hess, eds., Plasma Processing (Materials Research Society), 93-307.

Tachibana, K. (1984). in T. Takagi, ed., Proc. 8th Symp. on Ion Sources and Ion-Assisted Technology (Inst. Elec. Engr. Japan), 319-326.

Shirafuji, J., S. Nagata, and M. Kuwagaki (1986). Jpn. J. Appl. Phys., 25, 336-344.

## DISCUSSION

A. V. PHELPS: Does your model take into account the conversion of $SiH_3$ to $Si_2H_6$ at the surfaces?

M. KUSHNER: Yes, the plasma chemistry model includes a sticking coefficient for $SiH_3$ and includes the association reaction $2SiH_3$ (adsorbed) → $Si_2H_6$ (gas). In practice, this is only important for gas pressures of less than 10-20 mTorr. For gas pressures of a few hundred mTorr, volumetric association reactions dominate.

# SIMULATION OF THE BULK AND SURFACE PROPERTIES OF AMORPHOUS HYDROGENATED SILICON DEPOSITED FROM SILANE PLASMAS

Michael J. McCaughey and Mark J. Kushner
University of Illinois
Department of Electrical and Computer Engineering
Gaseous Electronics Laboratory
607 E. Healey
Champaign, Illinois 61820

## ABSTRACT

A Monte Carlo simulation for the growth of amorphous hydrogenated silicon (a-Si:H) thin films by plasma enhanced chemical vapor deposition (PECVD) is presented. The goal of the model is to predict the bulk and surface properties of films (eg., hydrogen content, deposition rate, buried hydride/dihydride ratios, porosity, and surface roughness) having thicknesses of $\lesssim$2000 Å. The effects on the film properties of the composition of the radical flux incident on the surface are examined. Film properties were found to be critically dependant on the ratio of $SiH_3/SiH_2$ in the radical flux. High values for this ratio results in film properties resembling chemical vapor deposition. Film properties obtained with small values resemble physical vapor deposition. Rough films (RMS roughness >10's of Å) accordingly result from radical fluxes having high $SiH_2$ fractions. We find that surface roughness and hydrogen fraction increase with increasing growth rate and

increasing film thickness, though thin films (<10's layers) have large hydrogen fractions due to there being a hydrogen rich surface layer with a thickness approximately equal to the surface roughness. We also find a correlation between porosity (subsurface voids) and hydrogen fraction, implying that the inner surfaces of voids are lined with ≡Si-H configurations. In simulating films grown from $Ar/SiH_4$ gas mixtures, we find that a decrease in the $SiH_3/SiH_2$ ratio in the radical flux, and increase in the ion/radical ratio incident on the surface are largely responsible for the degradation of film properties observed with decreasing silane fraction.

## I. Introduction

Thin films of hydrogenated amorphous silicon (a-Si:H) fabricated by plasma enhanced chemical vapor deposition (PECVD) are valuable materials for the manufacture of thin film transistors, direct-line contact sensors, xerographic materials, and solar cells.[1-4] The efforts of many researchers have resulted in a generally accepted working theory that device quality films (photoconductivity $> 10^{-5}$ $(\Omega\text{-cm})^{-1}$, low surface roughness, hydride/dihydride ratio >1, spin density $\lesssim 10^{16}cm^{-3}$) are obtained from pure silane plasmas having radical fluxes incident on the substrate composed dominantly of silyl ($SiH_3$). The mechanisms responsible for this behavior were proposed by Gallagher.[5] He observed that silyl cannot directly insert into hydrogen passivated (≡Si-H) silicon bonds on the surface and as a result they are highly mobile in the adsorbed state. The residence time and sticking coefficient of these radicals then depends on the generation of dangling bonds on the surface by ion bombardment or etching reactions. The diffusive motion of these adsorbed radicals, filling in surface roughness results in smooth films. Plasma conditions resulting in large fractions of silylene ($SiH_2$) in the radical flux, which can directly insert into passivated surface sites, or conditions which result in a high rate of activating surface sites by removing passivating H atoms, result in rougher poorer quality films.

In simulating the deposition of thin films of a-Si:H by PECVD one desires to predict physical and processing parameters such as growth rate, hydrogen fraction, hydride/dihydride ratio, local bond structure (Si-Si and Si-H bond angles), surface roughness and porosity. An extension of this predictive capability would be to relate these physical parameters to

electronic properties of the material, either on an ab initio or semi-empirical basis. Although the qualitative description of film growth described above is logical, there are few, if any, quantitative models for film growth which can predict these properties based on the cited mechanisms. In a similar fashion, many models and descriptions of the plasma kinetics of silane discharges have been presented[6-9] however few have correlated plasma properties to film characteristics. To date, Gleason et al.[10] has presented the most complete physical model of film growth based on first principles simulation techniques. Their model is capable of prediciting bond angles, hydride ratios, hydrogen fraction and local order. Their work, though, did not address thick films having many hundreds of layers. Therefore, bulk properties such as surface roughness and porosity were not predicted.

In this paper, we present a Monte Carlo simulation for the deposition of a-Si:H from silane glow discharges and we relate plasma properties (in the form of radical and ion fluxes to the substrate) to bulk and surface characteristics of the film. As described below, we do not address the issue of short range order (eg., bond angles) as discussed by Gleason et al.,[10] though, we do address bulk film properties such as porosity and surface roughness. By using computed radical fluxes from a companion model for the plasma chemistry of silane discharges,[6] a complete first order model for the growth of a-Si:H films is presented.

The model presented here emphasizes the bulk properties of the film as opposed to local bond structure. The modeling techniques we use are capable of simulating the deposition of thick films exceeding many hundreds of layers while de-emphasizing the details of the short range order, particularly bond angles. This tradeoff is accomplished by assuming that the film is composed

of a cubic lattice, where each lattice point may be occupied by either a silicon atom or a void. The use of the term lattice does not imply that there is any long range order in the occupation probability of a site by a silicon atom. No assumptions are made concerning the coordination partners of each silicon atom. The amorphous character of the film results from the random distribution of coordination partners for each silicon atom in the lattice, and from the finite but random probability that a lattice point is occupied by either a silicon atom or a void.

In Section II, the Monte Carlo model for film growth is described in detail. Simulated properties of a-Si:H films (roughness, hydrogen content, porosity) deposited from silane plasmas are discussed in Section III using parametric radical fluxes. The simulation of PECVD a-Si:H films grown from $Ar/SiH_4$ gas mixtures is discussed in Section IV followed by concluding remarks in Section V.

## II. Description of the Model

Our model for the growth of a-Si:H films uses Monte Carlo techniques to simulate the impingment and adsorption of gas phase radicals and ions on the surface of a growing film, as well as for the processes which occur after adsorption. These processes include the sputtering of surface species by energetic ions, diffusion of adsorbed radicals on the surface, the incorporation of radicals into the film, the desorption of radicals from the surface, and the elimination of hydrogen from the film by cross linking between Si-H bonds in the near surface layers of the film. Gas phase-surface reactions are also simulated by including reactions between the impinging flux and the surface lattice species when non-sticking radicals strike the surface.

For the results discussed here, we typically modeled the growth of a square patch of a-Si:H approximately 100-250 Å on a side having up to 1000 layers or a thickness of 2000-3000 Å. Periodic boundary conditions are used for the lateral dimensions of the film. In the discussion that follows, the term "site" denotes the x-y coordinate of a position on the film as viewed normally from the plasma. The term "lattice point" denotes the position of a particular atom or void in the film below a given site. There are many lattice points stacked vertically at each site.

The simulation proceeds schematically as follows. A flux of radicals is directed towards the surface, isotropically for neutrals and vertically for ions. The identity of the individual radical and the local morphology of the impingement site determines whether the radical adsorbs, sputters, bonds, or chemically reacts with the surface. An adsorbed, but non-bonded, radical may diffuse on the surface until encountering an activated site (ie., a dangling bond, $\equiv Si-\bullet$) at which time it bonds, a process which constitutes film growth. $SiH_n$ radicals which bond to the film, may later interconnect with adjacent surface species to form the amorphous network. Cross linking may occur between both nearest and next nearest neighbors, the latter possibly resulting in the formation of voids. Adsorbed species exceeding a specified residence time without bonding to the film may desorb, thereby enabling calculation of a sticking coefficient. By specifying characteristic frequencies for each process, the rate of occurance of a particular event is determined relative to the rate of arrival of radicals on the surface. The model then proceeds as an effective integration in time of the equation of motions of each particle in the simulation.

An important feature of the model is the categorization of lattice points as being either in the near surface layer or in the bulk film. Since we

desire to simulate volumes of a-Si:H films having $10^6$ - $10^7$ individual sites, it is not computationally practical to retain statistical information on each site. The model instead retains statistics for each lattice point in the near surface layer at each site. The near surface layer is typically 5-20 atoms deep. When a radical bonds to the surface at the top of the near layer, the lattice point at the bottom of the near layer is removed and its statistical information added to the average values for the bulk film. Although the near surface layers at each site are only 5-20 layers thick, the height of film at adjacent sites may differ by an arbitrary amount. Therefore, the rms difference in height (or roughness) of the film may exceed the near surface layer thickness.

A. Lattice Points and Site Heights

Lattice points in the near surface layers are classified as being either unoccupied or occupied by a silicon atom. An occupied site is identified by its coordination partners. For example a point identified as SSSS denotes occupation by a silicon atom having four other Si atoms as coordination partners. A point identified as SSHD has two Si atoms and an H atom as coordination partners, and a dangling bond. Lattice points at a particular site which are unoccupied and buried beneath an occupied point are denoted as a void. The fraction of voids beneath the surface layer is therefore an indication of the porosity of the film. The topmost occupied lattice point is the surface of the film at that site. The average thickness of the film is then the average of the topmost heights for each site. The roughness of the film is the rms deviation of the thickness of the film from its average value.

B. Radical Fluxes

The flux of neutral radicals incident on the surface may consist of an arbitrary mix of $SiH_n$ ($0 \leq n \leq 3$) or H. We do not presently consider disilane radicals. The flux of ions is assumed to consist of only a single generic charged species. The distribution of radicals is either specified as a part of a parametric survey, or is obtained from the results the electron kinetics and plasma chemistry model described in Ref. 6. The time interval between impingement of a neutral radical from the plasma onto the surface is

$$\Delta t_R = (\Phi \cdot L^2)^{-1}, \qquad (1)$$

where $\Phi$ is the total neutral radical flux and L is the physical length of the square of film we are simulating. The length is based on the width, in number of sites, of the lattice assuming an average lattice constant of 2.5 Å. Every $\Delta t_R$ during the simulation a radical is directed towards the surface based on selection of a random number r ($0 < r \leq 1$). The particular radical which is directed towards the surface is that radical satisfying

$$F_{i-1} < r \leq F_i, \quad F_i = \sum_{j \leq i} f_j \qquad (2)$$

where $f_i$ is the mole fraction of radical i in the flux of radicals incident on the surface. A similarly defined timer increment, $\Delta t_I$, for the ion flux determines the frequency with which ions are directed towards the surface.

The site on the surface $(x_i, y_i)$ at which the selected radical impacts is randomly selected by use of two additional random numbers:

$x_i = r_1 \cdot L$, $y_i = r_2 \cdot L$. The particular site is constrained in the following fashion. Assuming that the neutral radical flux is incident isotropically onto the surface, the probability that a radical impacts in a deep well (resulting from surface roughness) is small. The local morphology of the selected site is therefore inspected to determine whether the site sits at the bottom of a well. A well is defined as a site which is lower than the height of its nearest neighbor sites by an amount greater than or equal to the near surface layer. If this is the case, the radical which would have otherwise impacted in the well is placed on the surface site adjacent to the well. Assuming that ions are incident vertically, they may impact on any site including those in wells.

C. Selection Criteria for Plasma-Surface Reactions

The surface lattice points at any site may be classified as inert, passivated, or activated. An inert surface site is occupied by a silicon atom fully coordinated to other silicon atoms (ie., SSSS). A passivated surface site is occupied by a silicon atom having at least one Si-H bond and no dangling bonds (eg., SSHH) whereas an activated surface site is occupied by a silicon atom having at least one dangling bond (eg.,SSSD). All neutral silane radicals incident on an inert site are assumed to adsorb onto the surface. All neutral silane radicals incident on an activated site may directly incorporate into the lattice; for example,

$$SiH_2(g) + SSSD \rightarrow SSSS + SHHD. \qquad (3)$$

where (g) denotes a gas phase species.

Neutral silane radicals $SiH_n$, $n \leq 2$, may also incorporate into passivated sites by displacing a hydrogen atom from the surface species, a process which is nearly thermo-neutral. For example,

$$SiH(g) + SSSH \rightarrow SSSS + SHHD. \qquad (4)$$

$SiH_n$ radicals with $n \leq 2$ therefore effectively have sticking coefficients of near unity unless later sputtered off the surface. In the model, silyl radicals ($SiH_3$) may only incorporate into an active surface site and therefore most often move directly into an adsorbed state since the fractional surface density of active sites is small. This condition is important to determining the surface properties since the mole fraction of $SiH_3$ radicals in the incident flux is typically $\geq 0.9$ for plasma conditions which result in device quality films.

The rate of generation and passivation of surface sites is important in two respects. First, the removal of hydrogen from the surface is important in the accounting of the total amount of hydrogen in the film and in determining the characteristics of the hydrogen rich surface layers. Second, the net rate of generation of dangling bonds on the surface by removing passivating H atoms in part determine the sticking coefficient for $SiH_3$ radicals since this specie requires an activated surface site for incorporation.

New passivated and active surface sites are continually being generated by radicals which incorporate into the film and constitute the new surface specie at that site. Non-sticking radicals, molecules, and ions from the plasma may also react with the surface species to generate activated sites.

Specifically, in the model we assume that an H atom (in the incident flux) landing on an active site passivates the dangling bond, whereas H atoms landing on a passivated site extract a hydrogen thereby etching the surface. For example,

$$H(g) + SSSD \rightarrow SSSH \quad (5)$$

$$H(g) + SSSH \rightarrow SSSD + H_2(g). \quad (6)$$

The latter process is analogous to the gas phase hydrogen abstraction reaction

$$H + SiH_4 \rightarrow SiH_3 + H_2. \quad (7)$$

The analogous reactions to Eqs. 5 and 6 may also occur with $SiH_4$ as the reactant instead of H. The former reaction

$$SiH_4(g) + SSSD \longrightarrow SSSH + SiH_3(g) \quad (8)$$

may be important since the flux of $SiH_4$ striking the surface is large compared to that for H. The etching reaction

$$SiH_4(g) + SSSH \longrightarrow SSSD + SiH_3(g) + H_2(g) \quad (9)$$

is likely not to be rapid since it is endothermic by approximately 1.9 kcal/mole [11]. Nevertheless, as will be discussed in Sec. IV, the net rate of passivation of the surface by $SiH_4$ is important in accounting for film properties.

Dangling bonds may also be generated by sputtering off the passivating H atom by ion impact and by sputtering of loosely adhered silicon containing surface species, for example

$$M^{+}(g) + SSSH \rightarrow M^{+}(g) + SSSD + H(g). \qquad (10)$$

The model ignores the direct contribution of ion impact to the densification of the film, as addressed by Mueller[12] and by Drevillon.[13] The precise mechanism for hydrogen removal by ion impact is not specified in the model, though it is assumed to be a combination of sputtering and thermal spiking. In the simulation, a maximum number of H atoms is specified, typically 10, that may be removed from passivated bonds per incident ion subject to the availability of ≡Si-H bonds in the vicinity of the ion impact. In practice, the average number removed per incident ion is less than ten due to this requirement.

Ion impact may also sputter off loosely adhered $SiH_n$ groups on the surface, a process which has been described as "scouring" of the surface.[14] Typically, these groups are the terminous of polymeric chains which are not presently simulated in this model. To investigate the importance of this process, we defined loosely adhered $SiH_n$ groups as species on the surface which have only 1 silicon atom as a coordination partner (ie; SHHH, SHHD, SHDD, SDDD). We then included the process, for example,

$$M^{+}(g) + (SSSS\text{-}SHHH) \longrightarrow M^{+} + SSSD + SiH_3(g) \qquad (11)$$

in the model. The importance of this process is discussed in Section IV.

D. Surface Diffusion and Reactions

During the simulation, adsorbed radicals on the surface, principally $SiH_3$, diffuse from surface site to surface site. Adsorbed radicals are moved from their current surface site with each increment of the global timer. The direction of the move in the plane of the surface (one of eight directions including nearest and next nearest neighbors) is determined by choice of a random number. An adsorbed radical is allowed to make a specified number of such moves before being removed from the surface; that is, being desorbed. The specified number of moves is an input parameter chosen to give a reasonable sticking coefficient. Under conditions which experimentally yield high quality films, allowing 10 such moves for $SiH_3$ results in a sticking coefficient of 0.05 - 0.25, in fair agreement with recent measurements.[15,16]

The diffusive motion of the adsorbed radical is constrained in the following manner. The height of the film at a particular site is h. When an adsorbed radical is moved, we define the height of the film at the initial site as $h_i$ and the height of the film at the site to which the adsorbed radical is chosen to move as $h_f$. Moves with $h_i \geq h_f$ are allowed; that is the adsorbed radical is allowed to make a lateral move or fall onto a site of lower height. Moves with $h_i < h_f$ are not allowed; that is the adsorbed radical is not allowed to climb to a higher surface site. An adsorbed species may be trapped in a well as a result of a move. A trapped radical is one which does not move from a surface site for the maximum number of attempted moves. In this case the model assumes that the radical is permanently trapped and will eventually bond at that location. It is therefore bonded in place and if necessary $H_2$ is eliminated.

When an adsorbed radical moves over a new surface site, it may bond to the occupying Si atom and incorporate into the film in the same manner as described above for neutral radicals incident from the plasma. An adsorbed radical which does not bond to the surface site beneath it is moved again on the next cycle. When an adsorbed radical moves to a surface site where the height of the film at an adjacent site is higher than its present location these are additional considerations. Under those conditions, as well as when the radical attempts a move with $h_f > h_i$, the adsorbed radical may bond with the lattice atom having the same height at the adjacent site. This adjacent lattice atom is buried beneath its own surface site and constitutes part of the near surface layer for that site.

E. Cross Linking, Interconnection and Hydrogen Elimination

Cross linking is the process whereby ≡Si-• (eg., SSSD) and ≡Si-H (eg., SSSH) configurations, bond, and form the amorphous network of the film. Cross linking is also an important process for removing hydrogen previously incorporated into the lattice. Cross linking may occur between silicon atoms in adjacent sites having dangling bonds, for example,

$$SSSD + SSSD \rightarrow SSSS + SSSS \qquad (12)$$

or between silicon atoms in adjacent sites having passivated bonds, for example,

$$SSSH + SSSH \rightarrow SSSS + SSSS + H_2(g). \qquad (13)$$

The former process is exothermic. The latter process, though being endothermic, is believed be largely responsible for eliminating hydrogen from the film. An activation energy of 1.35 kcal/mole has been assigned to this process by observing hydrogen content as a function of substrate temperature.[17] Cross linking may occur between ≡Si-H configurations topmost on the surface and those buried beneath the surface but exposed on a sidewall, a process which constitutes film densification.

Cross linking, interconnection, and hydrogen elimination are simulated in the following fashion in the model. A characteristic site examination frequency for nearest neighbors, $\upsilon_n$, and for next nearest neigbors, $\upsilon_{nn}$ are specified. These frequencies yield intervals, $\Delta t_n = 1/\upsilon_n$, which specify the average time between inspecting adjacent lattice points. After $\Delta t_n$ has elapsed at a particular lattice point, a survey of nearest neighbor lattice points is made. The nearest neighbor lattice points are the ≡Si-• and ≡Si-H complexes within a lattice constant of the central point. If the central lattice point is a ≡Si-• complex, the survey consists of examining the nearest neighbor points in a random order searching for another ≡Si-• complex. A successful search results in an interconnection as shown in Eq. 12. If the central lattice point is a ≡Si-H complex, the survey searches for another ≡Si-H complex. If the search is successful, the choice of another random number determines whether there is enough thermal energy available for the endothermic process to take place. This is determined by having $-\ln(r) \geq \epsilon_a/T_s$, where r is a random number (0,1), $\epsilon_a$ is the activation energy, and $T_s$ is the substrate temperature. If these conditions are met, interconnection with hydrogen elimination occurs as shown in Eq. 13. The procedure described for nearest neighbor interconnection is also followed for next nearest neighbors, with the examination interval being $\Delta t_{nn} = 1/\upsilon_{nn}$.

F. Void Formation

Cross linking and interconnection with next nearest neighbors can result in the formation of voids (or porosity). The algorithm for these processes is identical to that described above for interconnection between nearest neighbors. The frequency of interconnection with next nearest neighbors, however, must be less than that for nearest neighbors as evidenced by the low porosity of films ($\lesssim$ 15%) which can be deposited. To account for this observation, a ratio of $\upsilon_n/\upsilon_{nn} \geq 50$ was typically used. As cross linking with at most next nearest neighbors is allowed, the voids generated in the model are at most one lattice constant wide. They may, however, have either vertical or horizontal extents of up to many hundreds of lattice constants. In forming voids in this fashion, low porosity films may occur in films which have an extremely rough surface, since it is not possible (in the model) to cross link at greater distances than next nearest neighbors which would otherwise bridge roughness and form large voids. The large surface roughness, though, gives the appearance of a porous near layer, and in measurements of surface roughness a void fraction is often cited based on the near layer roughness. Our definition of porosity is a void (vacant lattice points) below the topmost occupied lattice point at a site.

Occupied surface lattice points on both vertical and horizontal surfaces are usually passivated by hydrogen. Therefore, the formation of voids traps hydrogen below the surface. Our algorithms do not presently allow for evolution of hydrogen from sub-surface sites and voids. Therefore the bulk hydrogen fractions for porous material (void fraction >10's of percent) are likely to be overestimated. This effect is discussed below.

## III. Simulated Properties of a-Si:H Films

In this section, we will discuss results obtained from our model for the simulation of the growth of hydrogenated amorphous silicon films from silane plasmas when the radical fluxes are specified as part of a parametric survey. In Section IV, we discuss results for when the radical fluxes are obtained from a companion model for the electron kinetics and plasma chemistry of discharges sustained in silane[6].

Before beginning the parametric survey, we present a sample of a simulated surface of a-Si:H for typical plasma deposition parameters shown in Fig. 1. The radical fluxes for this case were obtained from the electron kinetics and plasma chemistry model. The discharge conditions are a silane pressure of 250 mTorr, substrate temperature of 500 K, and power deposition of 100 mW-cm$^{-3}$. The total mono-silane radical flux incident on the substrate is 2.5 x $10^{16}$ cm$^{-2}$s$^{-1}$ in the ratio of $SiH_3/SiH_2/SiH/H$ = 0.93/0.0064/1.8 x $10^{-4}$/0.06. The total ion flux incident on the surface is 1.3 x $10^{14}$ cm$^{-2}$s$^{-1}$ and at most 10 surface sites may be activated per incident ion. The frequencies for examination of nearest and next nearest neighbors are $\upsilon_n$= 3.9 s$^{-1}$ and $\upsilon_{nn}$ = 8x10$^{-2}$s$^{-1}$, respectively. The calculated deposition rate from the model using these parameters is 4.5 Å-s$^{-1}$. The hydrogen fraction of the simulated film is $f_H$ = 12%, and the ratio of hydride/dihydride bonds in the bulk material is 2.1, which does not include the hydrogen rich surface layers. By summing the $SiH_3$ flux incident onto the surface and comparing the fluence to the amount of $SiH_3$ desorbing, we obtain a sticking coefficient for $SiH_3$ of ~0.12. The calculated surface roughness (the rms deviation from the average film height of 750Å) is approximately 20 Å. All of these parameters are in good agreement with experimental results for device

quality films grown by PECVD.[1] The qualitative appearance of the surface agrees well with recent scanning tunneling microscopy measurements of the surface of plasma deposited a-Si:H films.[18] Our predicted spin densities are fractionally large (a few times $10^{-4}$, or $\approx$ 5-6 x $10^{18}$ $cm^{-3}$) for films which otherwise have good properties. Desirable spin densities are typically $\lesssim 10^{16}$ $cm^{-3}$.[1] We interpret this discrepancy as there being thermal structural relaxation of the Si network after burial of the surface species which reduces the spin density,[1] a process we do not include in the model.

A. Surface Roughness

The surface roughness of a-Si:H films is important with respect to their use in thin film devices and in multilayer structures where the lattice period may be comparable to the surface roughness.[19] Works by Knights,[20] Tsai, et al.,[21] Collins and Cavese,[22-24] and Collins and Pawlowski[25] have resulted in a qualitative understanding of the origin and scaling of surface roughness. In summary, plasma conditions which have a predominance of silane radicals which have high sticking coefficients ($SiH_n$, $n \lesssim 2$) generally result in rougher films and poor sidewall coverage. The low surface mobility for these radicals results in shadowing of precursor or random surface features, and magnify their roughness. These conditions are found in low pressure silane plasmas (<100 mTorr) or diluted silane plasmas where the probability of radical scavanging reactions, exemplified by

$$SiH_2 + SiH_4 \rightarrow Si_2H_6^*, \qquad (14)$$

is low. Deposition under these conditions resembles physical vapor deposition (PVD). It is generally believed that plasma conditions which result in radical fluxes dominated by $SiH_3$ result in smoother films and higher quality material, and resemble chemical vapor deposition (CVD).

To investigate the effect of adsorbant mobility on the roughness of a-Si:H films, we parameterized our model while varying the fraction of $SiH_3$ in an impinging flux consisting only of a mixture of $SiH_2/SiH_3$. Those results are shown in Fig. 2. We find that the surface roughness is relatively constant until the silyl fraction is less than 0.4, below which surface roughness increases markedly. As the growth rate is a function of $SiH_3$ fraction (see below) we performed our calculations for both constant growth rate and constant magnitude of the radical flux, and obtained similar roughnesses. The ion flux was kept constant throughout. These results imply that surface adsorbant mobility is most influential in determining the surface roughness. However, only moderate fractions of a highly mobile radical, such as $SiH_3$, is sufficient to fill in and smooth the surface. The sticking coefficient for $SiH_3$ is approximately 0.25 for these conditions. It appears, then, that the surface roughness generated by $SiH_2$ sticking in a PVD-like manner can be mitigated by having approximately $\gtrsim$0.1 (0.5 flux fraction x 0.25 sticking coefficient) of the deposition result from the higher mobility specie, $SiH_3$.

Surface roughness is a function of film height, as well as deposition specie. Collins and Cavese[22] found that for conditions dominated by PVD-like deposition surface roughness increased with increasing film height, whereas this dependence on film height was not as strong for CVD-like conditions. They found that roughness scales as $h^{0.33}$ for 0.2 $\mu$m < h < 2 $\mu$m. Drevillon[13]

has also found a correlation between growth rate and surface roughness. In that work, Drevillon viewed surface roughness as a porous overlayer on top of homogeneous bulk material.

We simulated a-Si:H films with different heights for CVD and PVD-like conditions by using incident radical fluxes of $SiH_3/SiH_2$ = 0.9/0.1 and 0.15/0.85, respectively. Our results are shown in Fig. 3. For PVD-like conditions surface roughness scales almost linearly with thickness. For CVD-like conditions surface roughness has only weak dependence on film thickness for thicknesses greater than 100 monolayers (about 250Å). The poor scaling of surface roughness for PVD-like conditions (ie., large ratios of $SiH_2/SiH_3$) results primarily from the shadowing effect of precursor or random roughness in the first few layers. Roughness increases with increasing thickness as the shadowing effect becomes more severe. This effect is likely exaggerated in our simulation by not including densification by ion impact and interconnection with more than second nearest neighbors (see below) though the roughness must clearly be greater than for the CVD-like conditions. For CVD-like conditions, a quasi-equilibrium is reached between shadowing and the "filling" effect of mobile surface species.

For CVD-like film growth, the deposition species with a high surface mobility, $SiH_3$, requires a finite residence time on the surface to fill in roughness. This residence time must be sufficient to allow the mobile radicals to diffuse a distance approximately equal to the transverse dimension of the surface roughness. One would then expect that the surface roughness would increase with increasing deposition rate as the average residence time of mobile species on the surface decreases. In simulating films for CVD-like conditions, though, we find only a weak dependence of surface roughness on growth rate, as shown in Fig. 4.

B. Hydride/Dihydride Ratio

The ratio of buried hydride to dihydride configurations in a-Si:H films is also an indication of film quality, with better films (e.g., higher conductivity) having large (SSSH)/(SSHH) bond ratios.[26] In our simulations, this ratio decreases with increasing growth rate as shown in Fig. 4. Slower growth rates allow longer residence times of SSHH configurations on the surface, and therefore there is more opportunity for interconnection and hydrogen elimination which increases the hydride/dihydride ratio. Many of the dihydride configurations are contained in voids which (see below), in our model, do not further interconnect. Therefore the dihydride density may be over-estimated. Low growth rates then appear to produce better material based on both roughness and hydride/dihydride ratio criteria.

C. Hydrogen Fraction and Porosity

Before discussing the relationship between hydrogen fraction and porosity, we are careful here to differentiate between surface roughness and voids. The former is an rms deviation of the surface height. The latter is the fraction of unoccupied lattice sites below the surface and is thus a measure of film porosity. We have therefore defined the term porosity to mean a true volumetric defect density. In the literature, the term porosity is often used to describe a defect density based on mean film thickness which includes surface roughness. For example, the (volumetric) void fraction of a typical film is 10-20%. A defect density based on mean film thickness, defined as

$$R_a = \text{(average roughness)/(mean film height)} \qquad (15)$$

would add an additional defect density level of about 5% for a film having a roughness of 20Å and height of 400Å.

The atomic fraction of hydrogen in a-Si:H films, $f_H$, is of interest with respect to its effect on electronic properties, such as the optical bandgap and photoconductivity. It is generally observed that $f_H$ increases with increasing deposition rate.[14,27,28] This dependence has been attributed to a "burial effect" where the shorter residence times of ≡Si-H configurations on the surface resulting from increasing growth rates reduce the probability for cross linking and hydrogen elimination. We found a similar dependence of hydrogen fraction on growth rate, as shown in Fig. 5; that is, $f_H$ increases with increasing growth rate. When we do not allow void creation, the same general dependence of $f_H$ on growth rate is obtained, however the value of $f_H$ is lower at slow growth rate. The increase in $f_H$ at low growth rate correlates directly with an increase in the porosity of the film with decreasing growth rate, also shown in Fig. 5. This correlation between voids and hydrogen fraction has been made experimentally for both a-Si:H films,[14,29] and a-Ge:H films.[30] We find that large amounts of hydrogen are being trapped in voids as a result of the sidewalls being passivated by H atoms.

The increase in void fraction we predict at low deposition rates is typically not observed. Void fractions are either constant with growth rate or tend to increase with increasing growth rates under some conditions.[28] Mathematically, our result is a consequence of the fact that interconnection with next nearest neighbors occurs at a fixed rate, so slower growth implies more void formation. These conditions imply that ion impact densification and

heating of the film, both of which will evolve hydrogen and close voids after burial, must be important.

The average void sizes obtained in our simulations are approximately 20-40Å$^3$. We find that the atomic hydrogen content increases, and the ratio of hydride to dihydride configurations decreases, as the average void size increases. (see Fig. 6). This correlation suggests that dihydride configurations are more likely to be found in voids, and by implication hydride configurations are more uniformly distributed. These predictions agree with the results of Reimer, et.al.[14] who, using NMR methods, were able to differentiate between isolated monohydride and grouped dihydride configurations in a-Si:H. Since films that have high monohydride fractions typically have better electrical properties, films having small void sizes should similarly have better properties.

The average void sizes in Fig. 6 are small, <40 Å$^3$, and have equivalent spherical diameters of 3.5-4.0 Å. The distribution of voids is compact, with the relative density falling to $<10^{-4}$ for voids having volumes of greater than a few hundred Å$^3$ (see Fig. 7). Beyond this size, the distribution has a long tail which extends to larger volumes. There are infrequent occurrances of voids having volumes greater than many thousand Å$^3$. These large voids tend to be long fissures, more often vertical than horizontal. For comparison, though, their equivalent spherical diameters are ≤20-25Å.

Void fractions, or porosity, tend to be constant for films >750 Å thick and for deposition conditions for which $SiH_3$ is the predominant deposition radical, as shown in Fig. 8. For the cases shown, the void fraction of PVD-like depositions is less than that for CVD-like conditions when only subsurface porosity is considered. The porosity of the PVD-like material may

be artificially low since the model limits void formation to those created by cross linking with next nearest neighbors, which as described above, is not able to bridge over large roughness and create large voids. Cross linking or bridging gaps across more than one lattice point is required to have PVD-like deposition have a higher porosity than CVD-like conditions. When including the apparent density defect due to surface roughness, as given by $R_a$ in Eq.15, the defect density of the PVD-like films exceeds that of PVD-like films as shown in Figure 8. The majority of density defect for thin PVD-like films (<2000 Å) can be attributed to surface roughness.

D. Hydrogen Rich Surface Layers

The growth mechanism for a-Si:H films suggested by Gallagher implies that both latteral and vertical surfaces of the film are saturated by ≡Si-H configurations.[5] This mechanism then requires that there be a hydrogen rich layer at the surface whose local depth is indicative of the depth of active growth, and whose average depth is approximately the surface roughness. Measurements of hydrogen evolution by post deposition sputtering of a-Si:H films have shown this layer to be 5 layers thick at room temperature, and a monolayer at >500K.[31] Simulations of film growth by Gleason et al. indicated that the active layer is 1.0 - 2.5 atoms deep[10] not including surface roughness. To account for the effect of this active layer on $f_H$, Gleason gives the expression $f_H = N_b f_b + N_s f_s$, where the subscripts denote bulk material (b) or surface layer material (s). N is the fraction of atoms in a particular region, and $f_i$ is the hydrogen fraction in region i. From our simulations we find that $f_s$ is 0.5-2.0 depending on conditions. The local thickness of the hydrogen rich active region in our model is <4-5 layers as

our results computed hydrogen fractions are insensitive to the depth of our near layer for values $\gtrsim 5$.

Extending this logic, the hydrogen content of the film should also scale proportionally to $\Delta h/h$, where $\Delta h$ is the surface roughness, since more roughness provides more exposed surfaces which are passivated by H atoms. Since the ratio $\Delta h/h$ decreases with increasing film thickness, one would expect that the hydrogen content of thin films to be higher than that of thick films. Simulated hydrogen content as a function of film thickness is shown in Fig. 9. In very thin films (less than a few hundred Å's) $f_H$ approaches 50% since the exposed surface areas contain a significant fraction of all atoms in the lattice. For moderately rough films, we have found that up to 30% (roughness 40 Å, height 750 Å) of the total atomic hydrogen present in the films may be in the near layer region and within ~25 Å of the average surface. PVD-like conditions result in a higher hydrogen fraction due to their higher growth rate and larger surface roughness.

## IV. a-Si:H Films from $Ar/SiH_4$ Plasmas

It has generally been observed that the properties of a-Si:H films degrade upon dilution of the input silane gas with argon. The films become rougher,[22] begin growing with a columnar structure,[32] and the fraction of hydrogen found in voids or poly-hydride configurations increases.[14] Concurrently, deposition rate and hydrogen fraction increase.[29] To simulate a-Si:H films using realistic deposition parameters, we computed radical fluxes using the plasma chemistry model described in Ref. 6 for a parallel plate rf PECVD reactor. The deposition conditions were 250 mTorr gas pressure and a substrate temperature of 500 K with an $Ar/SiH_4$ gas mixture. The power

deposition was varied about 50 mW-cm$^{-3}$ in order to give the same flux of silane radicals onto the surface.

Computed flux characteristics are shown in Fig. 10a as a function of silane fraction in argon. As the mixture is diluted with argon, the ratio of $SiH_3/SiH_2$ in the incident flux decreases, and the ratio of the total ion flux to silane radical flux increases. The $SiH_3/SiH_2$ ratio decreases with argon dilution due to the lower net rates of radical scavanging reactions such as that in Eq. 14 and

$$H + SiH_4 \rightarrow SiH_3 + H_2, \qquad (16)$$

both of which combine to increase the $SiH_3/SiH_2$ ratio. The ion to silane radical ratio increases due to there being a larger fraction of power coupled into argon which produces dominantly ions.

Simulated film properties for PECVD of a-Si:H in $Ar/SiH_4$ mixtures with a constant magnitude for the radical flux are shown in Fig. 10b. We find that the bulk hydride/dihydride ratio decreases, deposition rate increases and hydrogen fraction increases when pure silane is diluted with argon, in agreement with experiments.[14] The as buried spin density also increases with argon dilution, in spite of increased hydrogenation of the film. This effect is likely a result of the higher rate of arrival of $SiH_2$ and higher growth rate which reduces the time for interconnection on the surface. Film roughness remains fairly constant for these conditions at ≈20Å. This systematic agreement with experiment[14] was obtained by limiting the role of ions to sputtering loosely adhered $SiH_n$ groups, and having the net rate of passivation of the surface be a constant. These results imply that

net rate of passivation by gas phase species is dominated by $SiH_4$ but rate limited by an activation energy barrier for the reverse process which produces dangling bonds. One should, therefore, find a more sensitive dependency of passivation on substrate temperature than silane partial pressure.

## V. Concluding Remarks

A model for the growth of a-Si:H thin films from silane plasmas has been presented. From the results of the model, we find that the physical properties of the film depend on both the relative fraction of the radicals in the incident flux and on the rate at which the radicals impinge on the surface. The roughness of the a-Si:H films depends most critically on the sticking coefficients of the impinging radicals, and secondarily on the deposition rate. We find that $SiH_3$ fractions of >50% in the incident flux and deposition rates of <3-4 Å/s produce smooth films (roughness <20%). We also find a correlation between subsurface voids, hydrogen content, and high dihydride densities implying that hydrogen is trapped in voids when their passivated sidewalls are covered over. Subsurface evolution of the hydrogen trapped in these voids must likely take place in order to reduce the hydrogen fraction and void density of slowly growing films. In camparing our results to experiment, we find that passivation of dangling bonds on the surface is likely dominated by $SiH_4$, and not radical species. The observation the high quality films are obtained in moderate pressure pure silane plasmas having low dissociation fraction is therefore partly explained by the following criteria. The silane pressure must be sufficiently high that insertion and abstraction reactions of radicals with the feedstock maintain a high ratio of $SiH_3/SiH_2$ in the radical flux. Low dissociation fractions are required to insure that passivation of the surface by $SiH_4$ is complete.

## VI. ACKNOWLEDGEMENTS

The authors would like to acknowledge the support of the Army Research Office (contract No. DAAG29-85-C-0031), under the direction of Dr. Andrew Crowson. The authors would also like to thank Drs. A. Gallagher, N. Mali, and B. Stafford for valuable discussions. Prof. John Thornton, who died unexpectedly in November 1987, also contributed valuable insight to this work.

## FIGURE CAPTIONS

FIG. 1. Simulated surface of an a-Si:H film, being relatively smooth, deposited from a pure silane discharge (250 mTorr, power=100 $mW/cm^{-3}$). The film (area 125 x 125 $Å^2$) has an average thickness of 750 Å with an RMS surface roughness of 20 Å.

FIG. 2. RMS surface roughness as a function of composition of the radical flux ($SiH_3$, $SiH_2$). PVD-like deposition resulting from a large $SiH_2$ fraction in the radical flux ( >0.5) has a high surface roughness.

FIG. 3. RMS surface roughness as a function of film height for PVD-like conditions ($SiH_2/SiH_3$ = 0.15/0.85 in incident radical flux) and CVD-like conditions ($SiH_2/SiH_3$ = 0.1/0.9). The RMS roughness for PVD-like conditions increases with increasing film thickness due to shadowing effects. CVD-like conditions quickly reach an equilibrium when mobile adsorbed $SiH_3$ radicals on the surface fills in surface roughness at approximately its rate of generation.

FIG. 4. Film properties as a function of film deposition rate; RMS surface roughness and the ratio of buried hydride/dihydride configurations. The composition of the incident flux ($SiH_3/SiH_2$ = 0.9/0.1) was kept constant for all cases while the magnitude of the flux was varied. The average film thickness for all cases was 750 Å.

FIG. 5. The atomic hydrogen fraction and density defect due to porosity as a function of growth rate for the deposition conditions described in Fig. 4. The increase in hydrogen content at low growth rate for simulations where voids are created results from hydrogen being trapped in subsurface voids. The effect may be magnified by the model, which does not allow hydrogen evolution from voids after burial.

FIG. 6. Hydrogen content and hydride/dihydride ratio of a-Si:H as a function of average void size.

FIG. 7. Fractional distribution of voids as a function of void size. The average void volume is 40.9 $Å^3$ and the total void fraction is 16.3%. The sample size for this case is 125 x 125 x 750 $Å^3$.

FIG. 8. Density defect as a function of film thickness. The simulated deposition conditions are the same as for Fig. 3. The solid lines denote bulk porosity. The predicted values for PVD-like conditions may be artificially low due to the assumption in the model that cross linking can take place with at most next nearest neighbors (see text). When the effect of surface roughness ($R_a$, dashed lines) is included, PVD films have a larger density defect than CVD-like films.

FIG. 9. Atomic hydrogen fraction, $f_H$, as a function of film height for the same deposition conditions as used in Fig. 3. Thin films have higher $f_H$ since larger fraction of their atoms are contained in the hydrogen rich near surface layer.

FIG. 10. a) Computed parameters for the radical flux in $SiH_4$/Ar plasmas as obtained from the model described in Ref. 6. b) Deposition rate, hydrogen fraction, as buried spin density, and hydride/dihydride ratio for simulated a-Si:H films having a constant magnitude of silane radical flux for the conditions of Fig. 10 a). These results imply a degradation of film properties when diluting $SiH_4$ with argon.

## REFERENCES


1. K. Tanaka and A. Matsuda, Mat. Sci. Reports 2, 139 (1987).

2. H. Fritzsche, Solar Energy Mat. 3, 447 (1980).

3. F. Kampas, in Semiconductors and Semimetals, edited by J. I. Pankove (Academic, Orlando, 1984) Vol. 21A, p. 123.

4. J. A. Thornton in Amorphous Metals and Semiconductors edited by P. Maasen and R. I. Jaffee (Pergamon, New York, 1986), pp. 299-314.

5. A. Gallagher, J. Appl. Phys. 63, 2406 (1988).

6. M. J. Kushner, J. Appl. Phys. 63, 2532 (1988).

7. G. Turban, Y. Catherine, and B. Grolleau, Thin Solid Films 60, 147 (1979).

8. P. A. Longway, R. D. Estes, and H. A. Weakliem, J. Phys. Chem. 88, 73 (1984).

9. K. Tachibana, in Proceedings of the 8th Symposium on Ion Sources and Ion-Assisted Technology edited by T. Takagi (Institute of Electrical Engineering, Tokyo, Japan, 1984) p. 319.

10. K. K. Gleason, K. S. Wang, M. K. Chen, and J. A. Reimer, J. Appl. Phys. 61, 2866 (1987).

11. B. H. Boo and P. B. Armentrout, J. Am. Chem. Soc. 109, 3549 (1987).

12. K. Muller, J. Appl. Phys. 59, 2803 (1986).

13. B. Drevillon, Thin Solid Films 130, 165 (1985).

14. J. A. Reimer, R. W. Vaughan, and J. C. Knights, Phys. Rev. B 24, 3360 (1981).

15. J. Perrin and B. Allain, J. Non-Cryst. Solids 97/98, 261 (1987).

16. J. Perrin and T. Brockhuizen, Appl. Phys. Lett. 50, 433 (1987).

17. B. A. Scott, J. A. Reimer, and P. A. Longeway, J. Appl. Phys. 54, 6853 (1983).

18. R. Wiesendanger, L. Rosenthaler, H. R. Hidber, H.-J. Güntherodt, A. W. McKinnon, and W. E. Spear J. Appl. Phys. 63, 4515 (1988).

19. M. Tsukude, S. Hata, Y. Kohda, S. Miyazaki, and M. Hirose, J. Non-Crystal. Solids 97/98, 317 (1987).

20. J. C. Knights, Mater. Res. Soc. Proc. 38, 371 (1985).

21. C. C. Tsai, J. C. Knights, G. Chang, and B. Wacker, J. Appl. Phys. 59, 2998 (1986).

22. R. W. Collins and J. M. Cavese, J. Appl. Phys. 61, 1662 (1987).

23. R. W. Collins and J. M. Cavese, J. Appl. Phys. 62, 4146 (1987).

24. R. W. Collins and J. M. Cavese, J. Non-Cryst. Sol. 97 & 98, 1439 (1987).

25. R. W. Collins and A. Pawlwski, J. Appl. Phys. 59, 1160 (1986).

26. M. Pinarbasi, L. H. Chou, N. Maley, A. Myers, D. Leet, and J. A. Thornton, Superlattices and Microstructuring 3, 331 (1987).

27. R. C. Ross and J. Jalik, Jr. J. Appl. Phys. 55, 3785 (1984).

28. O. Kuboi, M. Hashimoto, and Y. Yatsurugi, App. Phys. Lett. 45, 543 (1984).

29. S. Kumar, K. K. Pandya, and K. L. Chopra, J. Appl. Phys. 63, 1497 (1988).

30. J. R. Blanco, P. J. McMarr, K. Vedam, and R. C. Ross, J. Appl. Phys. 60, 3724 (1986).

31. G. H. Lin, J. R. Doyle, M. He, and A. Gallagher, J. Appl. Phys. 64, 188 (1988).

32. J. C. Knights and R. A. Lujan, Appl. Phys. Lett. 35, 244 (1979).

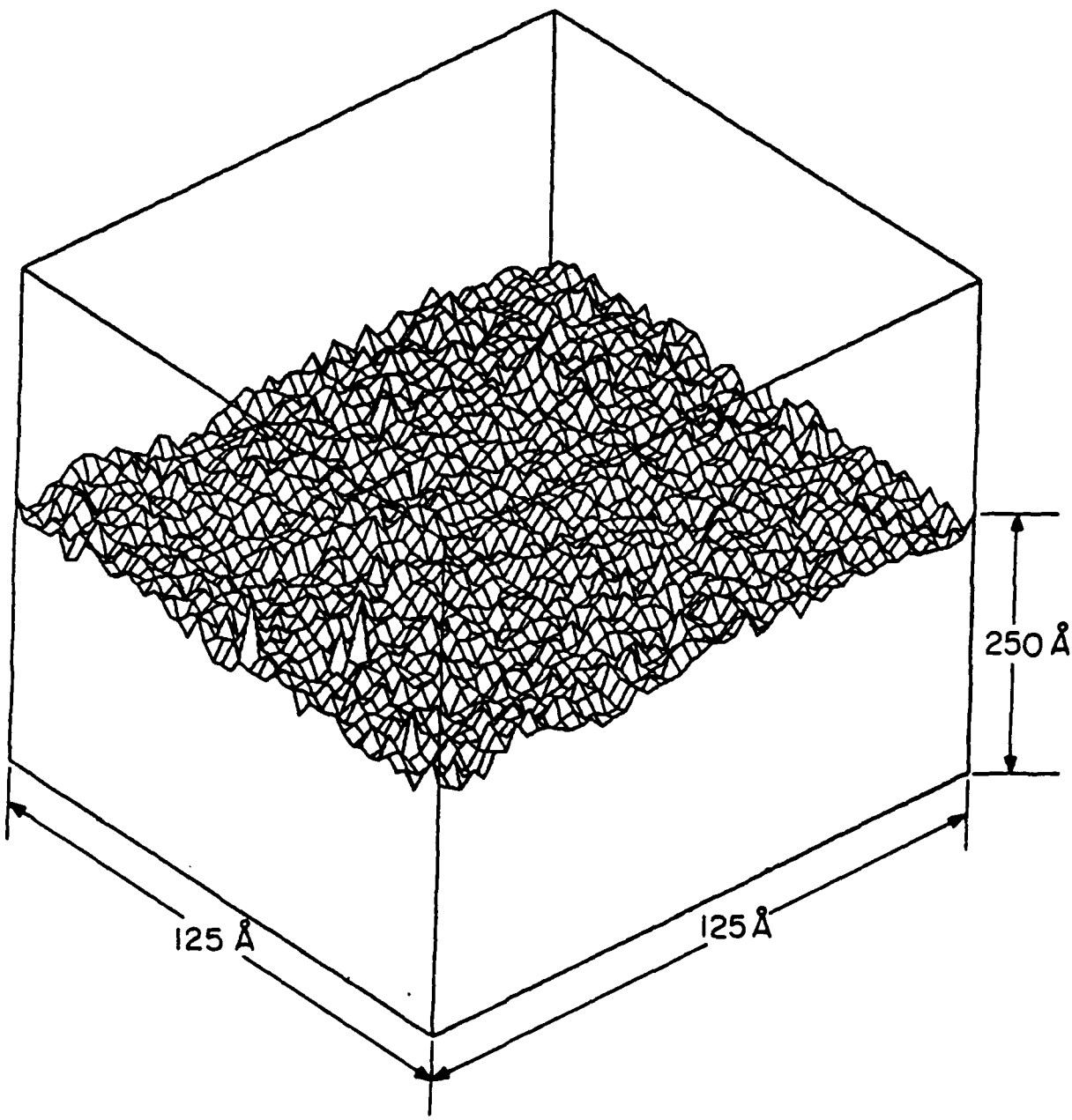


McCaughey and
Kushner

Fig. 1 of 10

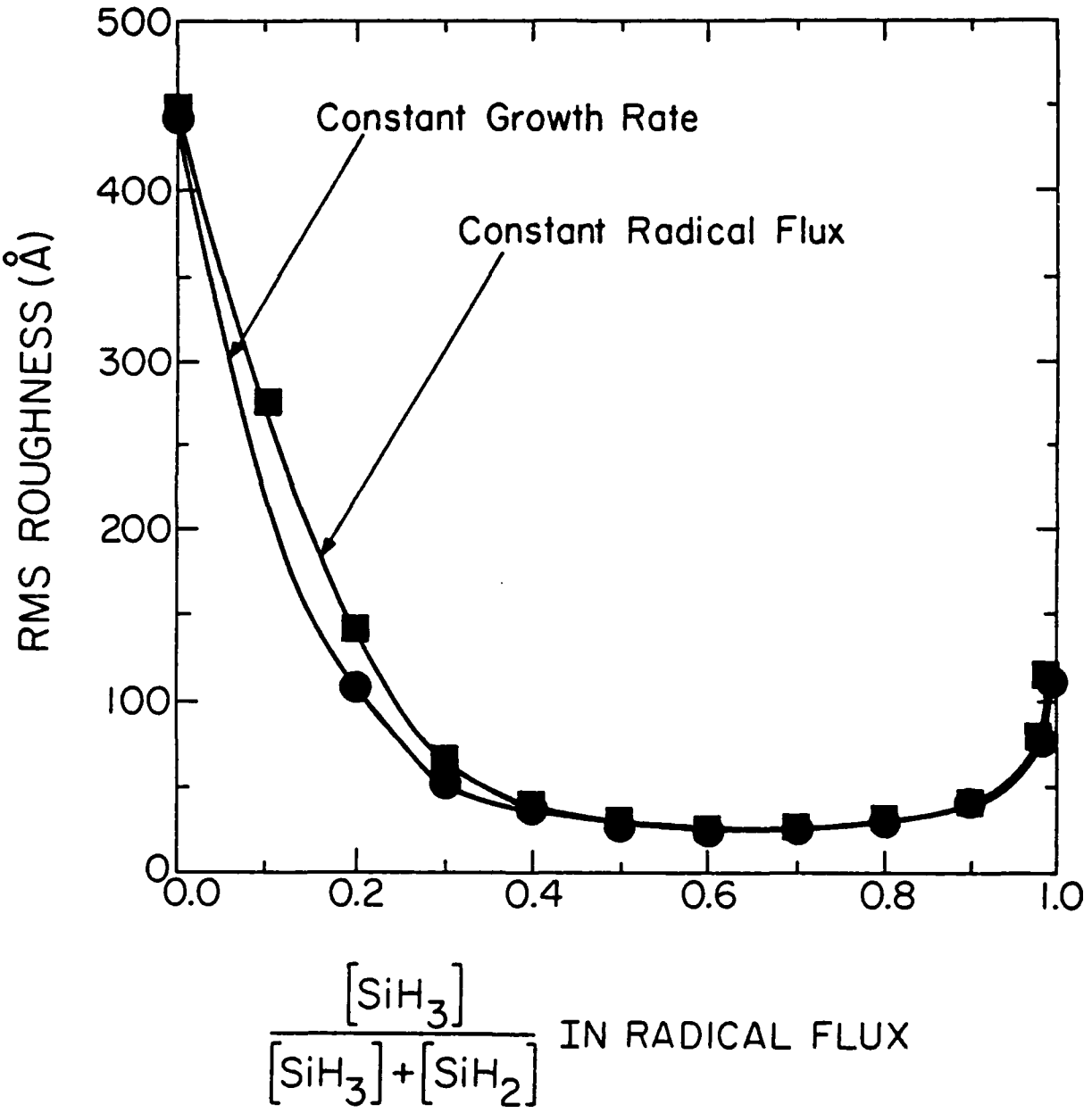


McCaughey and Kushner

Fig. 2 of 10

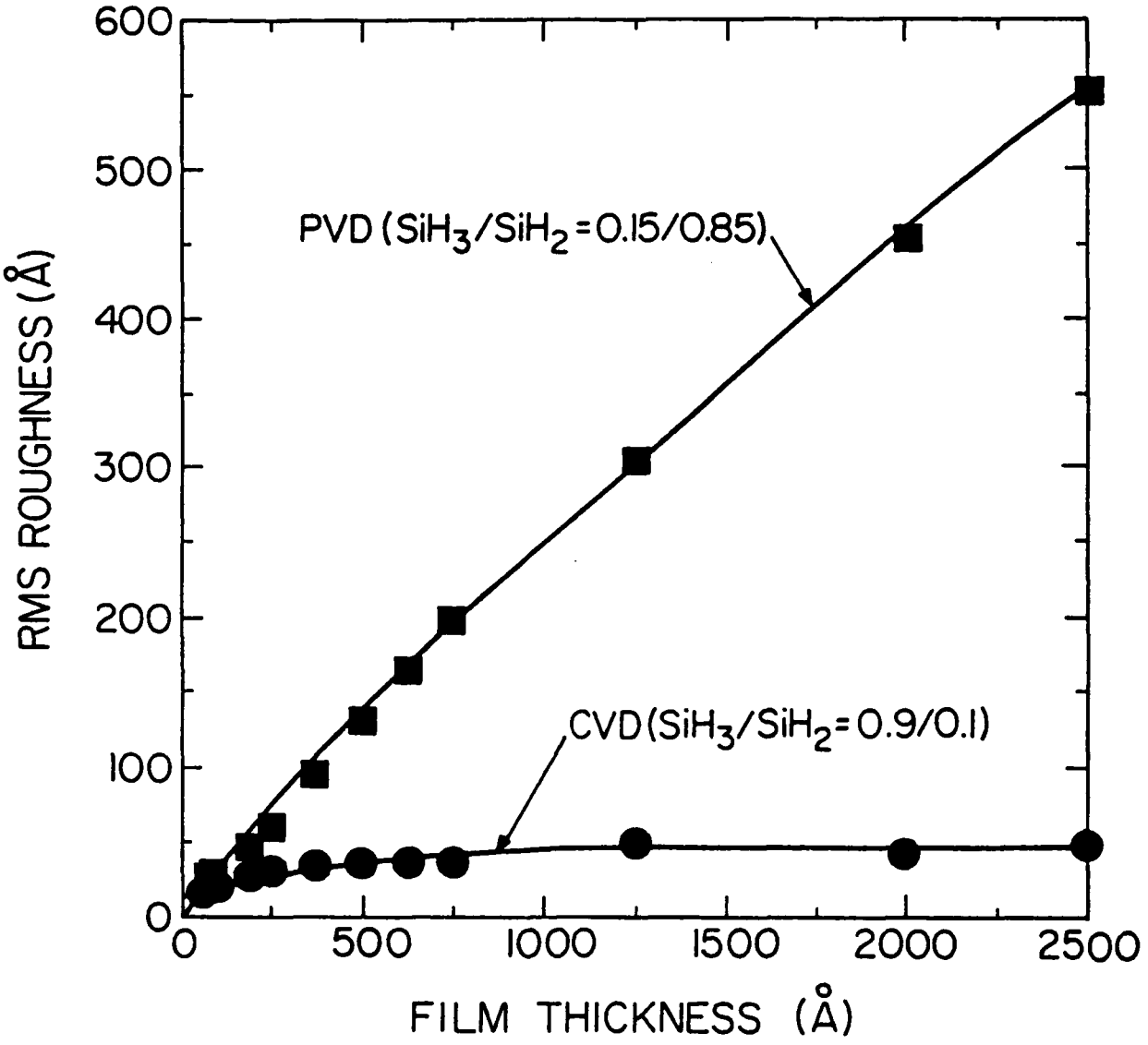


McCaughey and Kushner

Fig. 3 of 10

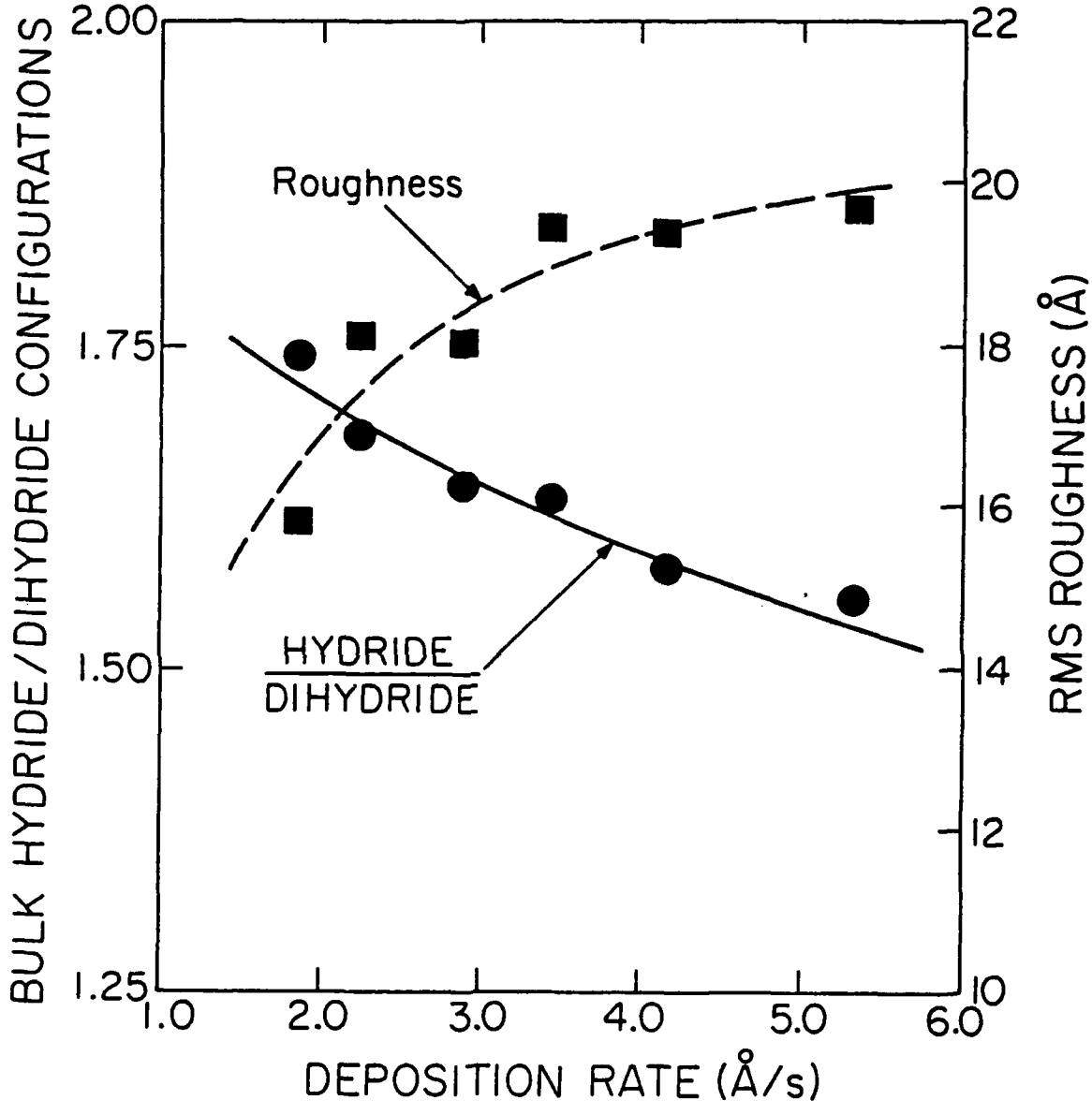


McCaughey and Kushner

Fig. 4 of 10

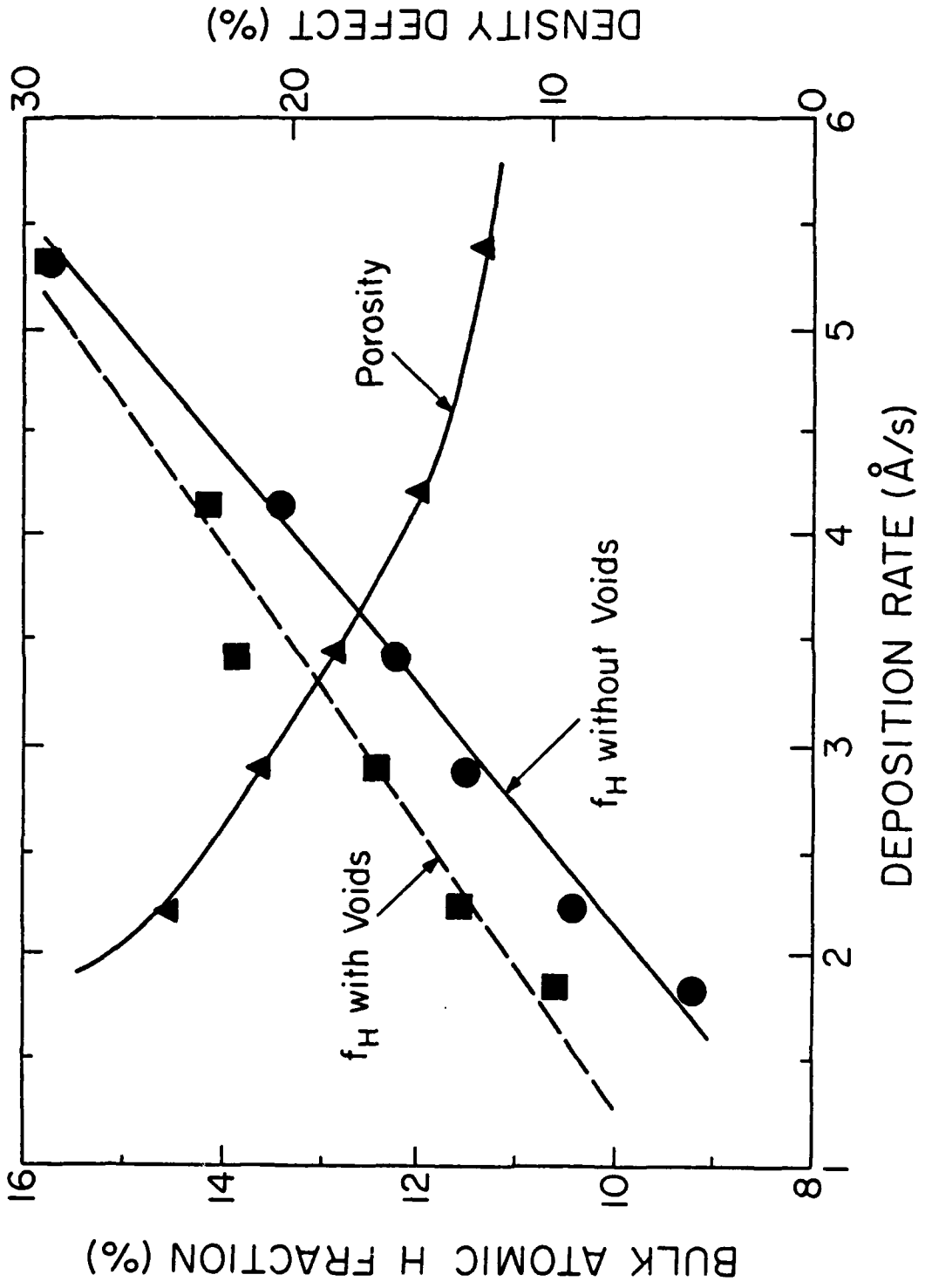


McCaughey and Kushner

Fig. 5 of 10

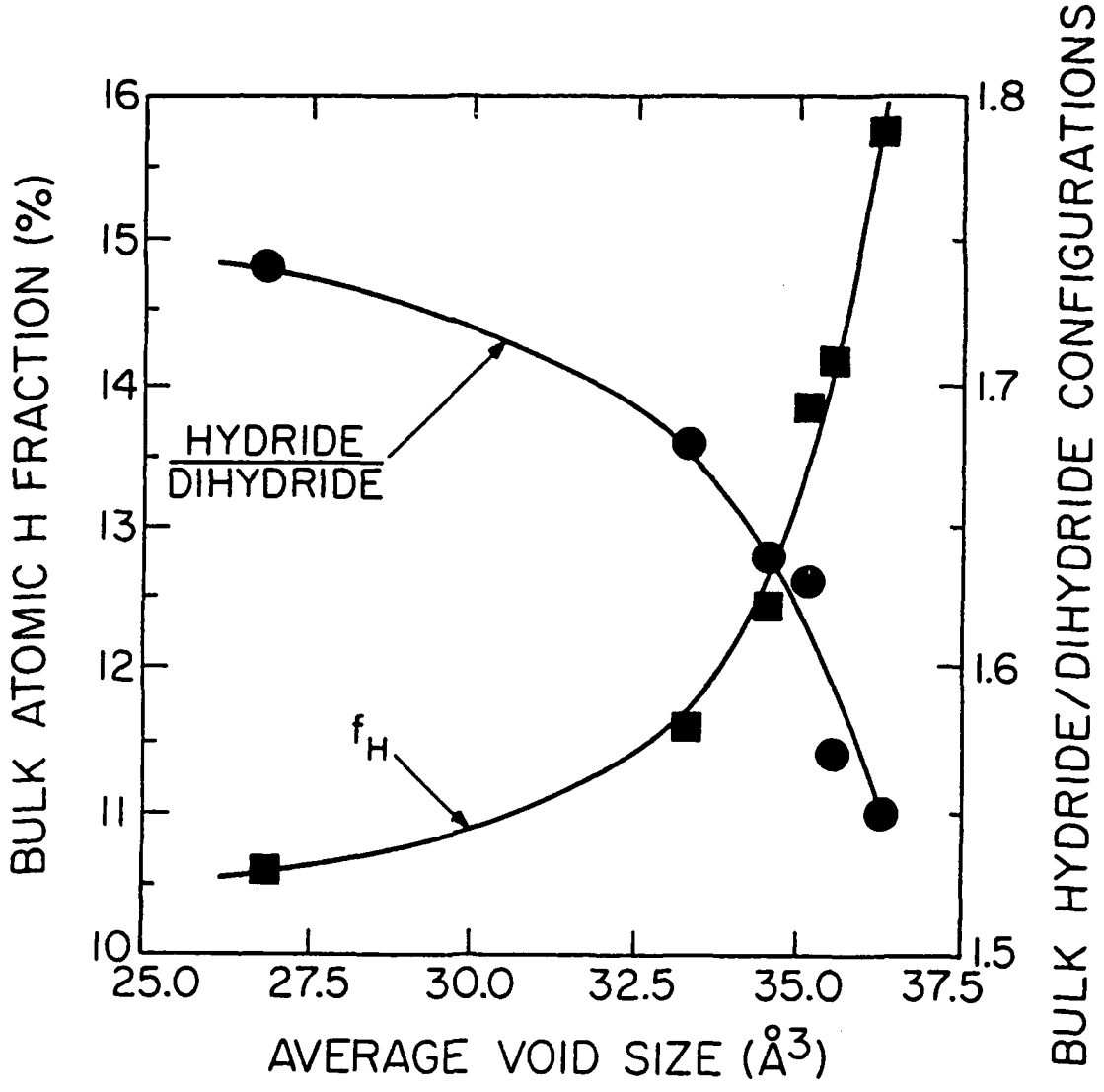


McCaughey and Kushner

Fig. 6 of 10

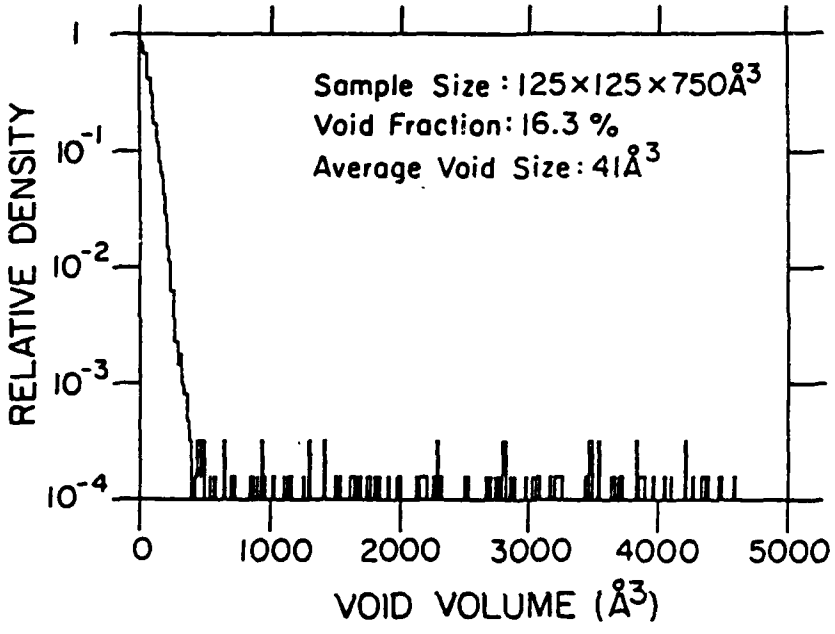
Sample Size : 125×125×750Å3
Void Fraction: 16.3 %
Average Void Size: 41Å3
RELATIVE DENSITY
1
10-1
10-2
10-3
10-4
0
1000
2000
3000
4000
5000
VOID VOLUME (Å3)

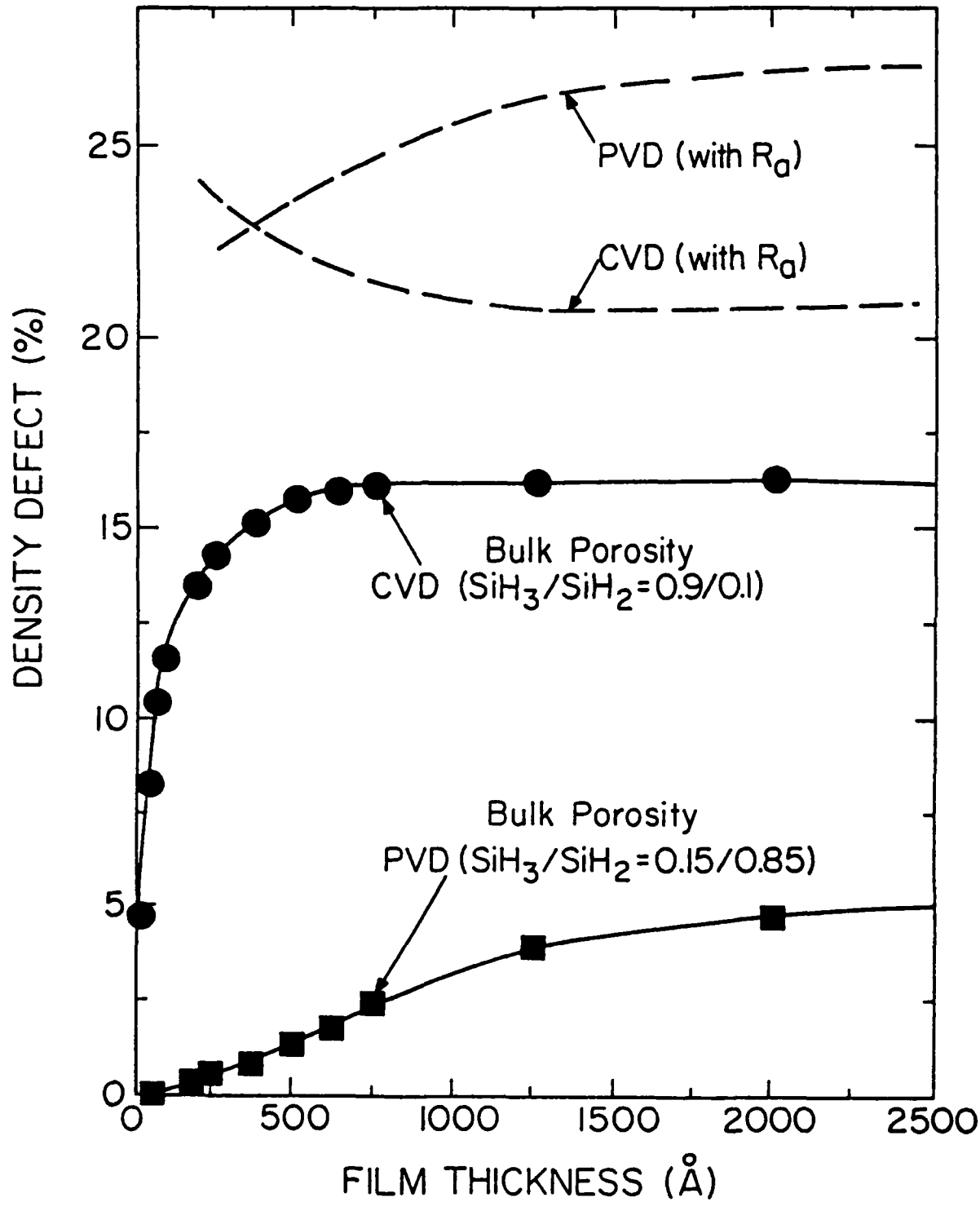


McCaughey and Kushner

Fig. 8 of 10

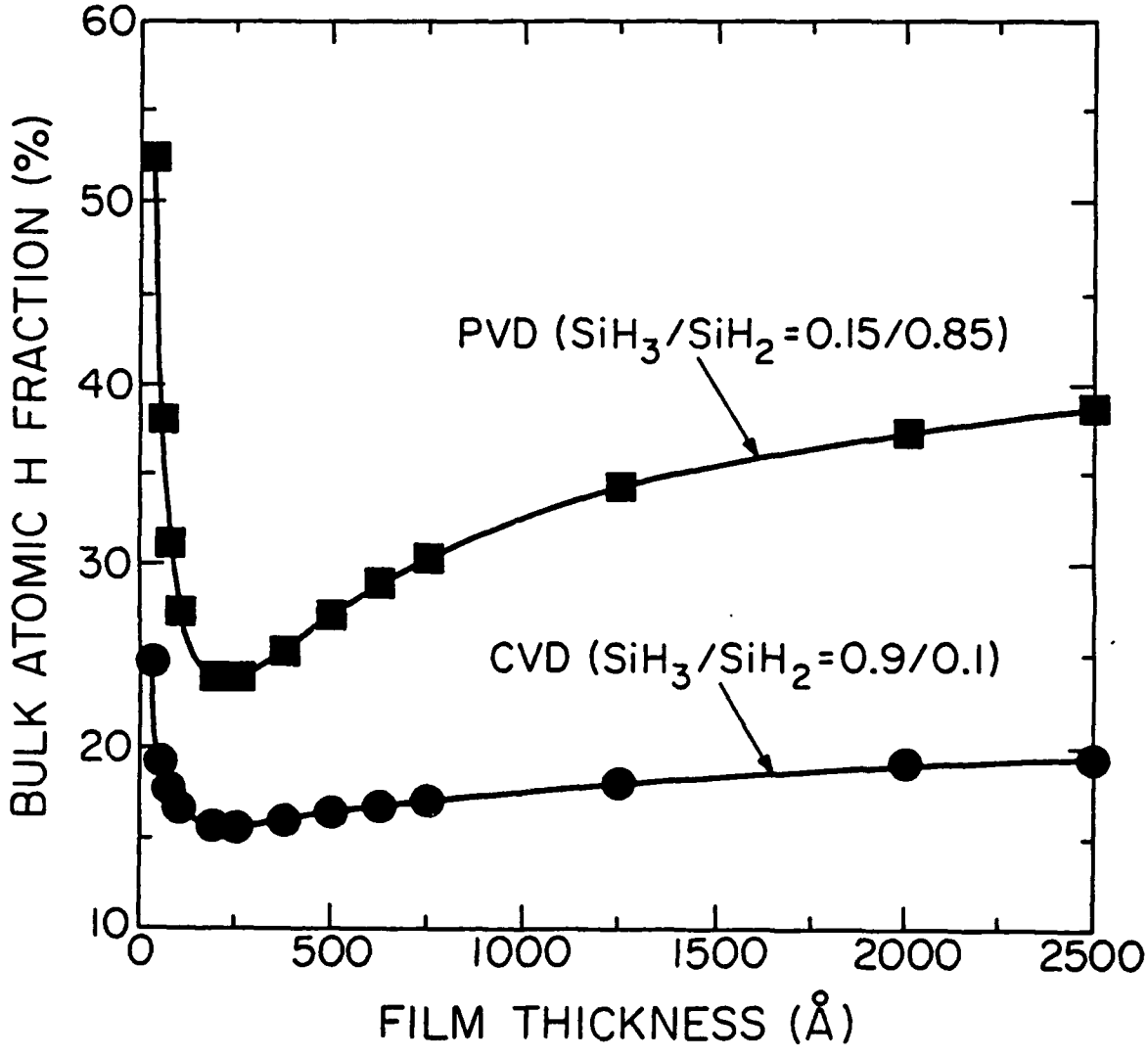


McCaughey and Kushner

Fig. 9 of 10

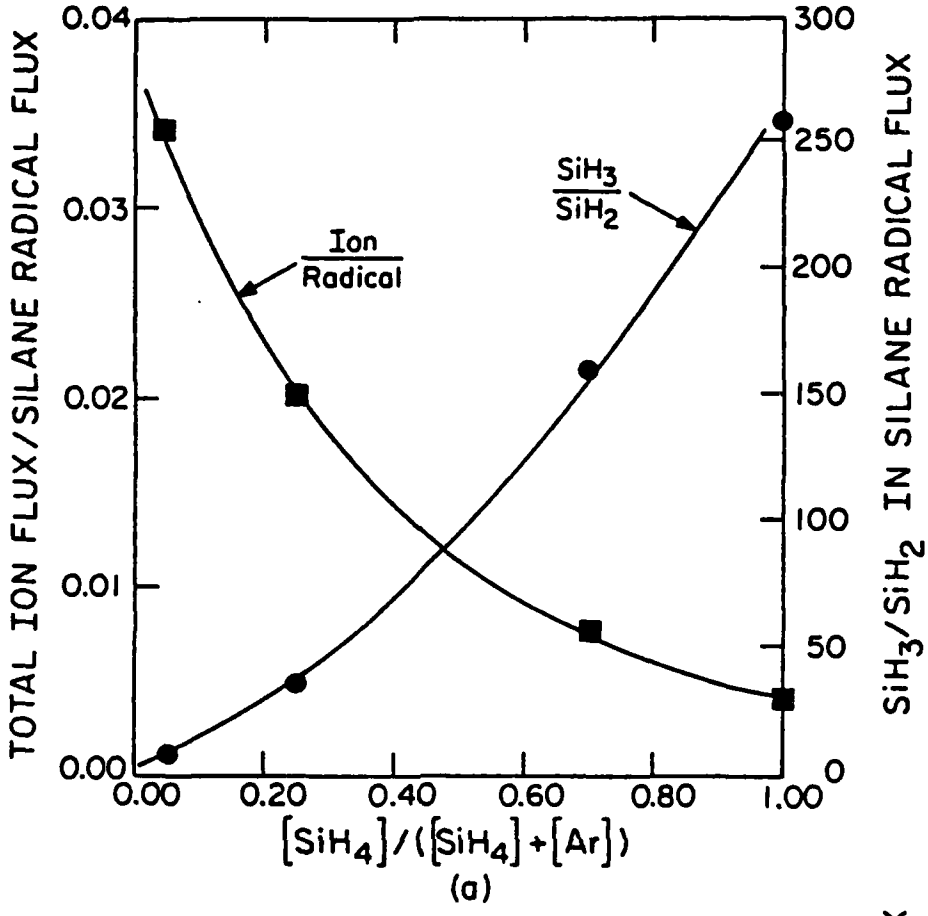


(a)

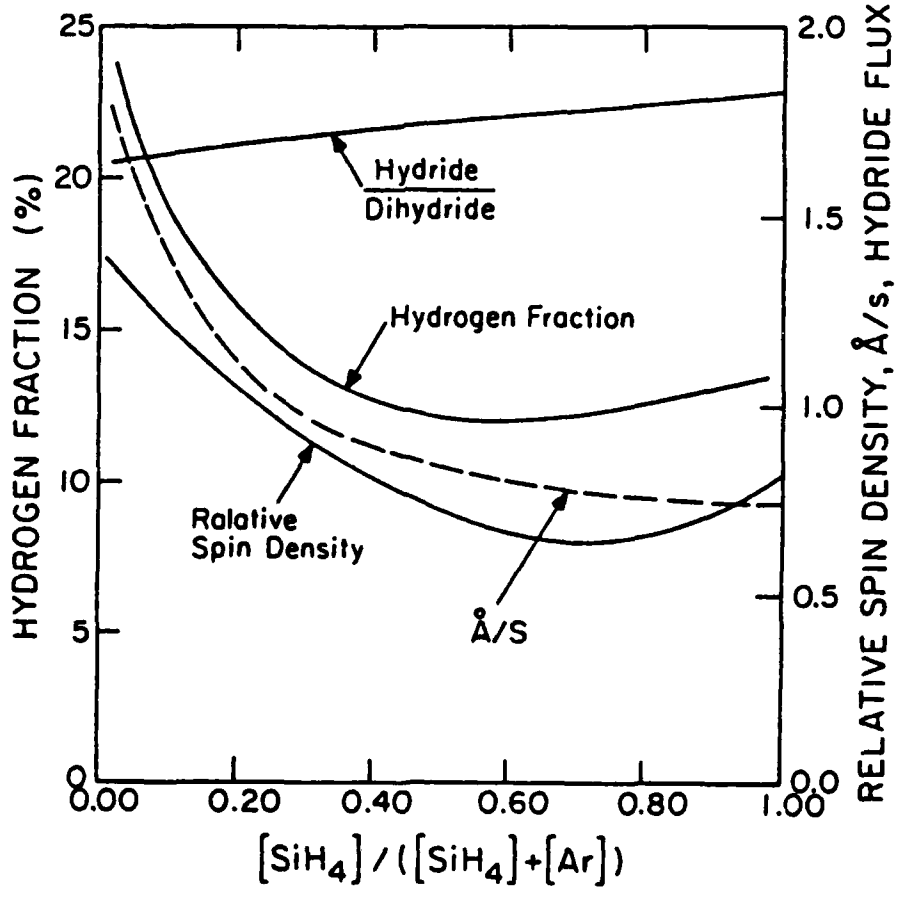


(b)

McCaughey and Kushner

Fig. 10 of 10